AN EXPERIMENTAL STUDY OF THE EFFECT OF MASS INJECTION AT THE STAGNATION POINT OF A BLUNT BODY

Thesis by

Howard Martin McMahon

In Partial Fulfillment of the Requirements

For the Degree of

Doctor of Philosophy

California Institute of Technology

Pasadena, California

1958

ACKNOWLEDGMENTS

I wish to express my deep appreciation to Professors Lester Lees and Clark Millikan for their constant guidance and encouragement during the course of this investigation. I would also like to acknowledge many valuable discussions with Dr. Toshi Kubota. I would like to thank the staff of the Hypersonic Wind Tunnel for their assistance and advice during many hours of testing, and the members of the Aeronautics Machine Shop for making superb experimental equipment from my very crude sketches. My thanks also to Mrs. Mary Dennison for much computational work, to Mrs. Betty Wood and to Mrs. Nell Kindig for preparing the many figures, and to Mrs. Geraldine Van Gieson for typing the manuscript.

This work is dedicated to Fran, whose confidence and understanding made it possible, to Patricia and Helen, who one day may understand why I never had time to read them stories, and to my parents.

ABSTRACT

An experimental study of the effect of the injection of nitrogen and helium coolant gases at the stagnation point of a blunt body was carried out in the GALCIT Hypersonic Wind Tunnel at a Mach number of 5.8. The gases were injected straight out of the stagnation point and also tangential to the body surface. The model was also fitted with flow separation spikes.

The injection of the coolant gas resulted in a marked reduction in the model equilibrium temperature, and this cooling effect persisted over the entire length of the model. For the same mass flow, helium was a better coolant than nitrogen.

The average heat transfer near the nose of the body was reduced almost to zero by injecting a mass of helium as small as $\frac{1}{2}$ per cent of the mass flow of free-stream air contained in the "capture" area πR^2 of the spherical nose.

Separation near the spike tip was observed up to a ratio of spike length to spherical nose diameter of 1.78 and a free-stream Reynolds number based on nose diameter of 2.84×10^5, resulting in a value of the foredrag coefficient which was one-third the value with no spike attached.

TABLE OF CONTENTS

LIST OF FIGURES

LIST OF SYMBOLS

a	radius of thermocouple wire
A	area
A^*	area at $M = 1$
b	thickness of model skin
c	specific heat
C_{D_F}	foredrag coefficient, $D_F/(\frac{1}{2}\rho_\infty U_\infty^2)(\pi R_B^2)$
C_p	pressure coefficient, $(p - p_\infty)/(\frac{1}{2}\rho_\infty U_\infty^2)$
$C_{p_{max}}$	pressure coefficient at stagnation point of spherically blunted cone model, no injection
D	diameter of outer surface of spherical nose
D_F	pressure drag, $\int p \cos\psi \, dA$
F	function of time appearing in Appendix B
$\tilde{F}$	Laplace transform of F
h	heat transfer coefficient in equation $q = h(T_2 - T_1)$; also, length of deflector cap stand-offs (Figure 6)
k	thermal conductivity
K_o	modified Bessel function of the second kind of order zero
K_1	modified Bessel function of the second kind of order one
L	spike length; also, a representative length
m_i	mass of coolant gas injected per unit time
M	Mach number
$\bar{n}$	vector normal to body surface
n	distance measured along normal vector
p	pressure

q, Q	heat transfer rate per unit area
q_{av}	average heat transfer to a segment of area per unit time
q_c	conduction term in local or average heat equation
q_s	storage term in local or average equation
q_T	total heat transferred locally per unit time, being the sum of the local storage term and the local conduction term
Q_w	heat transfer rate per unit area along thermocouple wire
r	radius in polar or spherical coordinates; also recovery factor $(T - T_\infty)/(T_o - T_\infty)$
R	radius of outer surface of spherical nose
R_{in}	radius of inner surface of spherical nose
R_B	radius of model base
Re	Reynolds number based on free stream conditions ahead of shock wave and with spherical nose diameter as characteristic length, i.e., $Re = \rho_\infty U_\infty D/\mu_\infty$
s	variable appearing in the Laplace transform of a function
S	distance along model surface measured from stagnation point
S_o	distance along conical skirt of model as measured from tip of 10^o half angle cone
S/R	nondimensional distance to a measuring station
t	time (seconds)
T	temperature (^oF or ^oR)
T_1	temperature on model surface measured at $S/R = 0.1$
T_{equil}	equilibrium temperature
T_{inj}	temperature of coolant as measured in plenum chamber
$\tilde{T}$	Laplace transform of temperature
u	velocity

U	free stream velocity
x	distance in rectilinear coordinates; distance along body axis
y	vertical distance from body axis to surface of model
α	angle of attack
β	nondimensional ratio $(1 - \lambda)/(1 + \lambda)$ in Appendix A
γ	ratio of specific heats
Γ	nondimensional injection parameter $(m_i/\rho_\infty U_\infty \pi R^2)$; also, gamma function in Appendix B
δ	boundary layer thickness
ϵ	a quantity small compared to one (Appendix B)
ζ	temperature difference (p. 34)
η	temperature level (p. 34)
θ	polar angle of spherical nose
θ_c	cone angle
κ	thermal diffusivity $k/\rho c$
λ	nondimensional ratio in Appendix A $\sqrt{\frac{k_1 \rho_1 c_1}{k_2 \rho_2 c_2}}$
μ	viscosity
ξ	distance from leading edge of flat plate (Appendix C)
π	constant, 3.1416
ρ	density
τ	nondimensional temperature ratio defined in Section IV. C, p. 33
ϕ	meridian angle of spherical nose
ψ	angle between normal vector and horizontal
∇	operator

Subscripts

$( )_{1,2}$	quantity evaluated at points one, two or for materials one, two
$( )_m$	quantity evaluated for model skin material
$( )_o$	quantity evaluated at stagnation conditions
$( )_w$	quantity evaluated at surface of model
$( )'$	quantity evaluated at conditions behind normal shock wave
$( )_\infty$	quantity evaluated at free stream conditions ahead of shock wave

Double Subscripts

$\Gamma = 0$	quantity evaluated for no-injection condition
$\Gamma \neq 0$	quantity evaluated with injection

I. INTRODUCTION

The problem of aerodynamic heating for aircraft and internal propulsion systems has become increasingly important in recent years. Considerable thought has been given to the problem of an optimum body shape to minimize the severe heating effects on a body entering the Earth's atmosphere[1], and also to the problem of cooling the vehicle[2]. * A method of cooling utilizing the injection of a coolant gas directly into the boundary layer has shown promise, and much theoretical work and experimental work at subsonic speeds has been carried out[3-7]. Some experimental results on transpiration cooling of flat plates and cones[8,9] in supersonic flow are also available.

Most of the investigations to date have been concerned with injection of the coolant gas over some porous surface area on a model such as a flat plate (see Appendix C) or a cone, where the situation is comparatively easy to treat theoretically. The experiment reported here was concerned with the effects caused by introduction of nitrogen and helium coolant gas through an orifice at the stagnation point of a blunt body when the body is immersed in a hypersonic flow. The purpose of the experiment was to search for new or unusual effects, both as regards the magnitude of these effects and their relative importance, so that the work would serve as a guide to theoretical analyses of the problem, and as a guide to more detailed experimental investigations. Measurements of pressure, temperature and heat

---

* Superscript numbers refer to the reference section beginning on page 51 .

transfer were carried out on a basic model shape with no injection. Then the same measurements were made with injection straight out of an orifice at the stagnation point, and also with the coolant stream directed tangential to the surface of the model by means of a deflector cap at the nose. Lastly, flow-separation spikes were mounted on the model to see whether the equilibrium temperatures or heat transfer rates were strongly affected in the separation region. This problem was considered to be of interest because a previous experiment[10] had shown an increased heat transfer rate in such a separated region.

The data obtained without injection are compared with theory and with previous experiments in order to establish a confidence level in the experimental methods; the results with injection are then expressed as comparative measurements of the quantities. No attempt is made to reduce the heat transfer rate data to the somewhat artificial form of an equivalent flat plate value for uniform wall temperature.

The experimental determination of heat transfer is not an easy problem. In many cases, a local measure of the heat transfer rate is required as well as an average over some portion of the model surface. To make a local measurement in the steady-state case requires the construction of an internally cooled model so that there is a heat "sink". The local value of q is determined either by measuring the temperature gradient through the model shell or by a direct measurement utilizing thermopile elements called heat meters[11]. Recently, the use of heat meters has shown great promise when the meters are "miniaturized", so that corrections for conduction caused by axial temperature gradients in the model are avoided[12, 13]. However,

the accuracy possible with these meters is obtained only after a difficult and time-consuming calibration.

A high degree of accuracy is not of paramount importance when one is looking for large effects or carrying out a preliminary survey, and the transient method offers certain advantages in such cases. The model is relatively easy to build and the only calibrations necessary are the straightforward calibrations of thermocouples and instrumentation. This simplicity is offset by the fact that the results are not known with exactness, because the conduction corrections may be appreciable and, by the nature of the method, cannot be determined accurately. It was decided to utilize the transient method for obtaining the comparative heat transfer measurements desired for this exploratory work.

An optimum utilization of the two techniques in wind tunnel research would seem to consist of using the transient method for exploratory work covering a wide range of conditions or model shapes. The most interesting cases could then be more critically examined by using a heat meter model, with the transient data acting as a guide to the best choice of meter sensitivity and location.

II. MODEL CONSTRUCTION

A spherically blunted cone with a 10 degree cone half-angle constituted the basic model shape for this experiment. Combinations of three different injection-deflector caps and four different drag reduction devices (spikes) were added to this basic shape.

A. Pressure Distribution Model

A model previously used by Machell and O'Bryant[14] (Model No. 6) was utilized for the pressure distribution studies. In order to minimize the effect of heat conduction along the surface (see Appendix A), a model with the largest possible nose radius was desired, and their work had shown that this model was the largest spherically blunted cone for which supersonic flow could be established in the wind tunnel.

The pressure distribution model was made of brass, and fitted with sixteen .016" diameter pressure orifices on the spherical and conical surfaces (see Figure 1). The pressure tap at the stagnation point was enlarged to .0625" diameter to a depth of approximately .040", where it joined a larger passage 0.083" in diameter drilled through the model from the rear. This hole was used as an injection orifice.

B. Heat Transfer Model

1. General Considerations

As shown in Appendix A, the criteria for the design of a transient heat transfer model are that the hemisphere radius should be as large as possible, that the model should have a thin skin of uniform thickness

with an air space behind it, and that the skin material should have a low thermal conductivity in order to make the ratio of the "heat storage" term to the conduction term as large as possible. However, there is the additional problem of the effect of the thermocouple wire on the measurements. An estimate of the conduction leakage loss along the thermocouple wire given in Appendix B shows that if the wire diameter is one-half the skin thickness, the error in the transient skin temperature measurement is less than 1 per cent at the end of five seconds if the skin is a good thermal conductor (e.g., metal), while it is about 20 per cent if the skin has a low thermal conductivity (e.g., glass).

Now the heat conduction correction in the heat balance equation can be determined from the measured data, while the thermocouple conduction correction can only be estimated. Therefore, it was decided to base the model construction on the requirement of a minimum thermocouple error and to use a plating process to form a thin-skin metal model.

2. Electroplating of Model and Installation of Thermocouples

A wall thickness of .020" was chosen, using Reference 15 as a guide for anticipated conduction corrections and time constants (see Appendix A), and a thermocouple wire diameter of .010" was selected.* According to Reference 16, page 104, example 43.1, the

---

* In order to test one of the conclusions from the calculations in Appendix B, three constantan wires having different diameters (.010", .021", .032") were installed at $\theta = 35^{\circ}$ and their readings compared during the no-injection tests. A 7 per cent scatter in the temperature-time slopes was noted, which showed no trend with wire size, hence the theoretical prediction that there would be a small error introduced even for wires of diameter comparable to the skin thickness would seem to be justified.

temperature gradient through such a thin metal shell is negligible, so that the location of the thermocouple in the normal direction is not critical. Attachment of the thermocouples to the inside of the skin (for example by soldering) could increase the local mass of the thin skin by a considerable amount. Thus, the local mass undergoing the temperature rise would not be known. A "zero mass" method of attachment was achieved by first making a core to the exact model dimensions, less .020" to allow for the skin which would be plated on later. Iron was chosen as the plating material. This choice simplified the model construction by allowing the use of one .010" diameter constantan wire at each station instead of a thermocouple pair. A common iron wire was attached at the rear of the model, and the iron shell provided the rest of the thermocouple circuit.*

The inside of the core was drilled out, and small holes about .008" diameter were drilled through the core wall at the designated thermocouple measuring stations. (The location of these holes is shown in Figure 2.) The ends of the .010" constantan wires were dipped in dilute nitric acid and withdrawn slowly so as to taper them. The wires were threaded through the large passages drilled in the core, forced up through the small holes to the surface, and pulled tight. Then they were cut off to a height of about .010" above the surface. When the

---

* Since the end of the common iron wire and the actual thermocouple junctions might be at different temperatures during the transient measurements, this simplification was possible only if the common wire and the shell were made of the same material. Otherwise a spurious thermocouple effect would be introduced. The correction introduced by the fact that the shell material and the common wire were perhaps not made from iron of identical purity was investigated and found to be negligible.

iron was plated over the core, these thermocouples became fused into the skin. The shell was plated to a depth of about .040" and then machined to the correct thickness and shape. The dimensions of the core and of the finished shell were both checked against a template using an optical comparator.

The fact that the core had to be removed while leaving the wires intact meant that it either had to be melted out or dissolved out. The plating solution had to be hot (about 200°F) since iron-plating in a room temperature solution sets up high internal stresses in the deposited iron and the shell tends to crack. This requirement precluded the use of wax or plastic as a core material. The core was made from aluminum and was removed by eating it away with a solution of sodium hydroxide. This etching had no effect on the shell or the wires.

This method of attaching the wires worked satisfactorily except for the wires near the stagnation point. Here the plating was most difficult because of the model shape, and when the core was removed the first five wires broke off. When these wires were replaced another method of attachment was tried which seemed to be equally satisfactory and was much simpler. Holes about .008" in diameter were drilled through the iron shell at the designated stations. The wire then was threaded through the holes from the inside and pulled very tight, forming a good force fit, after which the ends were cut off and stoned flush with the surface. No difference in behavior was noted between the wires attached by this method and by the first method described above.

The wires were led through a hole in the plastic base, then through a hollow bakelite sting attached to the base and through a

length of Saran tubing which came out through the tunnel wall. The model was checked for leaks by pressurizing it and immersing it in water. Thus the whole system was made leak-tight, so that the inside of the model was filled with still air at atmospheric pressure during the course of the tests and there were no heat transfer effects introduced by air flowing over the wires or over the inside of the shell[17]. A .083" diameter tube (.0625" I. D.) was fitted for injection at the stagnation point. A plastic plenum chamber inside the model provided space in which to measure the coolant gas temperature and pressure just prior to injection. The wall thickness of the injection tube between the end of the plenum chamber and the stagnation point was held to .005" in order to minimize heat flow along it from the skin. The heat transfer model is shown in Figures 3 and 4.

3. Spikes and Caps

In order to investigate the effect of injection tangential to the model surface three different deflector caps were used, as shown in Figures 5 and 6. They were made of brass, and were just large enough to contain the three mounting screws, which were placed in line with the legs to minimize their effects on the injection flow. The support legs for cap A were made of such a length that the circumferential outlet area for the injected gas was one-half the cross-sectional area of the injection tube. For cap B the ratio was 5:1; for cap C, 10:1.

Flow separation (drag reduction) devices in the form of three spikes of different lengths and one 20° half-angle cone were tested. These were made of brass and were fitted on the caps as shown in Figures 5 and 6.

III. INSTRUMENTATION AND TEST PROCEDURE

A. Hypersonic Wind Tunnel

The experiments were conducted in the GALCIT 5 x 5 inch Hypersonic Wind Tunnel (Leg 1), which is of the closed return, continuously operating type. A description of the wind tunnel and compressor plant is found in References 18 and 19, and a schematic drawing is shown in Figure 7.

Because of a large pressure drop caused by oil and scale-removal devices which had been installed after the fifth stage compressors, the stagnation pressure upper limit was 61 psig at the time the tests were run. One run was made at 82 psig by removing these devices from the system. The minimum reservoir pressure for starting the flow was about 25 psig. with the model installed, and the maximum stagnation temperature attainable was 300°F. The quantities p_o and T_o were maintained within $\pm$. 04 psi and $\pm$ 2°F, respectively, during the pressure distribution and equilibrium temperature runs. The stagnation pressure was controlled manually while in by-pass prior to the transient runs, and was held to about $\pm \frac{1}{2}$ psi.

The tunnel piping upstream of the throat had to be modified in order that a step function in the stagnation temperature could be provided for the transient heat transfer tests. Originally, the hot air flowing through the by-pass line was directed into a settling chamber (not shown) of about four cubic feet volume, and then through the throat. However, this arrangement gave a very poor approximation to the desired temperature step function in the test section because much of

the heat was lost to the walls of the settling chamber during the first few seconds. In order to sharpen the leading edge of the temperature step, piping was installed inside the settling chamber so that the air was led directly to the throat through an L-shaped pipe and a transition section. The transition section carried the air from the circular pipe to the rectangular nozzle contraction; it ended two inches upstream of the throat and was sealed in position. The temperature step now was sharper, but the amplitude of the temperature rise was small because of heat loss to the pipe walls. In order to minimize this heat loss the piping between the by-pass valve and the throat was pre-heated electrically by wrapping it with Nichrome wire and covering the wire with layers of glass cloth. The resulting temperature history is shown in Figure 8. This trace was measured with a thermocouple probe mounted one inch upstream of the throat. This throat probe was patterned after probe No. 3 of Reference 20 so that it had a fast time response.

A trace of the temperature history in the test section corresponding to the throat probe trace of Figure 8 is shown in Figure 9. This temperature was measured with a bare-wire thermocouple probe mounted in the center of the test section. The probe was U-shaped and was made of plastic. The thermocouple was made from .010" diameter wire and had a one-inch unsupported length across the open end of the "U" with a bead spot-welded in the center of this length. A recovery factor for this test section probe was calculated from the temperature read by the two probes at 115 seconds after flow was established. This factor had the value $r = 0.946$, and when it was

applied at 2, 5, and 10 seconds the computed temperatures as indicated on Figure 9 agreed with the throat probe temperatures within 3°F. Hence the T_o readings for the transient runs were measured with the throat probe. Since the magnitude of T_o depended partly upon the temperature of the pre-heated pipe, which could not be controlled accurately, T_o was monitored for each run by recording the throat thermocouple output on an Offner pen-type oscillograph.

Four fine-mesh screens were mounted inside the new piping and transition section in order to smooth out the flow. The stagnation temperature variation across the width of the tunnel was $\pm$ 1°F measured one inch upstream of the throat. The steady-state temperature distribution along a vertical centerline in the test section where the model was installed varied about $\pm$ 2°F.

B. Measurements of Injection Mass Flow

The nitrogen and helium gases which were used for the injection tests were taken from commercial bottles, passed through a pressure regulator, then through a gas flowmeter, and then into the model. A calibrated pressure gage just upstream of the flowmeter indicated the metering pressure. A small needle valve was located just downstream of the flowmeter. This valve location permitted the mass flow to be varied without changing the metering pressure, and hence kept the number of flowmeter calibrations to a minimum.

The gas flow was measured with Fisher and Porter variable-area flowmeters. The smaller mass flows were metered with a tube and ball-float meter which was calibrated for the two gases by running

it in series with a wet-test gas meter. The larger mass flows were measured with a flowmeter having a "tri-flat" tube for which calibration curves could be predicted for various gases and metering pressures.

The metering pressures were 20 and 30 psig. It is estimated that the mass flows were measured with $\pm$ 3 per cent error for the three lowest flow rates of each gas as measured with the small flowmeter, and $\pm$ 6 per cent error for the largest flow rate of each gas as measured with the large flowmeter.

C. Transient Temperature Instrumentation

The measurement of heat transfer by the transient method requires multi-channel recording equipment to record the output of the model thermocouples as a function of time. This equipment has to have a fast response and a relatively high sensitivity (in the microvolt range for some applications). The sensitivity has to be variable to take care of widely different heat rates at different points on the model; for example, for a blunt body the thermocouple outputs at the stagnation point and on the afterbody may differ by a factor of ten. The sensitivity also has to be variable in order to accommodate different heat rates at a given measuring station which may be brought about by changing the test conditions (e.g., p_o) or by injecting mass into the boundary layer.

The instrumentation described here was originally intended for use with a flat plate model (see Appendix C) where thermocouple outputs on the order of 100 microvolts at the end of ten seconds were expected. Therefore, high sensitivity was required in the recording

instrument. Although sensitivity was not as important for measurements on a blunt body, where the heat rates were considerably higher, the high sensitivity was useful for some tests with injection, and the instrumentation as developed had many advantages when compared with more conventional oscillograph equipment.

The temperature-time data were taken by sampling the output of the various thermocouples with a stepping switch, amplifying the output, and displaying the information on an oscilloscope.* Figure 10 shows a wiring diagram of the system. Each component will be discussed in detail.

Eighteen constantan wires and one common iron wire were brought from the model to the measuring area through a conduit, and were connected to terminal strips. In order to avoid ground loops, which were found to have an effect on the measured voltages, the model and wires were "floating" electrically before being connected to the terminal strips. This also reduced the noise level, which was found to be inadmissable when the model was grounded to the wind tunnel.** The conduit was electrically insulated, and grounded at one end. Eight constantan wires and one common iron wire led from the terminal strips to the stepping switch. These could be connected to the wires from the model in such a way that any eight stations could be monitored during

---

* This method was suggested by Mr. Paul Baloga of the wind tunnel staff, whose help with the development of the instrumentation is gratefully acknowledged.

** Once when the model was inadvertently grounded to the wind tunnel, the pulsing of the synchrotron magnets in the next building was picked up on the oscilloscope!

the cyclic measuring period or, if desired, fewer stations could be monitored with an increased frequency. All wiring up to levels 4 and 5 on the stepping switch was iron and constantan. A common cold junction was used for all thermocouples.

A 22 point, 5 level stepping switch was used, (see Figures 10 and 11) four levels being employed for the thermocouple signals and one (No. 3) for the triggering circuit for the oscilloscope. The stepping switch came equipped with a solenoid and ratchet to move the wipers, but the pulsing of the solenoid disturbed the oscilloscope trace. The solenoid was replaced by a small synchronous motor and a chain drive attached to an eccentric which moved the ratchet. This modification had the added advantage of allowing the cyclic measuring period to be changed simply by changing the gear ratio of the drive. The switch was wired so that a given thermocouple was sampled by the wipers with all other thermocouples disconnected and then, at the next point, the same thermocouple was sampled but with reverse polarity. The reversing was done by levels 4 and 5. This procedure kept the traces symmetrical about the horizontal centerline on the oscilloscope face. (See Figure 12(a).) It also decreased the reading error, since the total beam deflection represented twice the input, and eliminated any error caused by drift of the amplifier.

The thermocouple signal was fed from the stepping switch to a "Tektronix" type 122 low-level A. C. preamplifier which had a gain of 1000 times. The frequency response was adjustable, the low frequency cutoff being set at 0. 2 cycles and the high frequency cutoff at 1 kilocycle. From the preamplifier the signal went through the D. C. internal

amplifier of a "Tektronix" type 512 oscilloscope and was then displayed on a flat-face cathode ray tube. The traces were recorded by taking a picture of the tube with a Polaroid camera on type 46 film. The recording equipment, with the exception of the oscilloscope, was enclosed in a copper screen shield. The preamplifier, stepping switch, etc. were all insulated from the shield. The oscilloscope case was grounded.

A precision-resistance voltage divider was used to add to or subtract from the thermocouple output from the model just prior to making a run, so that the initial input to the oscilloscope was approximately zero. To provide for maximum utilization of the space available on the oscilloscope face, it was necessary to keep the initial deflection of the beam as small as possible.

The maximum sensitivity of the system was approximately 5 microvolts per centimeter of beam deflection on the oscilloscope face. The noise level of the measuring circuit with zero input was less than 5 microvolts, as shown in Figure 12(c). The contact noise level when the stepping switch was run with the input "shorted" is shown in Figure 12(d). Sensitivities of approximately 150 and 500 microvolts per centimeter were used when taking data, giving noise to signal ratios of less than 0.03.

By referring now to Figures 10 and 12(a), the sequence of events can be followed in detail: Just before the wipers reached the first point, the oscilloscope beam was waiting at the left-hand side of the trace. At point one the beam was triggered and began to move. Point two was a "short". At point three the first thermocouple was

sampled and the beam was deflected by an amount proportional to the thermocouple voltage. This D. C. voltage signal immediately began to decay because of the operating characteristics of the A. C. amplifier in the system. At point four the negative of the first thermocouple output was sampled. The beam returned by an amount equal to the original displacement (not back to zero because of the small displacement caused by the A. C. decay) and then kept going another equal amount in the same direction. The signal then again began to decay.* At point five the second thermocouple was sampled, and so on. Thus the total amount of the beam deflection corresponded to twice the input voltage. A "short" at point 11 provided easy identification of the traces, and three shorts at the end of the sequence allowed time for the beam to return to the left side, ready for the next trigger. Thus eight pieces of data were read in one second. Succeeding sweeps recorded the data for succeeding times, as shown in Figure 12(b). The time base was determined by timing several sweeps with a stop watch. The timing was estimated to be accurate to within 2 per cent.

This recording system has the following advantages: high sensitivity, versatility, low cost (about $100, not counting the oscilloscope which was already available, as opposed to several thousand dollars for multi-channel recorders), and the fact that the traces can be observed through a viewing hood while the run is being made. Of

---

* The preamplifier low frequency cutoff setting of 0.2 cycles gave the slowest decay rate and hence the nearest approach to a square wave trace on the oscilloscope. The high frequency cutoff setting of 1 kilocycle gave the sharpest wave peak for the sampling rate of 1 second per sweep.

course, the system works only if all the temperatures are either constantly increasing or constantly decreasing; otherwise, identification is impossible. The major disadvantage is the time necessary to reduce the data. It took about 35 minutes to read one picture (eight stations ten sweeps), plot the temperature-time curves, and determine the slope. The total time required for the data reduction of the heat transfer tests in these experiments was thus about eighty hours.

D. Test Conditions

All tests were conducted at a nominal Mach number of 5.8. The stagnation temperature was held constant at 250°F during the pressure distribution and equilibrium temperature measurements. For the transient heat transfer measurements the stagnation temperature ranged in value between 240-255°F. Once the temperature level was established it did not vary by more than 2 per cent during the interval 2 - 10 seconds after flow was started. The stagnation pressure was varied between 22 psig and 82 psig, corresponding to a range of free stream Reynolds numbers per inch of $0.79 - 2.03 \times 10^5$. The models were sting-mounted with the nose 22" from the throat and with the base about 3" ahead of the first strut support.

Nitrogen and helium gas were used as coolants. The mass of gas injected is expressed as the ratio of the mass flux out of the injection tube m_i divided by the free stream mass flux through a "capture" area equivalent to the cross-sectional area of the spherical model nose at $\theta = 90^\circ$, i.e., $\Gamma = m_i/\rho_\infty U_\infty \pi R^2$.

E. Pressure Distributions

The model was adjusted to zero angle of attack with respect to the free stream by differentially moving the sting support rods until the pressures read by the two orifices located at the same value of S/R were the same. This procedure was followed for each nose configuration for the no-injection case. These adjustments in angle of attack amounted to less than a $\frac{1}{2}^{o}$ change from the initial horizontal alignment of the model. Since numerous configurations and injection conditions had to be tried the model was not rotated about its axis to average out any cross-flow asymmetries. The pressures were read on vacuum-referenced manometers using silicone oil (for pressures less than about 6.5 cm. Hg.) or mercury. The estimated reading error was $\pm$ 0.5 per cent.

The stagnation pressure p_o was measured one inch upstream of the tunnel throat, and the quantity p_o'/p_o was determined from the measured pressure at the stagnation point (no injection). This quantity gave a free stream Mach number from which the free stream static pressure was computed. At the stagnation point,

$$C_{p_{max}} = \frac{p_o' - p_\infty}{\frac{1}{2} \rho_\infty U_\infty^2}$$

The pressure data is represented in the form $C_p/C_{p_{max}}$ vs. S/R, with the same value of $C_{p_{max}}$ being used to nondimensionalize the pressure readings measured with injection and with the spikes and caps.

F. Equilibrium Temperatures

The equilibrium temperatures for the various test configurations and conditions were read by measuring the output of the thermocouples in the heat transfer model while the tunnel was running in a steady-state condition. The temperatures were read on a Leeds and Northrup "Speed-O-Max" self-balancing potentiometer, and are estimated to be accurate within $\pm$ 1°F. The stagnation temperature T_o was measured by the thermocouple throat probe.

For these tests, and for the heat transfer tests, the model was aligned horizontally and was not moved thereafter.

The temperature of the coolant gas was measured in the plenum chamber $\frac{1}{2}$" upstream of the injection orifice. It is conservatively estimated that the gas may have increased in temperature at most 5°F because of heat being transferred from the tube to the gas as it traversed this short distance to the orifice.

G. Heat Transfer Test Procedure

The plant was started with valve Q (see Figure 7) in the "by-pass" position and valve B throttled, and the plant was allowed to reach some equilibrium temperature and pressure condition dependent upon the test section conditions desired. Before a test run the piping from valve Q to the throat was heated to approximately the stagnation temperature by varying the current to the nichrome heating wire with the aid of a "variac" voltage regulator, while the pipe temperature was monitored by means of several thermocouples soldered along its length. After about one hour of operation in by-pass, the test section was evacuated

by opening valve 3. When necessary, the coolant gas then was turned on. Next the voltage input to the oscilloscope was adjusted to approximately zero by using the precision voltage divider, and a picture of the "tare" sweep on the oscilloscope face was taken. Lastly, the recording oscillograph which monitored the stagnation temperature as measured by the throat probe was started.

The command to change valve Q to the "run" position was given when the beam was in the middle of a sweep. This point constituted time zero. At the start of the next sweep, the camera shutter was opened and left open for the remainder of the measuring period. When the transient measurement was concluded, normally in about 15 seconds, the air was directed back through the by-pass line. The model was allowed to cool down to some isothermal surface temperature condition (typically near room temperature), in about 10 - 15 minutes, and the sequence was then repeated.

H. Heat Transfer Data Reduction

The voltage-displacement relation for the oscilloscope was determined by "shorting" the eight inputs to the stepping switch and then sampling precise, known voltages which were applied to the circuit by means of the voltage divider. (This voltage source had been calibrated previously with a Leeds and Northrup K-2 potentiometer). The resulting oscilloscope traces were photographed. The polaroid type 46 film produced a transparency of the trace which was projected on the ground glass screen of an optical comparator. A magnification factor of 10 times was used, which corresponded to a net magnification of 4.1 times

compared to the true size of the trace on the oscilloscope. The lengths L (Figure 12(a)) were measured on the ground glass to within $\pm$ 1 mm., then divided by two to give the actual beam deflection corresponding to the input voltage. The resulting voltage-displacement curve was linear, and the slope was repeatable within 1 per cent over a period of months.

A sample iron-constantan thermocouple was made up and calibrated by suspending it in an oil bath of known temperature. The resulting temperature-voltage curve was linear within the temperature range used in the experiments. The slope of the curve differed by only 0.5 per cent from that predicted in the thermocouple tables.

By multiplying the calibration constants

(microvolts per cm.) x (^{o}F per microvolt)

a constant calibration factor was determined for each sensitivity setting of the oscilloscope.

The oscilloscope traces from the heat transfer runs were read by measuring the peak-to-peak lengths L on the optical comparator as described above. These lengths, when divided by two and multiplied by the appropriate constant, indicated the rise in temperature (^{o}F) above the initial wall temperature as a function of time. These data were then plotted, a curve faired through the points, and the slope measured by using a straight-edge with a prism attached to aid in determining the tangent. Sample curves for the no-injection condition are shown in Figure 13. For thermocouple 3, four thermocouples were each sampled twice during the cyclic measuring period; for thermocouple 14 eight thermocouples were each sampled once during the cyclic measuring period.

The initial wall temperature was determined by noting the cold junction temperature, the magnitude (and sign) of the voltage introduced by the voltage divider, and any differential temperature indicated by the "tare" trace.

The utilization of these temperature-time histories and the errors involved in the final determination of the heat transfer are discussed in Section IV. D. 1.

IV. RESULTS AND DISCUSSION

A. Schlieren Studies

Schlieren photographs of the flow over each model configuration were taken for each injection rate at a shutter speed of 1/25 of a second, using a steady BH-6 light source. The slit and knife edge were set horizontal for all of the exposures. Some of the more interesting pictures are included in Figures 14 through 29. All of the flow conditions described here appeared steady when viewed with the schlieren.

A photograph of the detached shock wave for the conventional no-injection case (Figure 14) is included for purposes of comparison. Figures 15 through 18 show the changes in the flow brought about by injection straight out of the stagnation point. The injection velocity in Figures 16 and 18 is estimated to be sonic at the exit of the injection tube. In Figure 15 the injection velocity is estimated at 400 feet per second; in Figure 17 it is about 2,000 feet per second. The shock wave bulges out around the point of injection in a manner similar to that observed when a thin blunt probe is extended a short distance in front of a hemispherical body[21]. Injection moves the centerline stagnation point somewhere upstream of the body, just as in the case of the short probe. The distorted shock wave has an inflection point as it approaches the body and then begins to assume its conventional shape. The inflection point and the shock wave continuing downstream from this point both lie closer to the body than the detached shock for the no-injection case because the air passing through the deformed shock is

not slowed down as much as through the usual detached shock. Thus the mass flux per unit area in the flow behind the shock is higher, and the shock lies closer to the body.

Figures 19 and 20, showing the flow field with a deflector cap installed and with injection, are representative of all of the deflector cap pictures both with and without injection. Here the shock shape is similar to that for injection straight out of the stagnation point, that is, the effect is that of a protruding short blunt probe. However, for the cap positioned closest to the nose (Cap A), the shock shape is altered only slightly.

Figures 21 through 24 show the effects of spikes on the flow around the model. Again, the schlieren pictures with and without injection are identical. The four spikes give rise to a conical separation region in front of the actual model, and the effective model shape changed from a blunt body to a conical body. The reasons for this flow separation are as follows: when a cylindrical spike is extended in front of a blunt body, the high pressure at the base of the spike is fed upstream through the subsonic portion of the boundary layer on the spike. The boundary layer cannot support this pressure gradient. It separates from the spike and forms a conical "dead air" region with a resulting conical shock wave. The separated region is conical because the cavity is a region of constant pressure, and a conical surface is a constant pressure surface in the three-dimensional case. The separation point moves forward along the spike until an equilibrium point is reached where the boundary layer can just support the pressure rise across the conical shock wave. Since it has been shown experimentally that a turbulent

boundary layer can support a larger pressure rise without separation than can a laminar layer, two regimes are possible. In one, the boundary layer on the spike is laminar and the separation point occurs near the tip; in the other the layer is turbulent, the separation point occurs somewhere downstream of the tip, and the conical shock is stronger.

The boundary layers on the spikes for this experiment are almost certainly laminar and thick.* For the 3/4" long spike and the 40° cone-spike the boundary layer appears to separate at the tip (Figures 21 and 24); for the other two spikes it appears to separate near the cone shoulder (Figures 22 and 23). This behavior is in agreement with results noted at lower Mach number for the laminar case[22, 23, 24, 25].** The basic mode of separation (i.e., separation near the spike tip, with no abrupt movement of the separation point) appears unchanged throughout a variation of free stream Reynolds number based on spherical nose diameter 1.11×10^5 to 2.84×10^5. This is in contrast to the results in Reference 10 at $M = 2.67$, when separation was observed far downstream of the cone shoulder for $L/D > 1.5$ at comparable values of free stream Reynolds number. Such a movement of the separation point indicates transitional or turbulent boundary layers on the spike, and the fact that this large movement is not observed here points up the increased stability of the laminar boundary layer at higher Mach numbers. For all four spikes the conical shock wave angle as measured from the photographs agrees

---

* Recent experiments in the Leg 1 tunnel by Mr. M. Matthews have shown laminar boundary layers of .10" thickness to exist 40 diameters back from the conical tip of a .083" diameter probe at a Reynolds number of 181,000 per inch.

** Mair[21] noted separation downstream of the probe shoulder for $L/D > 1.65$ with both a laminar and a turbulent probe boundary layer, but the separation phenomenon in the laminar case was unsteady.

with the angle predicted from tables for a flow deflection equal to the semi-vertex angle of the separated region. The agreement is within $\pm 1^{\circ}$ of angle, and the small scatter is caused by the slight uncertainty in determining the line defining the separated region. No change in the flow field for model HM + CA + S II could be distinguished from the pictures taken over a wide range of Reynolds numbers (see also Figure 38).

In all four cases, there is a second shock wave originating near the body, which indicates that the separated region is not tangent to the body and hence the flow still has to be turned. This shock wave moves around the nose of the body as the spike length is increased, until with the longest spike it was almost back to the sphere-cone tangency point. Also visible is the vortex line emanating from the intersection of this shock wave and the conical shock. (Figure 21)

Figures 25 through 29 show the flow about the yawed model (Figure 25 is a comparison photograph of the no-injection case.) Figures 26 and 27 show the changes in the flow when a large quantity of helium is injected out of the stagnation point along the axis of the model. At $\alpha = 4^{\circ}$ the detached shock wave has a hemispherical bulge similar in shape to that at zero angle of attack, while at $\alpha = 8^{\circ}$ the injection distorts the shock wave into somewhat of an ogive shape. At $\alpha = 8^{\circ}$ the shock wave shape around the lower surface appears to be almost independent of the injection. Thus it would seem doubtful that the injection had much of a blanketing effect over the lower surface at high angle of attack. No measurements were made with the model yawed.

Figures 28 and 29 show the effect of angle of attack on the spike-

induced separation. Around the lower surface the separated region and the resulting conical shock wave intersect the body close to the stagnation point so that the flow still has to be turned in almost the same manner as without the spike. Around the upper surface, the separated region envelopes the body and there is no shock wave emanating from the body. The separated region and the shock wave from the tip of the spike are both conical for a short distance downstream of the tip. Then, because of cross-flow caused by the high pressure on the lower surface, the separated region becomes concave in shape with a resulting change in the shock wave shape.

B. Pressure Distributions and Forebody Drag

1. Model with No Injection

The pressure distribution on the model with no injection (Figure 30) is used as a basis of comparison for the other conditions and configurations. For this case, the Reynolds number effect is small over a range of free stream Reynolds numbers from 0.79 - 2.03 x 10^5/inch, as was also demonstrated in Reference 14.

2. Injection Straight Out Stagnation Point

The pressure distributions on the model with varying nitrogen and helium injection are shown in Figures 30, 31, and 32. Here the gases were injected straight out of the orifice, i.e., injected opposite to the free stream direction.

The pressures show a severe disturbance of the flow field for the larger flow rates. A local pressure maximum appears at S/R = 0.2

with nitrogen injection at Re = 1.50×10^5 (Figure 30). In all cases steep pressure gradients are set up in the vicinity of the injection orifice. The local flow along the model is toward the orifice, and then this flow must be entrained in the jet, thus setting up a vortex flow pattern between the model and the distorted shock wave. The pressure distributions with this method of injection are similar to those noted in Reference 21, Figure 5, for very short spikes protruding in front of a hemisphere model. On the basis of these results, it was thought that injection out of the stagnation point would not be satisfactory as a heat transfer reduction device because of the very large disturbance introduced by the injection itself.* In order to minimize this disturbance, deflector caps were mounted over the end of the injection tube in an attempt to force the injected gas to flow in a direction parallel to the body surface.

3. Injection with Deflector Caps

The pressure distributions with the three different deflector caps mounted on the model are shown in Figure 33. As would be expected, the cap projecting farthest from the model produces the greatest change in the pressure distribution. The effect of nitrogen injection on the pressure distribution is slight, regardless of the spacing between the cap and the nose. A representative result for injection with Cap A installed is shown in Figure 34. The pressures measured by orifice No. 2 located behind the caps at S/R = 0.1 have been omitted in plotting.

---

* Later it was found that this mode of injection actually produced a more efficient "blanketing" of the body! (Section IV. C)

the data with caps and with injection, because they reflect the varying outlet pressure under the cap, and hence are not meaningful for this discussion.

The pressure peak in all of the pressure distributions occurred upstream of the location of the inflection point of the distorted shock wave. The same observation applies for the cases with injection straight out the nose.

Since none of the configurations with caps displayed any appreciable pressure effect with injection, cap A, which caused the least no-injection disturbance in the flow field, was chosen to be used on the heat transfer model.

4. Model with Spikes

The pressure distribution on the model was measured for the no-injection case with the four different spikes attached to each of the three caps in turn. The results were qualitatively the same for each cap. The pressures on the model with the spikes attached to cap A are shown in Figure 35. These results show a significant reduction in pressure over the spherical nose when the long spikes were attached. In particular, spike III reduces the pressure on the nose to 10 per cent of the value with no spike attached. The peaks in the pressure occur because there is a "zero" streamline defining the separated region, and its reattachment on the model results in a maximum pressure being measured at that point.

The cone angles of the separated regions were measured from the schlieren photographs and the corresponding cone surface pressures

determined from the Taylor-McCall theory. These pressures agree with the pressures measured on the nose inside the separated region to within $\pm$ 5 per cent, which is consistent with the accuracy of the separation angle measurement.

The pressure distribution with varying nitrogen injection was measured for each spike-cap combination. A representative result is shown in Figure 36. The change in the basic pressure distribution with increasing injection rate is small.

The Reynolds number effect on the model pressure distribution with the spikes was checked by testing cap A with three of the spikes over a range of p_o from 36.4 - 96.4 psia. The results are shown in Figures 37, 38, and 39. The Reynolds number effect on the pressure peaks is pronounced for spikes I and II, but not large for spike III. The reattachment in the case of spike II is thought to be laminar, from the results of a local heat transfer measurement on the conical afterbody.

The combination of cap A and spike II ($L = 1\frac{1}{2}$") was chosen to be used on the heat transfer model.

The pressure drag on a body of revolution is determined by integrating:

$$D_F = \int p \cos\psi \, dA = \int_o^{R_B} p \cdot 2\pi y \, dy$$

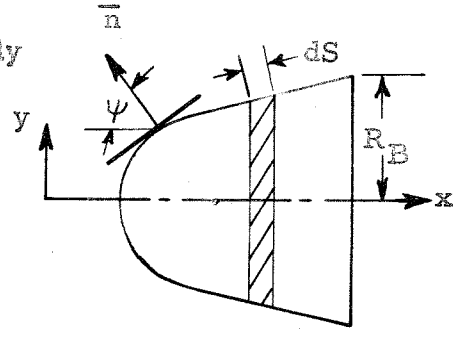

where

$dA = 2\pi y dS$

$dS \cos\psi = dy$

A foredrag coefficient referred to the base area may be formed as*

$$C_{D_F} = \frac{D_F}{(\frac{1}{2}\rho_\infty U_\infty^2)(\pi R_B^2)}$$

A foredrag coefficient thus can be determined from the measured pressure distributions.

The foredrag coefficient for the case of maximum helium or nitrogen injection straight out of the stagnation point was 15 per cent less than for the no-injection case, ignoring the drag penalty chargeable to the forward momentum of the injected gas.

The foredrag coefficients for the model alone and for the model with cap A and each of the three probe-spikes are shown in Figure 40. These are all for zero injection. Note that with the longest spike the drag was reduced by a factor of about three. This plot does not take into account the skin friction on the spike. Since the pressure in the separated region is constant, the same pressure should exist in front of and behind cap A, and no correction is made for the presence of the cap.**

---

* This definition of the coefficient neglects skin friction drag.

** The pressure drag on the cone tip is only 0.2 per cent of the drag with the longest spike attached; hence this incremental drag is disregarded.

C. Equilibrium Temperature Studies

1. Model with No Injection

Equilibrium temperature measurements on the model without caps or spikes for the no-injection condition are plotted for reference in Figure 46. None of these data are corrected for conduction or radiation effects, nor are the data with injection. The radiation loss from the model to the cooler wind tunnel walls is small; making a correction for it would raise the measured no-injection model temperatures less than $5^{\circ}F$, and the correction with injection would be less. However, on a model such as this there is considerable heat conduction through the skin, so that the measured temperature is lower than the adiabatic wall temperature near the front of the model and higher near the base. Although the net integrated heat transfer over the entire model surface should be zero (ignoring any heat loss to the sting), this internal conduction will have some effect on the history of the boundary layer growth.

2. Injection with Cap A

The equilibrium surface temperatures measured on the model when various rates of nitrogen and helium were injected using the deflector cap are plotted in Figures 41 and 42.* At station $S/R = 0$ are plotted the injection gas temperatures as measured in the plenum chamber. (See Figure 3.) The actual injection temperature as

---

* The temperature measured by the four thermocouples at $S/R = 0.61$ differed by at most $5^{\circ}F$ over the ranges of injection.

experienced by the model is rather difficult to define for this configuration. First, some heat is taken up by the coolant as it impinges on the hot cap prior to flowing into the boundary layer. Second, the temperatures at S/R = 0.1 for the largest helium rate indicate a lower temperature than the plenum chamber temperature. This fact is attributed to expansion of the coolant gas after it passes through the minimum section "throat" between the cap and the model. The injection temperature varied about 60°F over the range of injection rates because of varying amounts of heat picked up by the gas as it traversed the tubing between the wind tunnel wall and the base of the model. However, the variation in the ratio of the injection temperature to the tunnel stagnation temperature is about 10 per cent, while the injection mass flows varied by a factor of 10 for nitrogen and 6.4 for helium. Since the equilibrium model temperature would be expected to be dominated by the large changes in mass injected, and only weakly dependent upon the injection gas temperature variations, this small change in the injection temperature was not considered serious. In any event, the variation has been taken into account by non-dimensionalizing the data, and the results are shown in Figures 43 and 44.

The nondimensional parameter

$$\tau = \frac{T_{w_{r\neq 0}} - T_{inj}\left(\frac{T_{w_{r=0}}}{T_{l_{r=0}}}\right)}{T_{w_{r=0}} - T_{inj}\left(\frac{T_{w_{r=0}}}{T_{l_{r=0}}}\right)}$$

has been formed, where

$T_{w_{\Gamma \neq 0}}$ = measured wall temperature with injection

T_{inj} = injection gas temperature as measured in plenum chamber

$T_{w_{\Gamma = 0}}$ = measured wall temperature for no-injection condition

$T_{1_{\Gamma = 0}}$ = measured wall temperature at S/R = 0.1 for no-injection condition

The significance of this parameter can best be understood with the aid of a sketch:

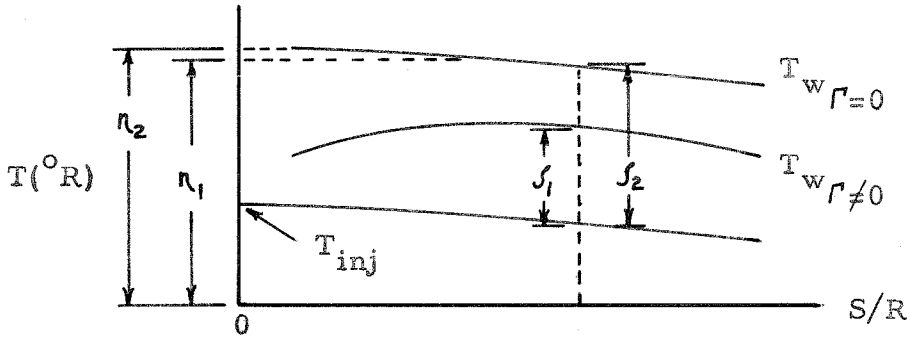

The injection temperature is plotted at S/R = 0 and is then computed for each S/R by multiplying it by the ratio η_1/η_2. The ratio ζ_1/ζ_2 is then formed, which is the temperature ratio parameter. If the injection process is of no value and the wall temperature with injection rises quickly to the no-injection value, the ratio approaches one. If the injection process is so effective that it keeps the model at an equilibrium temperature corresponding to a stagnation point temperature equal to the temperature of the injected gas, the ratio is zero. Thus the parameter ranges between zero and one, with the lower values indicating better cooling according to the criterion that the injected gas should keep the model equilibrium temperature equal to that expected for the corresponding "stagnation point" injection

temperature.

Before discussing these figures, it is well to get some feeling for the amounts of gas being injected. The volume flow of coolant corresponds to 0.053 - 0.53 standard cubic feet per minute of nitrogen, and 0.195 - 1.26 standard cubic feet per minute of helium. The mass flux in the boundary layer on the spherical nose with no injection was computed using References 26 and 27. The ratio of the mass injected at the stagnation point to the mass flux in the undisturbed boundary layer at $\theta = 80^{\circ}$ (tangency point) ranges between 3.6 per cent and 36 per cent for nitrogen and 1.9 per cent and 12 per cent for helium.

The temperature distributions in Figures 41 and 42 for injection with the cap are qualitatively similar to those which might be expected on the basis of theoretical treatments of injection (film cooling) into a flat plate boundary layer. Introduction of the coolant distorts the boundary layer profile and interposes a cool film near the surface. Because of mixing and heat conduction from the hot outer gas, this effect does not persist, and the surface temperature begins to rise. Then, unlike the flat plate, this rise is combined with the falling equilibrium temperature on the blunt body and the surface temperature decreases again.

Both gases show an increase in efficiency, as defined by the nondimensional temperature ratio τ defined above, with increasing injection rate, as is illustrated in Figures 43 and 44.

The degree of cooling effected by this injection process, and particularly the persistence of this cooling downstream, is surprisingly good, and would not be expected on the basis of some flat plate calcula-

tions[28]. A major difference between the two models is that in the flat plate case the gas is injected normal to the surface at a relatively low velocity, whereas here the gas is injected parallel to the surface at a very high velocity. Work is in progress at GALCIT on the theoretical aspects of this blunt body injection problem.

Figure 45 indicates the cooling efficiency of nitrogen and helium for the same mass injected. Helium is seen to be much the better coolant choice for this particular method of injection.

3. Injection straight out Stagnation Point

The equilibrium temperatures measured on the model when various rates of nitrogen and helium were injected straight out of the stagnation point are shown in Figures 46 and 47. The scatter in the four thermocouple readings at $S/R = 0.61$ caused by asymmetry was about $4^{\circ}F$. For all but the smallest injection rates for both gases, the injection velocity at the exit of the injection tube is estimated to be sonic velocity -- about 1200 feet per second for nitrogen and 3500 feet per second for helium.* This estimate is based on the fact that the pressure drop between the plenum chamber and the pressure as measured by the first pressure orifice is very large, indicating "choking" at the tube exit. Hence the injection flow is expanding supersonically into the relatively low pressure region surrounding the nose of the model. Figure 46 shows that, beyond a certain rate, increasing the nitrogen injection rate (and incidentally decreasing the injection temperature)

---

* The free stream velocity behind the undisturbed bow shock wave is 520 feet per second at this Mach number.

does not result in a decrease in model surface temperature. In contrast, the helium results in Figure 47 show a continued dependence of model surface temperature on injection rate.

For both gases, the model surface temperatures, once established near the injection region, decrease with increasing S/R at about the same rate as do the no-injection surface temperatures, in some cases falling below the measured plenum temperatures. This fact is illustrated in Figures 48 and 49 where the wall temperatures are nondimensionalized by the temperature measured at S/R = 0.1. The curves for all injection rates of both gases are superimposed upon the basic curve with no injection, whereas if the model temperatures with injection increased with increasing S/R the ratio would become greater than one and be in the neighborhood of the value listed in the box. This method of nondimensional plotting seemed more appropriate in bringing out this important point than plotting the data in the nondimensionalized ratio τ. One curve for helium plotted in terms of τ is shown for comparison in Figure 50.

For this method of injection, as in the previous case with the cap, the degree of cooling and the persistence of the cooling is unexpectedly good. The mechanism by which the cooling is brought about by this injection straight out of the stagnation point is complex, involving a mixing process which is difficult to analyze. However, some ideas are presented which may help to explain these two effects.

As regards the cooling effect, it would seem that the cool injected gas mixes with the hot free stream upon emerging from the tube and that this cool mixture of gases then flows along the body and

forms a protective blanket around it. In order to get some estimate of the relative masses involved in this mixing, a theoretical model has been assumed for the larger injection rates where the exit velocity is sonic. This model is admittedly over-simplified, and does not predict trends, but it does indicate the low-enthalpy blanketing effect described above. Consider a sonic jet emerging from the tube exit and over-expanding into the relatively low pressure region around the nose

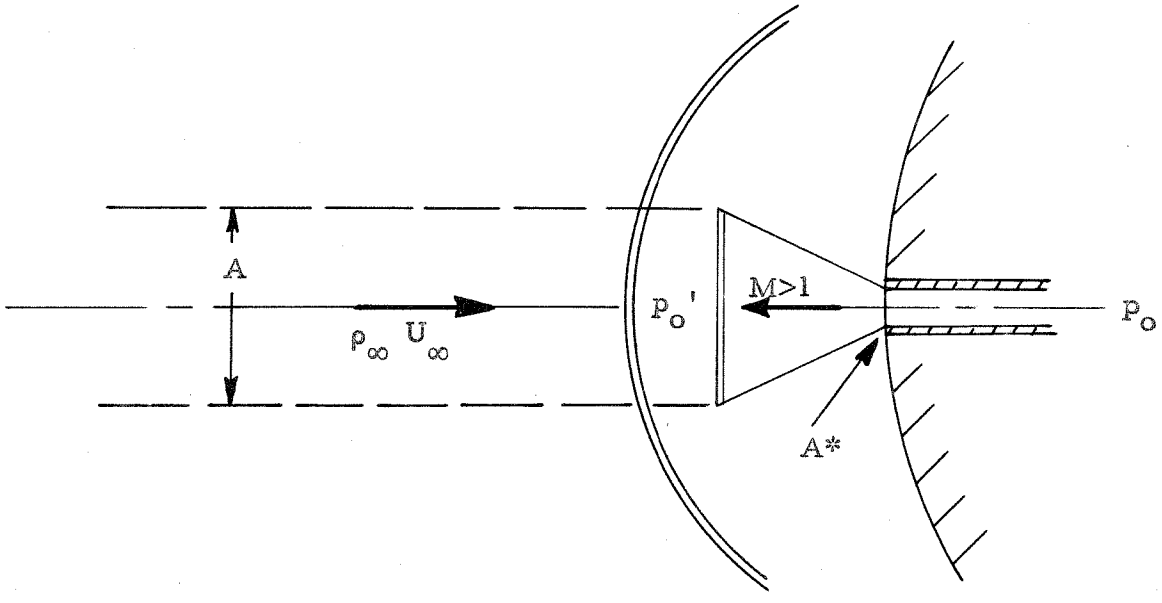

This jet is decelerated through a normal shock and brought to rest at a stagnation pressure equal to the stagnation pressure on the centerline behind the detached bow shock wave. Assuming the plenum pressure to be the reservoir pressure for this isentropic jet expansion prior to

the normal shock, the ratio p_o'/p_o is known and hence A/A^* may be determined. The free stream mass entering through this "capture area" is assumed to mix completely with the mass of cool injection gas. A mass balance of the stagnation enthalpies was carried out by this method for the injection conditions of the experiment. The resulting stagnation temperature of the mixture was 206^oF - 195^oF for the nitrogen rates and 175^oF - 160^oF for the helium rates. Thus the effective stagnation temperature which the body perceives is substantially lower than that with no injection. The defects of this model are apparent when these results are compared with the measurements. The predicted temperatures for the blanket are higher than the values measured on the model, and there is not enough temperature variation with changes in Γ.

Regarding the persistence of the cooling, the injected mass is greater than the mass that would be contained in the undisturbed boundary layer up to $\theta = 9^o$-30^o for the nitrogen and $\theta = 6^o$ - 17^o for the helium. The schlieren photographs (Figures 16 and 18) show that the inflection point in the distorted shock wave occurs at about $\theta = 40^o$. Within this "reattachment" region most of the free-stream air that would normally enter the undisturbed boundary layer has been mixed with the cool injected gas, and beyond this point the additional amount of hot free-stream air entrained in this cooling blanket is small. This may be seen from the following table:

θ	Mass Flux in Undisturbed Boundary Layer at Angle θ/Mass Flux in Undisturbed Boundary Layer at $\theta = 6^{\circ}$ (References 26 and 27)
11°	3.13
35°	21.5
50°	24.5
80°	55.7

Thus a cool "sub layer" is set up within the boundary layer and the model is immersed in a region of low enthalpy gas.

4. Injection with Cap A Plus Spike II

The measured temperatures and nondimensional temperatures for this case are shown in Figures 51 through 54. The fact that some of the points in Figure 53 lie above $\tau = 1$ is not considered to be significant, since the numerator and denominator in the τ ratio are nearly equal and hence the experimental error of $\pm 1^{\circ}F$ is reflected as a large change in τ.

The model surface temperatures with the spike in place and without injection are slightly lower than without the spike, as has been noted by other investigators.

The temperatures with injection show the same general trend as those with Cap A, because the spike is mounted on the front of the cap. However, the temperature peak occurs at a larger value of S/R with the spike in place.

D. Heat Transfer Studies

1. Local and Average Measurements; Accuracy

Measurements of local heat transfer rate with the model alone (Model HM) and with no injection yielded values of heat transfer which agreed with the values in Reference 15 within about 15 per cent. The magnitudes of the coefficients in the heat equation for the hemisphere (Equation A-3) used in the data reduction are

$$q_T = q_s + q_c$$

$$q_T = -6.04\times10^{-4}\frac{\partial T_w}{\partial t} + 3.94\times10^{-5}\left[\cot\theta\,\frac{\partial T_w}{\partial\theta} + \frac{\partial^2 T_w}{\partial\theta^2}\right] \qquad (1)$$

$BTU/in^2\,sec$

The degree of accuracy possible with this measurement was felt to be marginal, because the conduction term was 20 - 70 per cent of the total heat transferred at stations near the stagnation point and was repeatable only to 40 per cent because of the graphical double differentiation involved. For the larger injection rates the storage term became very small and the temperature gradients became very large. Thus, the accuracy and repeatability obtainable with this size of model by the transient technique precluded the determination of reliable <u>local</u> heat transfer values for the runs with injection. However, reliable <u>average</u> values of theheat rate over certain segments of the model surface can be obtained from the transient data. By assuming axial symmetry and integrating the basic equation for the hemisphere one obtains:

$$q_{AV} = \frac{-2\pi}{3}\rho_m c_m\left(R^3-R_{IN}^3\right)\int_{\theta_1}^{\theta_2}\frac{\partial T_w}{\partial t}\sin\theta\,d\theta + 2\pi k_m\left(R-R_{IN}\right)\left[\sin\theta\,\frac{\partial T_w}{\partial\theta}\right]_{\theta_1}^{\theta_2} \qquad (2)$$

or

$$q_{\theta AV} = -1.86 \times 10^{-3} \int_{\theta_1}^{\theta_2} \frac{\partial T_w}{\partial t} \sin\theta \, d\theta + 1.21 \times 10^{-4} \left[\sin\theta \frac{\partial T_w}{\partial \theta} \right]_{\theta_1}^{\theta_2} \frac{BTU}{sec} \quad (3)$$

Thus the second graphical differentiation is eliminated by the integration, and the magnitude of the storage term is increased compared to the conduction term because it is the sum of the heat transferred over an area.

The above equation was used to reduce the data over three segments of model surface: $\theta = 0 - 30^{\circ}$; $\theta = 0 - 60^{\circ}$; and $\theta = 0 - 80^{\circ}$. Not all of the thermocouples on the model could be read in a single run, but overlapping readings were taken in each sequence of runs. In general, a set of three "blow-down" runs was necessary to get all of the data for one test condition. The slopes of the temperature histories in the first run of the set were read at 4 seconds, with a repeatability in the slope reading of any curve of $\pm$ 2 per cent, and the slopes of the repeated readings in the other two runs were taken at a point in time so that they matched the value in the first run. This procedure meant a shift in the absolute time scale of up to $\pm \frac{1}{2}$ second to account for uncertainties in the absolute time zero location. The wall temperatures were estimated to be accurate within $\pm \frac{1}{2}$ F, which corresponds to an error of about $\pm$ 5 per cent in the absolute accuracy of the conduction term. The measurement of any $\partial T/\partial\theta$ was repeatable within $\pm$ 4 per cent. The results of four runs for the no-injection case, two with model HM and two with model HM + CA were averaged and compared with theory and the experimental results reported in Reference 15 to establish the validity of the present heat transfer method. The results

were as follows:

Segment θ =	q_{av} (BTU/sec.) No Injection			q_c/q_{av} (per cent)	Maximum Difference q_{av}; 4 runs (per cent)
	Present Experiment	Theory (References 12 and 29)	Previous Experiment* (Reference 15)		
$0 - 30^\circ$	3.25	3.64	3.89	43	14
$0 - 60^\circ$	9.26	9.25	9.63	34	11
$0 - 80^\circ$	10.5	10.9	11.7	10	17

A considerable portion of the difference between runs noted in the last column above can be attributed to the fact that the stagnation temperature and the model temperature were not identical for each run. The stagnation temperature established at 4 seconds varied about 8 per cent from one run to the next, and the initial wall temperature varied about 10 per cent. The data are plotted as they were obtained, and are not corrected for this variation in test conditions. In view of these test conditions, agreement with theory and previous experiment (about $\pm$ 10 per cent) is thought to be satisfactory, and encouraging enough to warrant employing the same technique for determining the effect of mass injection.

2. Injection Results with and without Cap

The average heat transfer over the three segments for the configurations Model HM and Model HM + CA is plotted in Figures 55, 56, and 57 as a function of the injection parameter. The repeatability is thought to be sufficient to illustrate the large effects under investigation.

---

* q_{av} obtained by integrating local values of q determined from given experimental values of Nusselt number.

As expected, the no-injection results with and without the cap are the same within the accuracy of the experiment and the results obtained with injection are nondimensionalized by the arithmetical average of four no-injection runs (two with cap A and two without).

For all of the transient runs the inlet tubing to the model was at approximately room temperature, so that the injection gas temperature also was at about room temperature and remained constant during the transient measuring period.

Referring to Figure 55, the negative values of the ordinate mean that for this segment, at the larger helium flow rates, heat is given up by the model to the air, i. e., the storage term was extremely small and the conduction term showed more heat entering the segment by conduction than could be accounted for by the storage term increase. Heat flows into the segment $0 \leq \theta \leq 30^{\circ}$ from further aft where the heat transfer rate is higher and thence out into the coolant surrounding the skin. Thus the interpretation of these negative values is simply that the heat transfer rate from the boundary layer is extremely small.

The results for all three model segments show a marked advantage in using helium rather than nitrogen as a coolant. The one exception is helium injection with Model HM + CA for the segment $\theta = 0 - 80^{\circ}$. Between $60^{\circ} \leq \theta \leq 80^{\circ}$ the heat transfer rate exceeds the value for no injection, so that the over-all average is above the no injection value. No explanation can be given for this effect, though it is unlikely that it is caused by laminar-turbulent transition, since the equilibrium temperatures do not indicate any increase in this neighborhood.

According to Figure 55, the average heat transfer rate over the

segment $0 \leq \theta \leq 30^{\circ}$ is reduced practically to zero by injecting a mass flow of helium as small as $\frac{1}{2}$ per cent of the mass flow of air intercepted by the body cross-sectional area πR^2, with or without the deflector cap. For the entire segment $0 \leq \theta \leq 80^{\circ}$ the average heat transfer rate is reduced appreciably only when helium is injected directly out of the forward stagnation point, i.e., without the deflector cap.

The results are not quoted in terms of a heat transfer coefficient. However, a feeling for the magnitude of the coefficient is obtained by finding an approximate equilibrium temperature from the nondimensional temperature ratio τ with T_{inj} of about room temperature. Then using $q \doteq h(T_{equil} - T_w)$ it is found that the primary reason for the reduction in the heat transfer rate is the reduction in the equilibrium temperature, and that the heat transfer coefficient in most cases increases with injection. With nitrogen, the heat rate remains about the same and the equilibrium wall temperatures decrease, so that the net effect upon h is an increase of about 50 per cent over the no-injection value. With helium, the heat rate decreases, but not as fast as the equilibrium temperature, and the net effect upon h is an increase of about 70 per cent over the region $\theta = 0 - 80^{\circ}$ and of about a factor of 5 in the segment $\theta = 0 - 30^{\circ}$. This increase is probably due to jet action. With the cap on, a very large tangential velocity is introduced at the surface, and $\partial u/\partial n$ increases. With straight injection, the air near the wall in the region $\theta = 0 - 30^{\circ}$ is entrained in the jet.

Although no nondimensional parameter could be found from this experiment to correlate the different effects of nitrogen and helium, two factors must play an essential role: (1) the larger specific heat of

helium, about 5 times that of nitrogen, and (2) the higher velocity of injection of helium compared with nitrogen, for the same mass flow.

3. Injection Results with Spike II

The average heat transfer measured with Spike II in position was lower than with no spike, even with no injection. Specifically:

Model Segment	$\frac{q_{av}\ (\text{spike})}{q_{av}\ (\text{no spike})}$	q_c/q_s
$\theta = 0 - 30^\circ$	-0.163 (heat leaving model)	100
$\theta = 0 - 60^\circ$	0.767	40
$\theta = 0 - 80^\circ$	1.027	30

The result for the first segment ($0 - 30^\circ$) is probably not reliable quantitatively, since both the conduction and storage terms were very small. But in no case were the average heat rates appreciably higher than without the spike. This would seem to be correct physically, since the pressure decrease caused by the spike would lower the heat transfer coefficient by about 1/3, and near the nose the coefficient in the separated region is about one-half that for a laminar boundary layer[30]. This result is in disagreement with the data obtained in Reference 10 wherein the average heat transfer rate with a spike mounted on a blunt body was reported to be approximately double that for the laminar boundary layer on the body alone. In this case almost the entire increase occurred over the forward half of the surface area of the hemisphere. These data were obtained at $M = 2.67$, and at comparable

free stream Reynolds numbers and values of L/D; the results were in fact independent of spike length. The key to the situation may lie in the remark made by Chapman[30] to the effect that the separated flow induced by the spikes in the experiment of Reference 10 was apparently of the "transitional" type, i. e., with transition occurring between separation and reattachment, whereas the comparison was made with the attached flow of a completely laminar boundary layer.

In the present experiment the separated flow for the spike of L/D = 1.07 was almost certainly of the "pure laminar" type, i. e., no transition before reattachment. This statement is based on the fact that a local measurement of heat transfer was made on the cone skirt at thermocouple No. 14 for the case of model alone, no injection, and for model HM + CA, no injection.* This local value changed only 3 per cent for the two cases, which is within the experimental accuracy, and the average heat transfer results up to the shoulder agree with the laminar theory, for model HM.

It would appear, then, that the heat rates to the forward part of the model with a spike attached are very much dependent upon the type of separation involved.

The results with model HM + CA + S II and with injection are shown in Figures 58 and 59, nondimensionalized by the no-injection heat rate values for the same model. The accuracy was not as good here as in the previous cases, because the storage term remained relatively small while the conduction term got very large, so that only a qualitative

---

* On the cone skirt the temperature gradients are flat, and the value of q_c/q_s was only 0.05.

discussion should be made. The direction of heat transfer over the $0 - 30^{\circ}$ segment was from the model to the coolant in all cases, and hence is not plotted. The results for the other segments do not show the large decrease in heat transfer predicted in Reference 30, but the mechanism is probably not the same. In the theory the mass is injected into the front of the recirculation region; in the present experiment the mass is injected against cap A and thence along the model surface at the rear of the recirculation region.

V. CONCLUSIONS AND RECOMMENDATIONS

The most important results of the various studies are:

(1) The schlieren studies show that flow separation devices (spikes) result in separation at or near the spike tip over a range of Reynolds numbers based on spherical nose radius from $1.11 - 2.84 \times 10^5$ and values of L/D up to 1.78 at a Mach number of 5.8. This value of L/D for laminar separation is greater than that achieved at a Lower Mach number and comparable Reynolds number, thus demonstrating the increased stability of the Laminar boundary layer at a higher Mach number.

(2) The separation caused by the spike with L/D = 1.78 results in a foredrag coefficient of one-third the value with no spike attached.

(3) The injection of cool nitrogen or helium gas at the stagnation point furnishes a powerful method of reducing the equilibrium wall temperature. The downstream persistence of this cooling effect is surprisingly good. Injection straight out of the stagnation point seems to blanket the whole body with a low enthalpy gas, and the equilibrium surface temperatures are substantially reduced over the whole model surface. Injection of the coolant gas tangential to the surface results in equilibrium surface temperature distributions qualitatively like those expected for injection into a boundary layer, but the boundary layer profile is severely distorted by the high tangential injection velocity and the cooling effect persists further downstream than would be anticipated from flat plate injection theory.

(4) With either method of injection, for the same mass flow, helium is a better choice of coolant than nitrogen.

(5) The average heat transfer over a segment near the nose of the body is decreased almost to zero by injecting a mass of helium as small as $\frac{1}{2}$ per cent of the mass flow of free-stream air intercepted by the spherical cross-sectional area πR^2.

(6) The primary reason for the reduction in the heat transfer rate would seem to be the reduction in the equilibrium wall temperature. Both methods of injection (straight out the stagnation point and tangential to the body surface) tend to increase the value of the heat transfer coefficient.

The results of this experiment indicate that it would be valuable to do the following:

(i) Repeat the experiment at much higher values of T_o.

(ii) Obtain <u>local</u> values of heat transfer with injection, particularly at angle of attack.

(iii) Measure surface shear with injection.

(iv) Determine the role played in the cooling process by the different gas properties.

(v) Determine velocity, temperature, and concentration profiles near the model surface with different methods of injection.

(vi) Determine local values of heat transfer with spikes and the change in this heat transfer with transition prior to reattachment of the separated region.

REFERENCES

1. Allen, H. J.; Eggers, A. J., Jr.: A Study of the Motion and Aerodynamic Heating of Missiles Entering the Earth's Atmosphere at High Supersonic Speeds. NACA TN 4047, October, 1957.

2. Masson, D. J.; Gazley, C., Jr.: Surface-Protection and Cooling Systems for High Speed Flight. Rand Report RM-1735, March, 1956. (Also, IAS Preprint 638)

3. Broadwell, J. E.; Sherman, P.: Survey of Porous-Wall Heat Transfer Literature. WADC Contract AF 18 (600)-51, Engineering Institute, University of Michigan, 1951.

4. Eckert, E. R. G.; Schneider, P. J.; Kechler, F.: Mass Transfer Cooling of a Laminar Air Boundary Layer by Injection of a Light-Weight Gas. Univ. of Minnesota, TR 8, April, 1956.

5. Klunker, E. B.; Ivery, Reese H.: An Analysis of Supersonic Aerodynamic Heating with Continuous Fluid Injection. NACA TN 1987, December, 1949. (Also, NACA TR 990)

6. Eckert, E. R. G.; Livingood, John N. B.: Comparison of Effectiveness of Convection-, Transpiration-, and Film-Cooling Methods with Air as Coolant. NACA TN 3010, October, 1953.

7. Mickley, H. S.; Ross, R. C.; Squyers, A. L.; Stewart, W. S.: Heat, Mass, and Momentum Transfer for Flow over a Flat Plate with Blowing or Suction. NACA TN 3208, July, 1954.

8. Leadon, B. M.; Scott, C. J.: Measurement of Recovery Factors and Heat Transfer Coefficients with Transpiration Cooling in a Turbulent Boundary Layer at M = 3 Using Air and Helium as Coolants. Univ. of Minnesota, Research Report 126, February, 1956.

9. Leadon, B. M.; Scott, C. J.; Anderson, G. E.: Mass Transfer Cooling of a 20 Degree Porous Cone at M = 5. Univ. of Minnesota Research Report 143, July, 1957.

10. Stalder, J. R.; Nielson, H. V.: Heat Transfer from a Hemisphere-Cylinder Equipped with Flow-Separation Spikes. NACA TN 3287, September, 1954.

11. DeLauer, R. D.; Nagamatsu, H. T.: Experimental Heat Transfer at Hypersonic Mach Number. GALCIT Hypersonic Wind Tunnel Memorandum No. 14, April, 1953.

12. Hartwig, F. W.: Development and Application of a Technique for Steady State Aerodynamic Heat Transfer Measurements. GALCIT Hypersonic Wind Tunnel Memorandum No. 37, June, 1957.

13. Richards, H. K.: An Experimental Investigation of Heat Transfer Rates on a Blunt Body in Hypersonic Flow. California Institute of Technology, Aeronautical Engineer Thesis, June, 1957.

14. Machell, R. M.; O'Bryant, W. T.: An Experimental Investigation of the Flow over Blunt-Nosed Cones at a Mach Number of 5.8. GALCIT Hypersonic Research Project, Memorandum No. 32, June, 1956.

15. Crawford, D. H.; McCauley, W. D.: Investigation of the Laminar Aerodynamic Heat-Transfer Characteristics of a Hemisphere-Cylinder in the Langley 11-Inch Hypersonic Tunnel at a Mach Number of 6.8. NACA TN 3706, July, 1956.

16. Carslaw, H. S.; Jaeger, J. C.: Conduction of Heat in Solids. Oxford University Press, 1950.

17. Boelter, L. M. K.; Lockhard, R. W.: An Investigation of Aircraft Heaters XXXV -- Thermocouple Conduction Error Observed in Measuring Surface Temperatures. NACA TN 2427, July, 1951.

18. Eimer, M.; Nagamatsu, H. T.: Direct Measurement of Laminar Skin Friction at Hypersonic Speeds. GALCIT Hypersonic Wind Tunnel Memorandum No. 16, July, 1953.

19. Baloga, P. E.; Nagamatsu, H. T.: Instrumentation of GALCIT Hypersonic Wind Tunnels. GALCIT Hypersonic Wind Tunnel Memorandum No. 29, July, 1955.

20. Stickney, T. M.: Recovery and Time-Response Characteristics of Six Thermocouple Probes in Subsonic and Supersonic Flow. NACA TN 3455, July, 1955.

21. Jackson, P. H., Jr.: Effect of a Probe on the Drag and Pressure Distribution of a Hemispherical Nose. CONVAIR, Pomona, CVAC/CF-2140, June, 1954.

22. Mair, W. A.: Experiments on Separation of Boundary Layers on Probes in Front of Blunt Nosed Bodies in a Supersonic Air Stream. Philosophical Magazine, Vol. 43, No. 342, p. 695, July, 1952.

23. Moeckel, W. E.: Flow Separation Ahead of a Blunt Axially Symmetric Body at Mach Numbers 1.76 to 2.10. NACA RM E51I25, December, 1951.

24. Jones, J. J.: Flow Separation from Rods Ahead of Blunt Noses at Mach Number 2.72. NACA RM L52E05a, July, 1952.

25. Beastall, D.; Turner, J.: The Effect of a Spike Protruding in Front of a Bluff Body at Supersonic Speeds. (British) R.and M. 3007, January, 1952.

26. Lees, L.: Recent Developments in Hypersonic Flow. Jet Propulsion, Vol. 27, No. 11, p. 1162, November, 1957.

27. Smith, A. M. O.: Improved Solutions of the Falkner and Skan Boundary Layer Equation. S. M. F. Fund Paper No. FF-10, March, 1954.

28. Rubesin, M. W.; Inouye, Mamoru: A Theoretical Study of the Effect of Upstream Transpiration Cooling on the Heat-Transfer and Skin-Friction Characteristics of a Compressible, Laminar Boundary Layer. NACA TN 3969, May, 1957.

29. Lees, L.: Laminar Heat Transfer over Blunt-Nosed Bodies at Hypersonic Flight Speeds. Jet Propulsion, Vol. 26, No. 4, pp. 259-269, April, 1956.

30. Chapman, D. R.: A Theoretical Analysis of Heat Transfer in Regions of Separated Flow. NACA TN 3792, October, 1956.

31. Rabinowicz, J.; Jessey, M. E.; Bartsch, C. A.: Resistance Thermometer for Heat Transfer Measurement in a Shock Tube. GALCIT Hypersonic Research Project, Memorandum No. 33, July, 1956.

32. Cooper, M.; Mayo, E. E.: Normal Conduction Effects on Heat Transfer Data During Transient Heating of Thin-Skin Models. Readers' Forum, Journal of the Aeronautical Sciences, Vol. 24, No. 6, p. 461.

33. Churchill, R. V.: Modern Operational Mathematics in Engineering. McGraw-Hill, New York, 1944.

34. Korkegi, R. H.: Transition Studies and Skin Friction Measurements on an Insulated Flat Plate at a Hypersonic Mach Number. GALCIT Hypersonic Wind Tunnel Memorandum No. 17, June, 1954.

APPENDIX A

THE MEASUREMENT OF HEAT TRANSFER BY THE TRANSIENT TECHNIQUE

The transient technique as applied in wind tunnel testing (see Reference 31 for a discussion of the transient technique as applied in the shock tube) consists of measuring the local heat transfer rate indirectly by measuring the time rate of change of temperature at selected points on a body when the body is suddenly exposed to a heated air flow. The local heat transfer rate is then determined by balancing the rate at which heat enters a unit volume of the skin with the rate at which it is stored and leaves the volume. The general heat conduction equation in a homogeneous material is given by

$$\frac{\partial T_w}{\partial t} = \frac{k_m}{\rho_m c_m} \nabla^2 T_w \qquad \text{(A-1)}$$

In spherical coordinates this equation becomes

$$\frac{\partial T_w}{\partial t} = \frac{k_m}{\rho_m c_m}\left[\frac{1}{r^2}\frac{\partial}{\partial r}\left(r^2\frac{\partial T_w}{\partial r}\right) + \frac{1}{r^2\sin\theta}\frac{\partial}{\partial\theta}\left(\sin\theta\frac{\partial T_w}{\partial\theta}\right) + \frac{1}{r^2\sin^2\theta}\frac{\partial^2 T_w}{\partial\phi^2}\right] \qquad \text{(A-2)}$$

This equation could be simplified if the model could be made in the form of a shell which is thin compared to the other dimensions, and if the heat loss from the inside surface of the shell could be considered to be negligible. Then it would be safe to assume that the first and second derivatives of T with respect to θ and ϕ, as well as the quantity $\partial T/\partial t$, would all be independent of the radius and that $\partial T/\partial r = 0$ at the

inner surface of the shell. Thus by assuming $\partial^2 T / \partial \phi^2 = 0$, integrating equation A-2 once with respect to r, and using the boundary conditions $\partial T/\partial r = 0$ at the inner surface of the shell where $r = R_{in}$ and $q_T = - k_m (\partial T/\partial r)_{r=R}$, where q_T is the total heat transferred from the boundary layer, one would obtain

$$\frac{q_T}{k_m} = -\left(\frac{\partial T_w}{\partial r}\right)_{r=R} = -\left(\frac{R^3 - R_{IN}^3}{3R^2}\right)\frac{\rho_m c_m}{k_m}\frac{\partial T_w}{\partial t} + \left(\frac{R - R_{IN}}{R^2 \sin\theta}\right)\frac{\partial}{\partial \theta}\left(\sin\theta \frac{\partial T_w}{\partial \theta}\right) \quad \text{(A-3)}$$

Now, what restrictions do these assumptions impose upon the model construction? If the skin were thin enough, the independence of the above-named derivatives with respect to the radius would be assured even if the skin were a poor thermal conductor; it would certainly be true if the skin were thin and made of metal. The assumption of zero heat leakage from the inside surface requires more careful examination. For structural reasons, it might be desirable to back up the thin skin with a layer of reinforcing material. The magnitude of the heat leakage to the reinforcing material must be estimated. An approximate method for making this estimate is given in Reference 32 for the case of variable heat input. An exact solution of the heat conduction equation for the case of a constant heat input to a slab is given here.

Consider the following one-dimensional heat transfer problem. Given a thin metal skin mounted on a low-conductivity backing material, with a constant heat input step function at the surface of the skin at time zero. If the skin is thin and a good conductor compared to the backing, the latter may be considered to be semi-infinite. The question arises as to how much heat leaks out of the metal skin through the

interface in some given time interval, as measured by the ratio Q/q (see sketch).

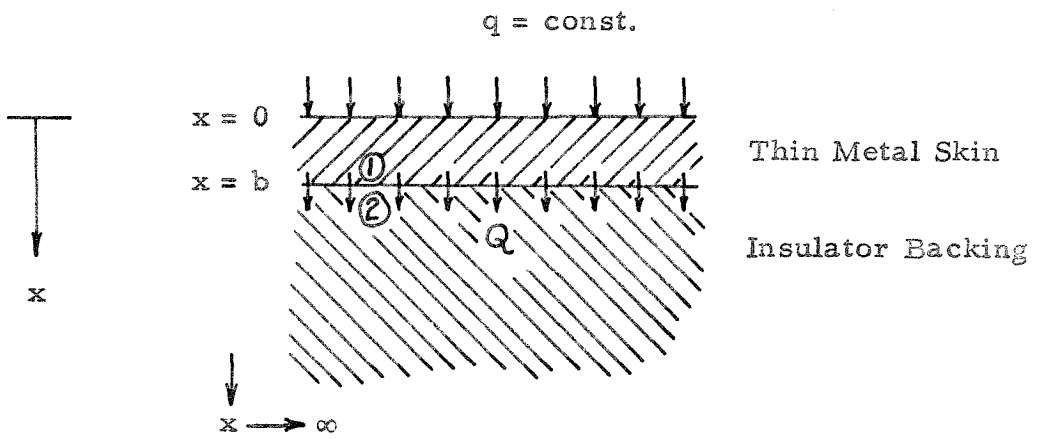

Equations:

$$\frac{\partial T_1(x,t)}{\partial t} = \kappa_1 \frac{\partial^2 T_1}{\partial x^2} \qquad 0 < x < b$$

$$\frac{\partial T_2(x,t)}{\partial t} = \kappa_2 \frac{\partial^2 T_2}{\partial x^2} \qquad b < x < \infty \qquad \text{(A-4)}$$

Initial Conditions:

$$T_1(x,0) = 0$$

$$T_2(x,0) = 0 \qquad \text{(A-5)}$$

Boundary Conditions:

$$k_1 \frac{\partial T_1(0,t)}{\partial x} = -q$$

$$k_1 \frac{\partial T_1(b,t)}{\partial x} = k_2 \frac{\partial T_2(b,t)}{\partial x} \qquad \text{(A-6)}$$

$$T_1(b,t) = T_2(b,t)$$

$$T_2(x,t) \longrightarrow 0 \quad \text{as} \quad x \longrightarrow \infty$$

By applying the Laplace transform to equations A-4 with zero initial conditions, and applying the transformed boundary conditions, the solution of the transformed equation is:

$$\tilde{T}_1(x,s) = \frac{q}{k_1 s\sqrt{\frac{s}{\kappa_1}}}\left[\frac{e^{-\sqrt{\frac{s}{\kappa_1}}x}}{1+\beta e^{-2\sqrt{\frac{s}{\kappa_1}}b}} - \frac{\beta e^{-\sqrt{\frac{s}{\kappa_1}}(2b-x)}}{1+\beta e^{-2\sqrt{\frac{s}{\kappa_1}}b}}\right] \quad 0<x<b \qquad (A-7)$$

where

$$\tilde{T}(x,s) = \mathcal{L}\{T(x,t)\} \equiv \int_0^\infty T(x,t)e^{-st}dt$$

$$\beta = \frac{1-\lambda}{1+\lambda} \qquad \lambda = \frac{k_1\sqrt{\frac{s}{\kappa_1}}}{k_2\sqrt{\frac{s}{\kappa_2}}} = \sqrt{\frac{k_1\rho_1 c_1}{k_2\rho_2 c_2}}$$

Hence

$$\frac{\partial\tilde{T}_1(x,s)}{\partial x} = \frac{q}{k_1 s}\left[-\frac{e^{-\sqrt{\frac{s}{\kappa_1}}x}}{1+\beta e^{-2\sqrt{\frac{s}{\kappa_1}}b}} - \frac{\beta e^{-\sqrt{\frac{s}{\kappa_1}}(2b-x)}}{1+\beta e^{-2\sqrt{\frac{s}{\kappa_1}}b}}\right] \qquad (A-8)$$

$$\frac{\partial\tilde{T}_1(x,s)}{\partial x} = \frac{q}{k_1}\left[\sum_{n=1}^{\infty}\frac{(-1)^n\beta^n e^{-\frac{(2nb-x)\sqrt{s}}{\sqrt{\kappa_1}}}}{s} - \sum_{n=0}^{\infty}\frac{(-1)^n\beta^n e^{-\frac{(x+2nb)\sqrt{s}}{\sqrt{\kappa_1}}}}{s}\right] \qquad (A-9)$$

Then inverting, evaluating the expression at x = b, and using the definition that $Q = k_1\frac{\partial T_1(b,t)}{\partial x}$:

$$Q = -\frac{2q}{1+\lambda}\sum_{n=0}^{\infty}\left(\frac{\lambda-1}{\lambda+1}\right)^n \operatorname{erfc}\left[\frac{b(2n+1)}{2\sqrt{\kappa_1 t}}\right]$$

Hence

$$\left|\frac{Q}{q}\right| = \frac{2}{1+\lambda}\sum_{n=0}^{\infty}\left(\frac{\lambda-1}{\lambda+1}\right)^n \operatorname{erfc}\left[\frac{b(2n+1)}{2\sqrt{\kappa_1 t}}\right] \qquad \text{(A-10)}$$

where $$\lambda = \sqrt{\frac{k_1\rho_1 c_1}{k_2\rho_2 c_2}}$$

For completeness, equation A-7 may also be inverted to obtain the expression for the temperature distribution in the metal skin. The result is

$$T_1(x,t) = \frac{q\sqrt{\kappa_1}}{k_1}\left\{\sum_{n=0}^{\infty}(-1)^n\beta^n\left[2\sqrt{\frac{t}{\pi}}\,e^{-\frac{(x+2nb)^2}{4\kappa_1 t}} - \frac{(x+2nb)}{\sqrt{\kappa_1}}\operatorname{erfc}\left(\frac{x+2nb}{2\sqrt{\kappa_1 t}}\right)\right] + \right. \qquad \text{(A-11)}$$

$$\left.\sum_{n=1}^{\infty}(-1)^n\beta^n\left[2\sqrt{\frac{t}{\pi}}\,e^{-\frac{(2nb-x)^2}{4\kappa_1 t}} - \frac{(2nb-x)}{\sqrt{\kappa_1}}\operatorname{erfc}\left(\frac{2nb-x}{2\sqrt{\kappa_1 t}}\right)\right]\right\}$$

where

$$\kappa_1 = \frac{k_1}{\rho_1 c_1} \qquad \lambda = \sqrt{\frac{k_1\rho_1 c_1}{k_2\rho_2 c_2}} \qquad \beta = \frac{1-\lambda}{1+\lambda}$$

Equation A-10 is evaluated for two cases: steel of thickness .030" with a laminated plastic backing, and steel of thickness .030" with a balsa wood backing. At the end of five seconds, $Q/q = 0.35$, (to 5 terms), that is, 35 per cent of the heat that has entered the skin surface has leaked through into the plastic reinforcing material. The value of Q/q for balsa wood backing is 7.6 per cent. Thus the heat leakage effect is appreciable even for these materials. The effect must either be made negligible or be accounted for in the heat balance.

For a small wind tunnel model, where there are no particular structural problems, the simplest thing to do is to make the model a thin hollow shell. With air as material (2) the heat leakage is 0.40 per cent after five seconds, and the assumption $\partial T/\partial r = 0$ at the inner surface which was used in simplifying equation A-2 to A-3 is a good one.

Some further conclusions regarding the model design are apparent from examination of Equation A-3. The first term on the right is the local net heat storage, while the second term represents the local net heat conduction along the model shell. (Corrections should be made for radiation if necessary. No radiation correction was made in the heat transfer data of this experiment, since the model and the wind tunnel walls were both initially near room temperature and the radiation effect during the first few seconds was judged to be small.) The value of $\partial T/\partial t$ for a particular point on the model is determined by measuring the temperature rise at that point as a function of time (after the hot air flow has started) and finding the slope of the resulting curve for some particular time. For this same instant of time, the model temperatures are plotted versus θ and $\partial/\partial\theta$ $\left(\sin\theta \frac{\partial T}{\partial \theta}\right)$ is found by taking slopes of the faired curves. The double graphical differentiation is difficult to do with accuracy, so it is desirable to keep the coefficient in the second term small, that is, make the model shell of low conductivity material and use as large a sphere radius as possible. Of course the shell dimensions should be accurately known and, for simplicity, the thickness should be constant. The decision as to the most desirable shell thickness is not as clear-cut. (See also Reference 15.) For a fixed material and sphere radius, the thinner the shell the

smaller is the ratio of the conduction correction to the storage term. But there is a time constant which also must be kept in mind. The magnitude of the storage term is approaching zero as time progresses, while the magnitude of the conduction term is approaching some maximum with time. Thus if the model shell is extremely thin, the conduction term will be some satisfactorily small percentage of the storage term only for times that may be so small as to prohibit recording the data with the available instrumentation. If the model shell is very thick, the instrumentation time scale is expanded but now the correction term is large for all times. Therefore there must be an optimum skin thickness for a given material, sphere radius, and instrument response time.

The whole problem of the conduction correction can be avoided in certain cases. Usually the initial wall temperature before the air flow starts is constant over the entire model. Thus if the quantity $\partial T/\partial t$ could be measured at exactly time zero the conduction correction would be zero. Since this slope is difficult to determine because of the response of the instrumentation, the slope may be read at several different time intervals and plotted against time. The resulting curve of raw data measured in the presence of conduction should intersect the ordinate at time zero at the same point that the true curve (i. e., no conduction in the model) would intersect. Thus a true $\partial T/\partial t$ with zero conduction correction may be inferred. This method is applicable only if the slope-time curve is well behaved so that it may be extrapolated with certainty. Since the stagnation temperature in this experiment had not reached a constant value until almost two seconds after the flow

had started, such an extrapolation was deemed too uncertain and was not used.

The temperature gradients on the conical afterbody would be expected to be small, hence that portion of the model poses no particular problems. The equation for the afterbody is

$$q_T = b\left[-\rho_m c_m \frac{\partial T_w}{\partial t} + \frac{k_m}{S_o}\frac{\partial T_w}{\partial S_o} + k_m \frac{\partial^2 T_w}{\partial S_o^2}\right] \qquad \text{(A-12)}$$

where b is the skin thickness and S_o is the distance along the surface from the tip of a 10^o half angle cone.

APPENDIX B

EFFECT OF A THERMOCOUPLE WIRE ON TRANSIENT MEASUREMENTS*

Consider a thin sheet (1) to which is attached a small thermocouple wire (2). There is a constant heat input step function applied to the upper surface at time zero. The problem is to determine the effect of the heat conduction along the wire on the quantities T and $\partial T/\partial t$. The region (3) is considered separately since this simplifies the writing of the boundary conditions for the other two regions.

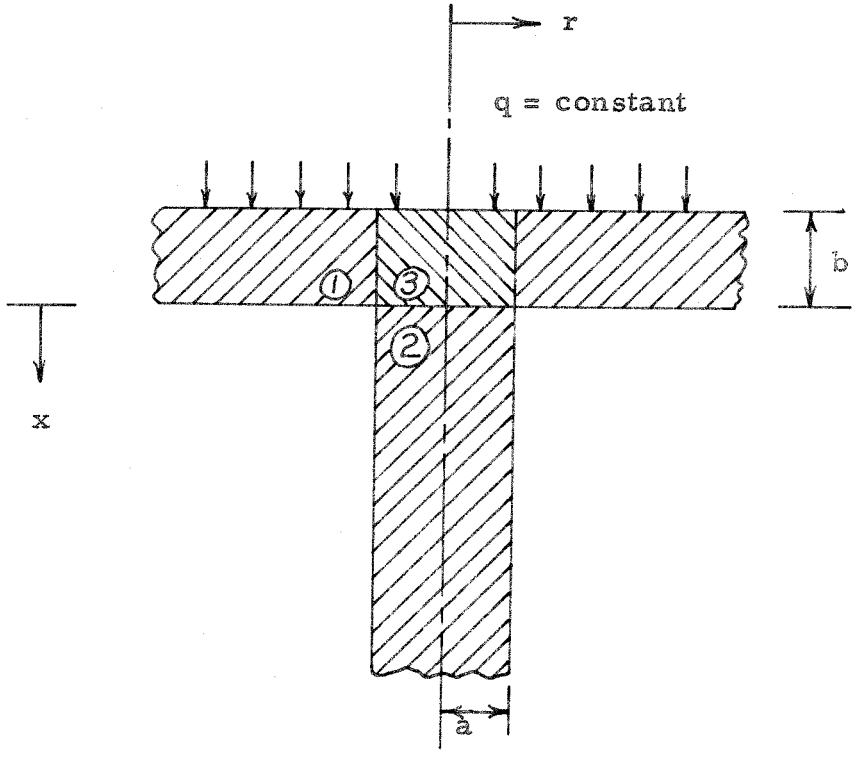

* The help of Dr. T. Kubota in the formulation and solution of this problem is gratefully acknowledged.

Assume:

(i) $T(R = a, t) = T(x = 0, t)$, that is, region (3) has an infinite conductivity but a finite heat capacity, so that the heat storage term for this region will be included.

(ii) There are no temperature gradients through sheet (1) normal to the surface.

(iii) There is no heat loss from the underside of the sheet nor from the surface of the wire.

For simplicity, also assume that $\rho_1 c_1 = \rho_3 c_3$. The heat equation in polar coordinates for region (1) is:

$$\rho_1 c_1 \frac{\partial T_1}{\partial t} = \frac{q}{b} + \frac{k_1}{r} \frac{\partial}{\partial r}\left(r \frac{\partial T_1}{\partial r}\right) \tag{B-1}$$

The initial and boundary conditions are:

$$\begin{aligned} &T_1 (r, 0) = 0 \\ &T_1 (r \longrightarrow \infty, t) = \text{finite} \\ &T_1 (a, t) = F(t) \end{aligned} \tag{B-2}$$

where $F(t)$ is to be determined later from the heat balance for region (3).

For region (2):

$$\rho_2 c_2 \frac{\partial T_2}{\partial x} = k_2 \frac{\partial^2 T_2}{\partial x^2} \tag{B-3}$$

with initial and boundary conditions:

$$\begin{aligned} &T_2 (x, 0) = 0 \\ &T_2 (x \longrightarrow \infty, t) = \text{finite} \\ &T_2 (0, t) = F(t) \end{aligned} \tag{B-4}$$

where $F(t)$ is the same function as appeared in Equation B-2. Writing the heat balance for region (3) and letting $T_3 = F(t)$:

$$\frac{\partial F}{\partial t} = \frac{q}{\rho_3 c_3 b} + \frac{2k_1}{\rho_3 c_3 a}\frac{\partial T_1(a,t)}{\partial r} + \frac{k_2}{\rho_3 c_3 b}\frac{\partial T_2(0,t)}{\partial x} \qquad \text{(B-5)}$$

Applying the Laplace transform to Equation B-1,

$$r\frac{\partial^2 \tilde{T}_1}{\partial r^2} + \frac{\partial \tilde{T}_1}{\partial r} - \frac{sr}{\kappa_1}\tilde{T}_1 = -\frac{qr}{\rho_1 c_1 \kappa_1 sb} \qquad \text{(B-6)}$$

where

$$\tilde{T}_1(r,s) = \mathcal{L}\{T_1(r,t)\} \equiv \int_0^\infty T_1(r,t)e^{-st}dt$$

$$\kappa_1 = \frac{k_1}{\rho_1 c_1}$$

The solution of this equation, satisfying the boundary conditions is

$$\tilde{T}_1(r,s) = \frac{\tilde{F}(s) - q/\rho_1 c_1 bs^2}{K_0\left(a\sqrt{\frac{s}{\kappa_1}}\right)} K_0\left(r\sqrt{\frac{s}{\kappa_1}}\right) + \frac{q}{\rho_1 c_1 bs^2} \qquad \text{(B-7)}$$

where

$$\tilde{F}(s) = \mathcal{L}\{F(t)\}$$

and $K_0\left(a\sqrt{\frac{s}{\kappa_1}}\right)$ is the modified Bessel function of 2nd kind of order zero. Applying the Laplace transform to Equation B-3:

$$s\tilde{T}_2(x,s) = \kappa_2 \frac{\partial^2 \tilde{T}_2(x,s)}{\partial x^2} \qquad \text{(B-8)}$$

where

$$\tilde{T}_2(x,s) = \mathcal{L}\{T_2(x,t)\} \qquad \kappa_2 = \frac{k_2}{\rho_2 c_2}$$

The solution of this equation is

$$\tilde{T}_2(x,s) = \tilde{F}(s)\, e^{-\sqrt{\frac{s}{\kappa_2}}\,x} \qquad \text{(B-9)}$$

Applying the Laplace transform to Equation B-5,

$$s\tilde{F}(s) = \frac{q}{\rho_3 c_3 b s} + \frac{2k_1}{\rho_3 c_3 a}\frac{\partial \tilde{T}_1(a,s)}{\partial r} + \frac{k_2}{\rho_3 c_3 b}\frac{\partial \tilde{T}_2(0,s)}{\partial x} \qquad \text{(B-10)}$$

Thus F(s) is determined by forming $\partial\tilde{T}_1/\partial r$ from Equation B-7 and $\partial\tilde{T}_2/\partial x$ from Equation B-9 and evaluating at the appropriate r and x.

Substituting and simplifying:

$$\tilde{F}(s) = \frac{q}{s\rho_3 c_3 b}\,\frac{1 + \frac{2\kappa_1}{as}\sqrt{\frac{s}{\kappa_1}}\,\frac{K_1\left(a\sqrt{\frac{s}{\kappa_1}}\right)}{K_0\left(a\sqrt{\frac{s}{\kappa_1}}\right)}}{s + \frac{\rho_2 c_2}{\rho_3 c_3}\frac{\kappa_2}{b}\sqrt{\frac{s}{\kappa_2}} + \frac{2\rho_1 c_1}{\rho_3 c_3}\frac{\kappa_1}{a}\sqrt{\frac{s}{\kappa_1}}\,\frac{K_1\left(a\sqrt{\frac{s}{\kappa_1}}\right)}{K_0\left(a\sqrt{\frac{s}{\kappa_1}}\right)}} \qquad \text{(B-11)}$$

where $K_1\left(a\sqrt{\frac{s}{\kappa_1}}\right)$ is the modified Bessel function of 2nd kind of order one.

This expression represents the transform of $T_1(a,t)$ and $T_2(0,t)$.

Equation B-11 will now be inverted by using approximations for the Bessel functions $K_0\left(a\sqrt{\frac{s}{\kappa_1}}\right)$ and $K_1\left(a\sqrt{\frac{s}{\kappa_1}}\right)$.

For $\left(a\sqrt{\frac{s}{\kappa_1}}\right)$ small, i.e., $a\sqrt{\frac{s}{\kappa_1}} \ll 1$

$$K_0\left(a\sqrt{\frac{s}{\kappa_1}}\right) \doteq -\log\left(a\sqrt{\frac{s}{\kappa_1}}\right) \qquad \text{(B-12)}$$

$$K_1\left(a\sqrt{\frac{s}{\kappa_1}}\right) \doteq 1/\left(a\sqrt{\frac{s}{\kappa_1}}\right)$$

Substituting these expressions in Equation B-11 would yield a solution for "small" s, that is, for "large" time. Taking material (1) to be pure iron, and the wire radius to be .005", then at t = 1 second, $\left(a\sqrt{\frac{s}{\kappa_1}}\right) \doteq .03$ and its value at 10 seconds is .01. Evaluating the complete series expansions for K_o and K_1 (see page 375 of Reference 16) for this material and wire radius and for the largest "small" s of $s = 1 \Longrightarrow t = 1$ second, the error involved in the approximation B-12 of discarding all but the first term in the expansions is about 3 per cent for K_o and 0.2 per cent for K_1. Thus the "long" time approximation is considered valid for $t \geq 1$ second and is of primary concern for a transient experiment in a wind tunnel.

Substituting the asymptotic expressions for K_o and K_1 into Equation B-11 would yield a solution for "large" s or "small" time. But this would yield solutions valid for time considerably less than one second, and this approximation is not of interest here.

Now substituting Equations B-12 into Equation B-11, simplifying, and factoring the denominator:

$$\tilde{F}(s) = \frac{g}{\rho_3 c_3 b s} \frac{\frac{a^2 s}{2}\log\left(\frac{a^2 s}{\kappa_1}\right) - 2\kappa_1}{-2\kappa_1 s\left[1 - \frac{a^2}{4\kappa_1}\log\left(\frac{a^2 s}{\kappa_1}\right)\left\{s + \frac{\rho_2 c_2}{\rho_3 c_3}\frac{\sqrt{\kappa_2 s}}{b}\right\}\right]} \qquad \text{(B-13)}$$

In the denominator there is (s log s) and ($\sqrt{s}$ log s). For small s, s and $\sqrt{s} \longrightarrow 0$ faster than log $s \longrightarrow \infty$, hence the square bracket in the denominator of Equation B-13 is $[1 - \epsilon]$ and may be expanded by the binomial theorem. Then

$$\tilde{F}(s) = \frac{q}{\rho_3 c_3 b}\left\{\frac{1}{s^2} + \frac{a^2}{4K_1}\frac{\sqrt{K_2}}{b}\frac{\rho_2 c_2}{\rho_3 c_3}\frac{1}{s^{3/2}}\log\left(\frac{a^2 s}{K_1}\right) + \mathcal{O}(\log^2)\right\} \quad \text{(B-14)}$$

This transform may be inverted by using tables of inverse transforms[33]. Then F(t) is

$$F(t) = \frac{q}{\rho_3 c_3 b}\left[t + \frac{a^2\sqrt{K_2}}{4K_1 b}\frac{\rho_2 c_2}{\rho_3 c_3}t^{1/2}\left\{\frac{\Gamma'(3/2)}{\Gamma(3/2)\Gamma(3/2)} - \frac{2}{\sqrt{\pi}}\log\frac{K_1 t}{a^2}\right\}\right] \quad \text{(B-15)}$$

which is in the form

$$F(t) = \frac{q}{\rho_3 c_3 b}\left[t + \varepsilon\right]$$

where

$$F(t) = T_3 = \frac{q}{\rho_3 c_3 b}t$$

is what would be expected without the wire, i.e., $\rho_3\, c_3\, b\, \frac{\partial T_3}{\partial t} = q$.

Thus evaluation of the square bracket in Equation B-15 for the particular materials and dimensions in question will give the error involved in measuring the temperature of the sheet caused by the presence of the thermocouple wire.

To illustrate, for materials (1) and (3) pure iron and material (2) constantan, with b = .020" and a = .005",

$$F(t) = (\text{const})\left[1 - 7.14 \times 10^{-3}\right] \quad \text{for } t = 1 \text{ second}$$

$$= (\text{const})\left[1 - 2.88 \times 10^{-3}\right] \quad \text{for } t = 10 \text{ seconds}$$

Thus the error in the temperature measurement which is introduced by the wire is less than 1 per cent.

The next question to be investigated is the error in the measure-

wire and the skin were of comparable dimensions, the error introduced by the presence of the wire would be very large. Some insight into the physical reason for this small error is obtained by solving for the heat flux per unit area along the wire.

The heat flux along the wire is given by

$$Q_w = k_2 \left.\frac{\partial T_2}{\partial x}\right|_{x=0} \tag{B-18}$$

Now from Equation B-9,

$$\frac{\partial \tilde{T}_2}{\partial x} = -\sqrt{\frac{s}{\kappa_2}}\,\tilde{F}(s)\, e^{-\sqrt{\frac{s}{\kappa_2}}\,x} \tag{B-19}$$

Then evaluating Equation B-19 at x = 0 and then substituting the "large" time expression for F(s) from Equation B-14,

$$\left.\frac{\partial \tilde{T}_2}{\partial x}\right|_{x=0} = -\frac{q}{\rho_3 c_3 b\sqrt{\kappa_2}}\left\{\frac{1}{s^{3/2}} + \frac{a^2\sqrt{\kappa_2}}{4\kappa_1 b}\,\frac{\rho_2 c_2}{\rho_3 c_3}\,\frac{1}{s}\log\left(\frac{a^2 s}{\kappa_1}\right)\right\} \tag{B-20}$$

Inverting from tables, and using the definition of Q_w from Equation (B-18):

$$Q_w = -\frac{q k_2}{\rho_3 c_3 b}\left\{\frac{2}{\sqrt{\kappa_2}}\sqrt{\frac{t}{\pi}} + \frac{a^2}{4\kappa_1 b}\,\frac{\rho_2 c_2}{\rho_3 c_3}\left[\Gamma'(1) - \log\frac{t\kappa_1}{a^2}\right]\right\} \tag{B-21}$$

Evaluating for the same materials, and for b = .020", a = .005",

Q_w/q = 5.9 for t = 1 second

= 18 for t = 10 seconds.

Thus the heat flow per unit area along the wire is large compared to the heat flow per unit area into the slab. But this heat lost down the wire is replaced almost completely by heat flowing in from the radial direction through the sheet. The net effect of the wire is then small

compared to the overall level of the temperature. An analogy may be made, as suggested by L. Lees, by considering water flowing into a large tank at a constant rate, the level of the water corresponding to the temperature of the sheet. If a small hole is made in the bottom of the tank, some water will flow through it and be lost, but water will move from the rest of the tank to make up this local deficit, and the net effect on the water level in the tank is small.

To illustrate the fact that heat flows along the sheet to make up the local temperature deficit, consider the case where b = .020" and a = .005" but now material (1) is plate glass, which has a thermal conductivity about 1 per cent that of pure iron. The error involved in making the "large" time approximation B-12 is now about 10 per cent for K_o and 5 per cent for K_1 at t = 1 second, and 5 per cent and 1.4 per cent, respectively, for t = 5 seconds.

By evaluating Equations B-15 and B-17 at 5 seconds, the error is found to be 18 per cent in the temperature measurement and 12 per cent in $\partial T/\partial t$.

The flow analogy here would correspond to the tank being filled with sand. The sand cannot flow toward the hole quickly enough to make up the local deficit, and the level of the sand near the hole is substantially lowered.

In order to keep the thermocouple conduction error small, it is therefore necessary that the skin be made of material with a comparatively high thermal conductivity. To keep the error less than 1 per cent at 5 seconds while using a glass skin would require a wire diameter of about .001".

APPENDIX C

TRANSIENT HEAT TRANSFER WITH FLAT PLATE MODEL

The investigation discussed in this report was originally planned as a study of pressures, temperatures, and heat transfer rates on a flat plate with injection into a laminar boundary layer. For this purpose a wind tunnel flat plate model was constructed as follows:

$0 \leq \xi \leq 3''$: solid nose

$3 \leq \xi \leq 5''$: woven stainless steel wire porous strip

$5 \leq \xi \leq 18''$: film cooled portion instrumented with thermocouples

The film-cooled portion of the plate was to be used for heat transfer studies with and without injection. The top surface was made of a sheet of stainless steel 1/64" thick which was mounted on a base made of thin plastic ribs. The resulting thin skin with an air space behind it was to be used as the mass for a local heat transfer determination by the transient technique. However, no satisfactory zero-injection values of heat transfer could be obtained for use as a basis of comparison for the efficiency of the injection. The local heat transfer coefficients at $\xi = 6''$ ($Re_\xi = 1.6 \times 10^6$) with no injection were about the correct laminar value, but aft of this region the coefficient increased rapidly as if a transition region existed there. But the results of Reference 34 showed laminar boundary layers to exist at much higher Reynolds numbers than were involved here, and steady-state velocity profiles measured at various stations on the heat transfer portion of the plate substantiated the fact that the boundary layer was laminar

at least until ξ = 15". These results were in agreement with the fact that the measured steady-state recovery factors were typically laminar.

There was a possibility that the boundary layer was not two-dimensional, with perhaps higher heating rates occurring off the centerline, so that the resulting heat conduction into the center part of the skin, which had not been taken into account, would yield a higher value of $\partial T/\partial t$ than the expected laminar result. The spanwise uniformity of the boundary layer was checked by measuring a series of total pressure profiles on the centerline and $\frac{1}{2}$" and 1" on either side of the centerline. The results at a high stagnation pressure are shown in Figure 60; the same effect was present at p_o = 61 psia. There was about a one-inch-wide strip of constant boundary layer thickness down the center of the plate, but further away from the centerline the boundary layer was unaccountably thin. It still appeared possible to get the desired results along the centerline with a negligible conduction correction if the data were obtained within about 15 seconds after the flow was established. After this time the errors resulting from spanwise heat conduction would be large. A test was made but the transient heat transfer results still indicated transition. To investigate this phenomenon further, some exploratory hot-wire surveys were made by Mr. A. Demetriades. Mass flow profiles were taken across the boundary layer on the centerline at a fixed value of ξ during the first few minutes after flow was established. These measurements showed a qualitative change in the profile as a function of time, with the biggest change occurring at a value of n/δ of about 0.3, where δ is the steady-state boundary layer thickness at a particular value of ξ. The probe

was then fixed at this value of n/δ at different ξ stations along the centerline, and the root-mean-square output of the hot-wire was read as a function of time. The results are shown in Figure 61. Qualitatively, a large RMS value corresponds to a turbulent boundary layer and a small RMS value indicates a laminar boundary layer. Thus, the hot-wire signal indicated that the boundary layer was initially turbulent or transitional and then, as time progressed, the boundary layer became less turbulent, eventually reaching some steady-state laminar configuration. The time duration of this varying RMS signal was found to depend upon Reynolds number and upon the plate or tunnel wall temperature. If the flow were started with the plate and tunnel walls at room temperature, the effect persisted for some minutes; if the plate and walls were near equilibrium temperature when the "blow-down" was made, the effect lasted only a few seconds.

On the premise that perhaps this effect was caused by the surface roughness of the porous section the same hot-wire measurements were carried out on a smooth flat plate. The results as regards the presence of transition and the temperature dependence were the same, although the duration of the phenomenon was shorter than for the film-cooling plate for the same wind tunnel conditions. The surface temperature history of the two plates was quite different, because the solid plate had a high heat capacity while the cooling plate had a thin skin and a low heat capacity. One other check was made, and that was to mount the hot-wire in the empty tunnel and see if any large disturbances were present in the flow during the period just after the flow was established. None were observed.

An explanation of this curious transition effect has not yet been found. It is possible that this effect is related to "transverse contamination" from the turbulent boundary layers on the tunnel sidewalls. The presence of this effect, and the fact that it was not repeatable, made it impossible to obtain reliable zero-injection heat transfer results. The effects of injection as regards the severe spanwise differences in the steady-state boundary layer thickness were not known, and it was uncertain whether reliable steady-state boundary layer measurements could be made. So the decision was made to retain the same instrumentation and techniques but to perform the injection experiment on a body of revolution where this phenomenon would not occur. No such transition effect was observed on the blunt-nosed cone model utilized in this investigation.

TABLE I

Notation	Description (See Figures 5 and 6)
HM	Basic hemisphere-cone model
CA	Deflector Cap A (h = .013")
CB	Deflector Cap B (h = .088")
CC	Deflector Cap C (h = .167")
S I	Spike I (L/D = .536)
S II	Spike II (L/D = 1.07)
S III	Spike III (L/D = 1.78)
S IV	Spike IV (20° half angle cone)

Sample Configuration	Description
HM + CA + S I	Spike I attached to Cap A and both mounted on front of basic model

TABLE II

COOLANT GAS PROPERTIES

Property	Nitrogen	Helium	Units
Density (32°F, 1 atm.)	.07807	.01114	lb./ft.^{3}
Specific Heat at Constant Pressure (- 310°F)	0.256	1.25	BTU./lb.
Ratio of Specific Heats	1.40	1.66	--
Thermal Conductivity (32°F)	.0127	.082	BTU/hr. ft.^{2} °F/ft.
Viscosity (50°F)	1.15×10^{-7}	1.32×10^{-7}	slug/ft. sec.
Molecular Weight	28	4	slug/mole
Gas Constant	1,780	12,460	ft.^{2}/sec.^{2} °F
Velocity of Sound (90°F)	1,169	3,370	ft./sec.

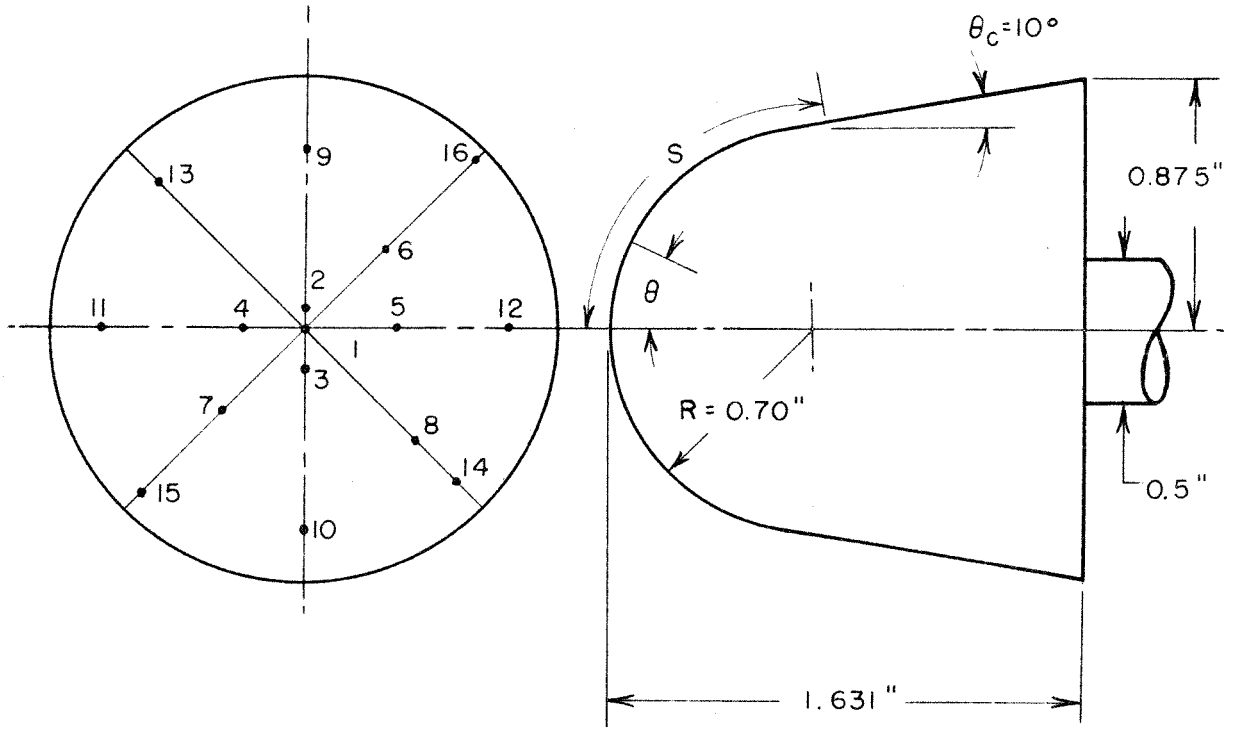

Station	S (inches)	S/R	θ (degrees)
1	0	0	0
2	0.07	0.10	6
3	0.14	0.20	11
4	0.21	0.30	17
5	0.34	0.48	28
6	0.42	0.60	34
7	0.42	0.60	34
8	0.63	0.90	52
9	0.84	1.20	69
10	0.91	1.30	74
11	0.98	1.40	80
12	1.05	1.50	--
13	1.12	1.60	--
14	1.26	1.80	--
15	1.54	2.20	--
16	1.82	2.60	--

FIG. 1

PRESSURE DISTRIBUTION MODEL

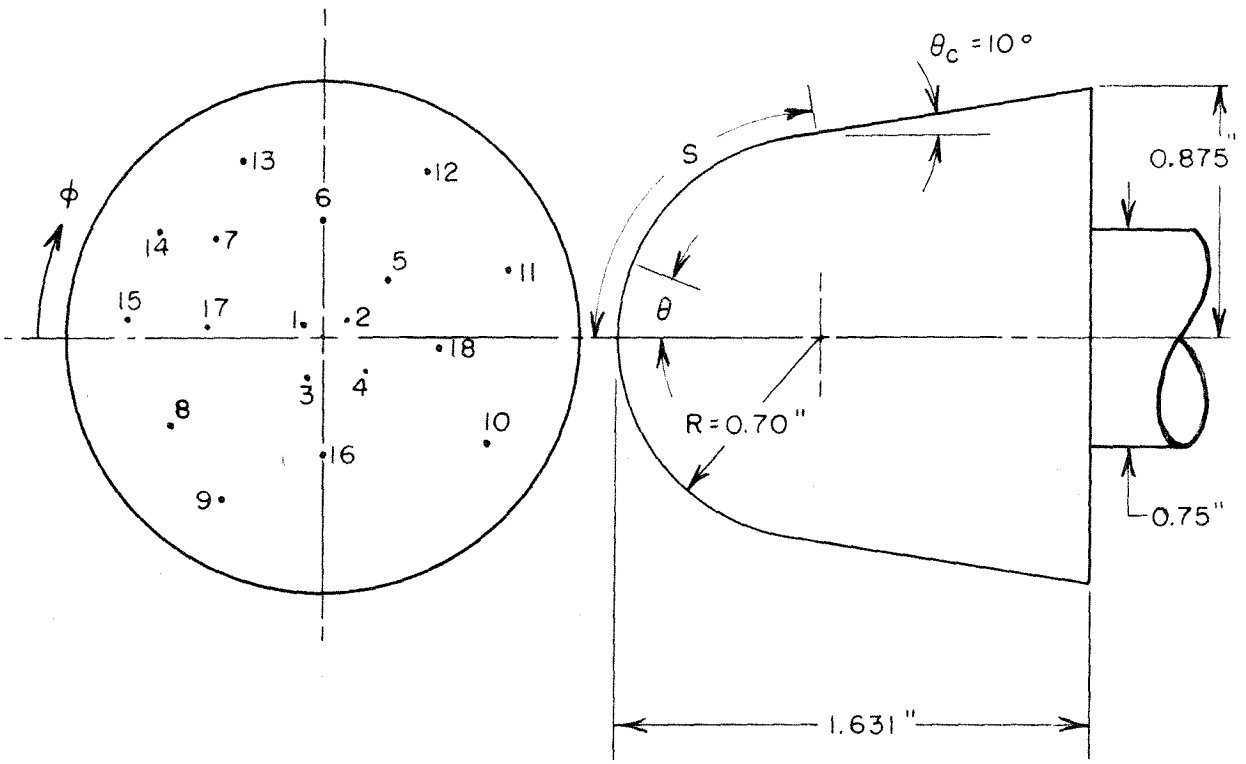

Station	S (inches)	S/R	θ (degrees)	
1	0.07	0.10	6	
2	0.10	0.14	8	
3	0.15	0.21	12	
4	0.18	0.26	15	
5	0.31	0.44	25	
6	0.43	0.61	35	
7	0.55	0.79	45	
8	0.73	1.04	60	
9	0.86	1.23	70	
10	0.98	1.40	80	
11	1.03	1.47	--	
12	1.08	1.54	--	
13	1.18	1.69	--	
14	1.38	1.97	--	
15	1.58	2.26	--	
16	0.43	0.61	35	(0.010" D wire)
17	0.43	0.61	35	(0.021" D wire)
18	0.43	0.61	35	(0.032" D wire)

FIG. 2

HEAT TRANSFER MODEL

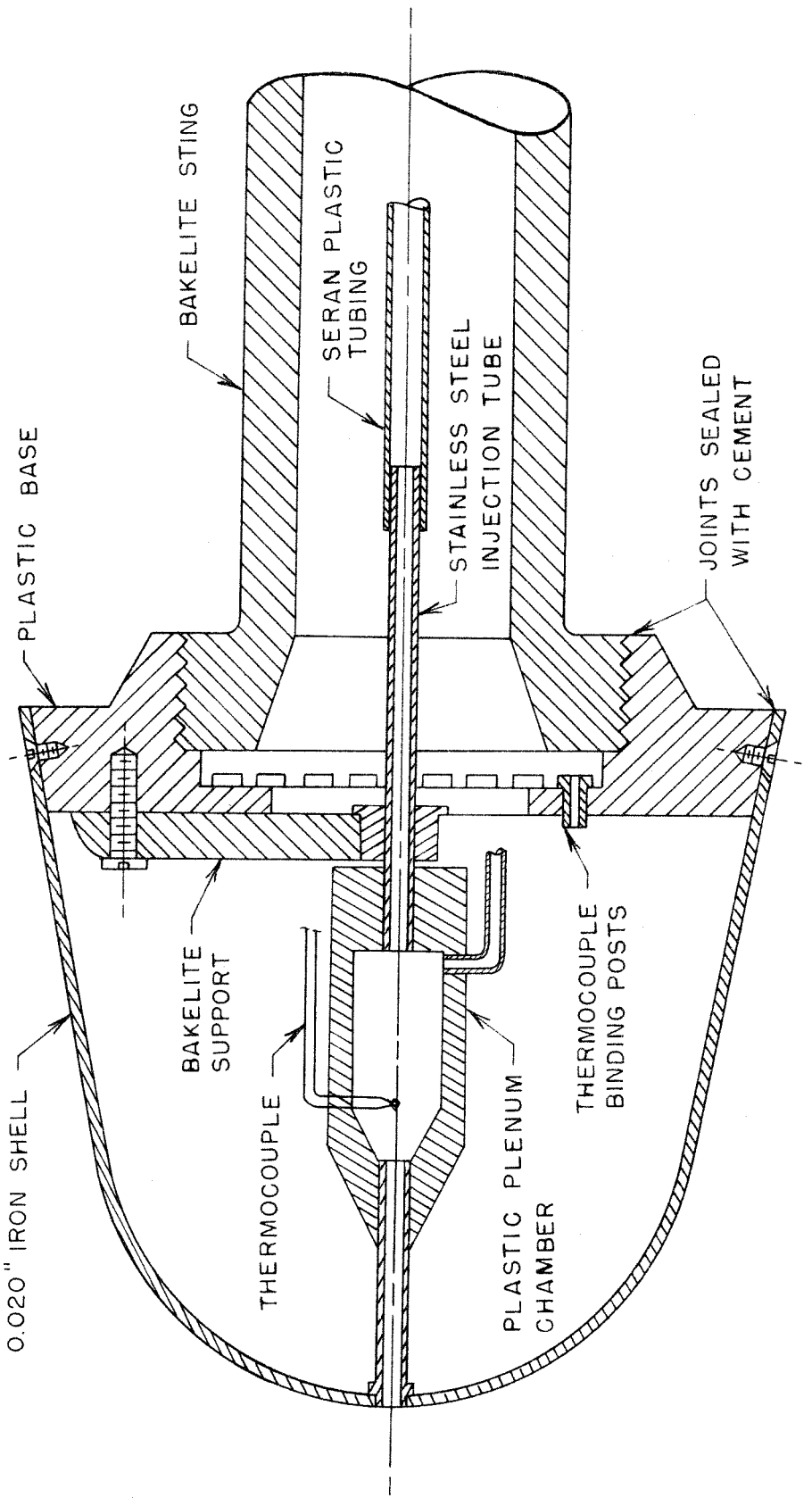

FIG. 3 — CROSS SECTION OF HEAT TRANSFER MODEL

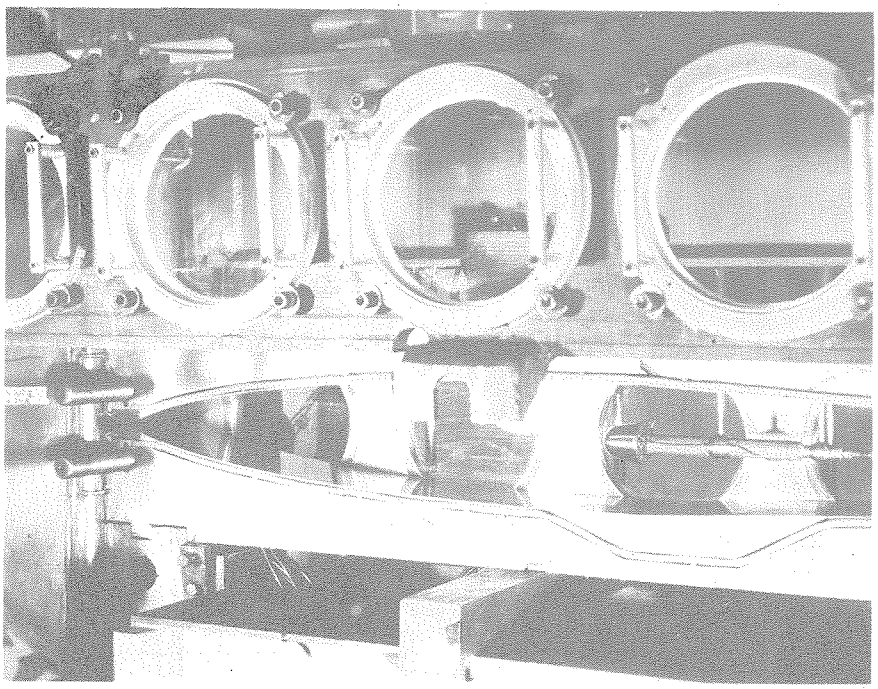

FIG. 4

HEAT TRANSFER MODEL INSTALLED IN LEG 1 TEST SECTION

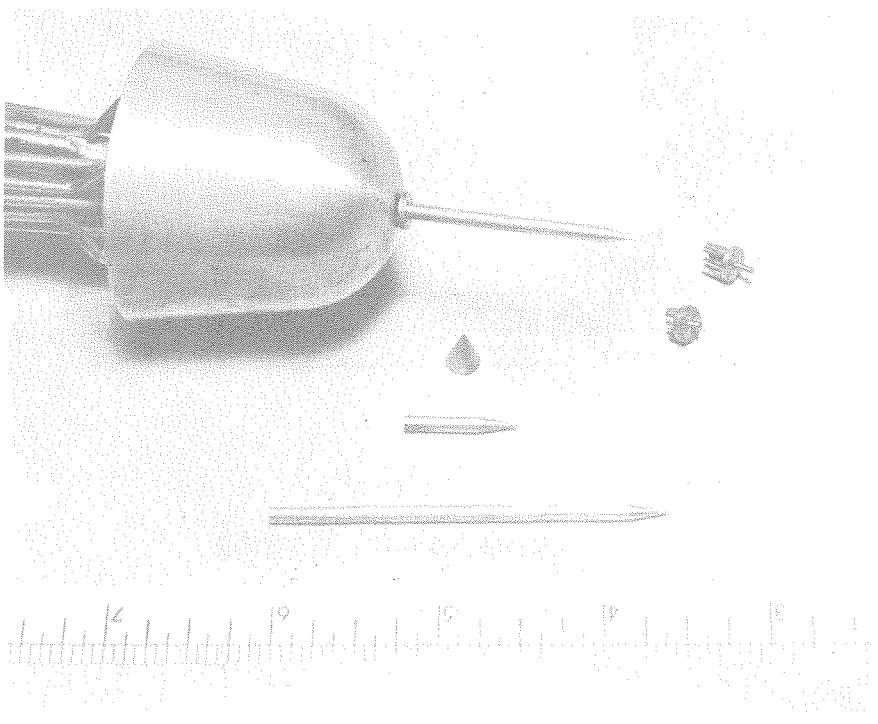

FIG. 5

PRESSURE MODEL SHOWING SPIKES AND DEFLECTOR CAPS

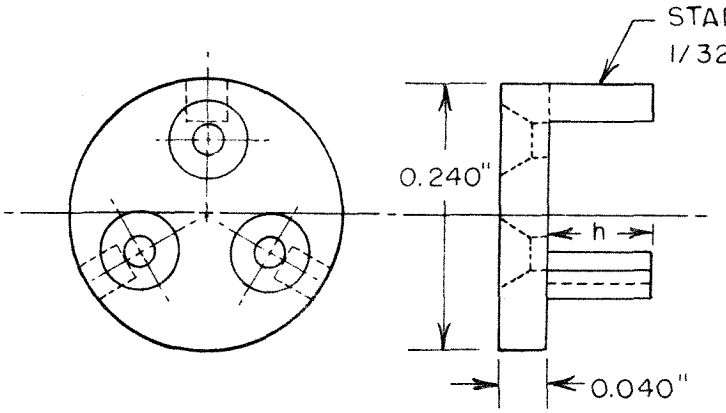

	h
CAP A	0.013"
CAP B	0.088"
CAP C	0.167"

DEFLECTOR CAPS

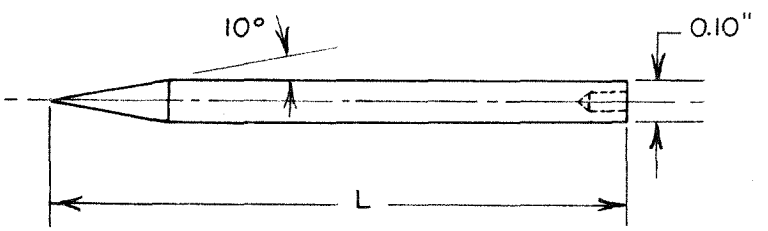

	L
SPIKE I	0.75"
SPIKE II	1.50"
SPIKE III	2.50"

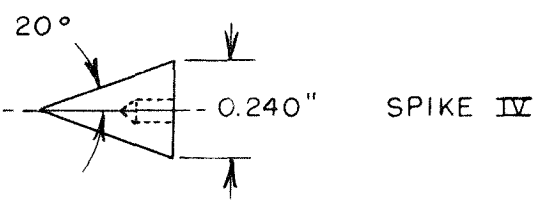

SPIKES

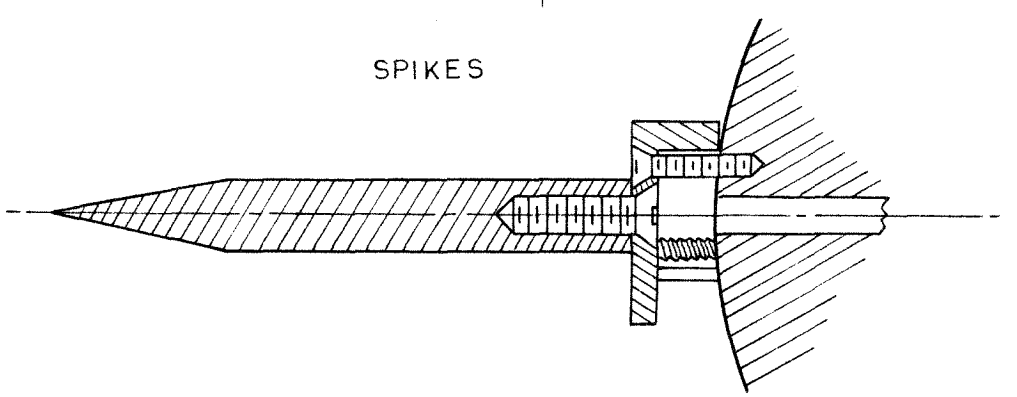

SPIKE I, CAP B, MOUNTED ON
NOSE OF PRESSURE MODEL

FIG. 6 — DEFLECTOR CAPS AND SPIKES

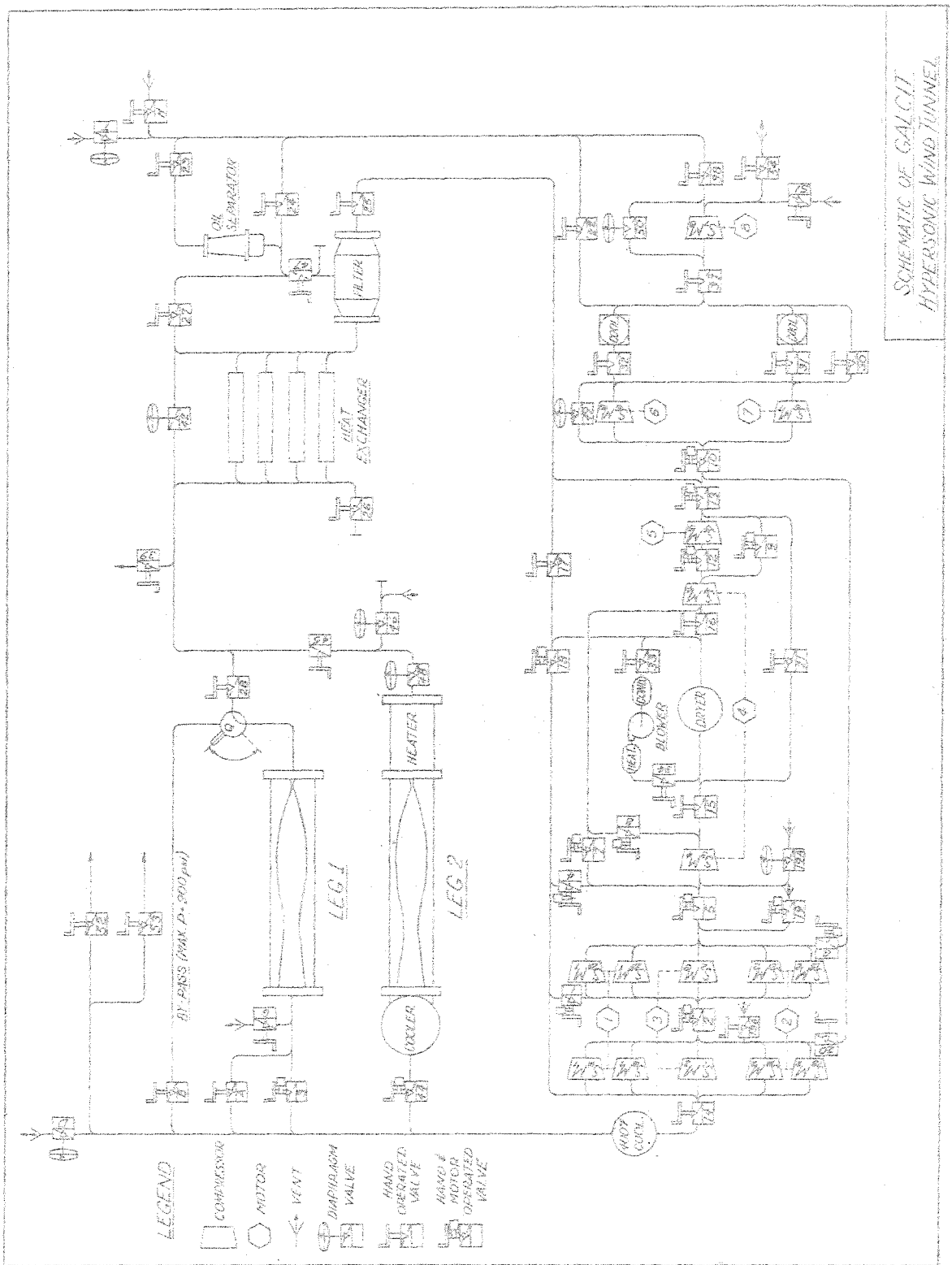
SCHEMATIC OF CALCIT HYPERSONIC WIND TUNNEL
LEGEND
COMPRESSOR
MOTOR
VENT
DIAPHRAGM VALVE
HAND OPERATED VALVE
MANUAL MOTOR OPERATED VALVE
LEG 1
LEG 2
HEATER
COOLER
DRYER
BLOWER
HEAT EXCHANGER
FILTER
OIL SEPARATOR
BY-PASS (MAX. P = 200 psi)
HOT GAS

FIG. 7

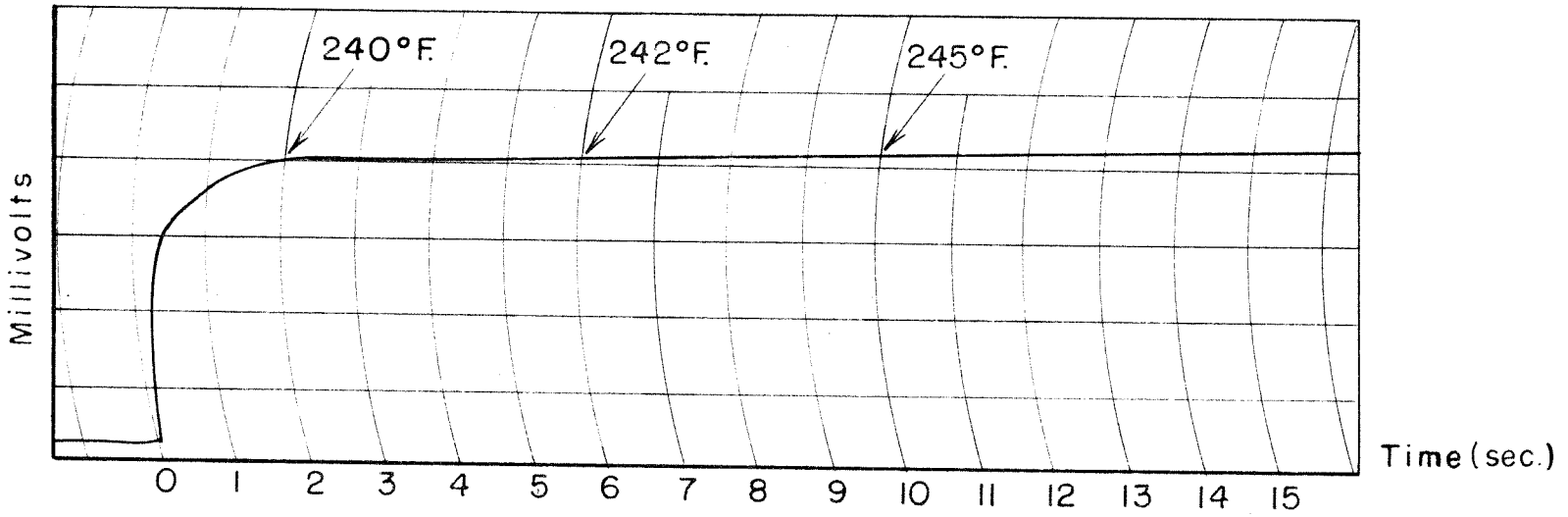

FIG. 8 – SAMPLE OSCILLOGRAPH TRACES OF THROAT PROBE OUTPUT

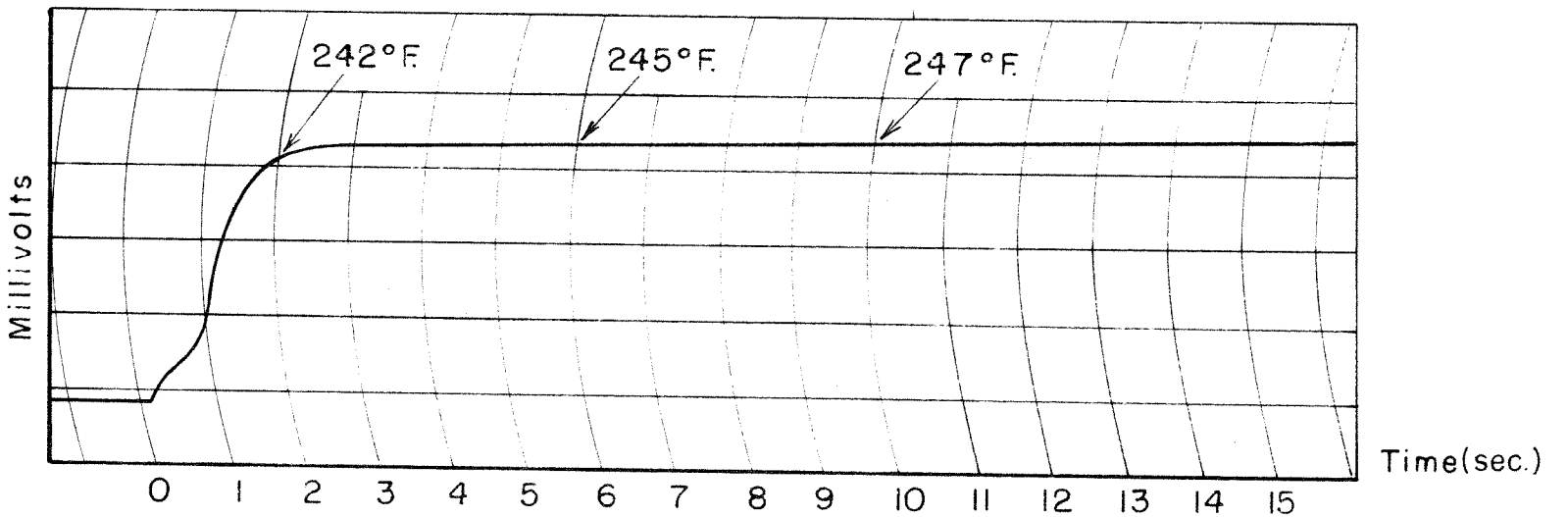

FIG. 9 – SAMPLE OSCILLOGRAPH TRACES OF TEST SECTION PROBE OUTPUT

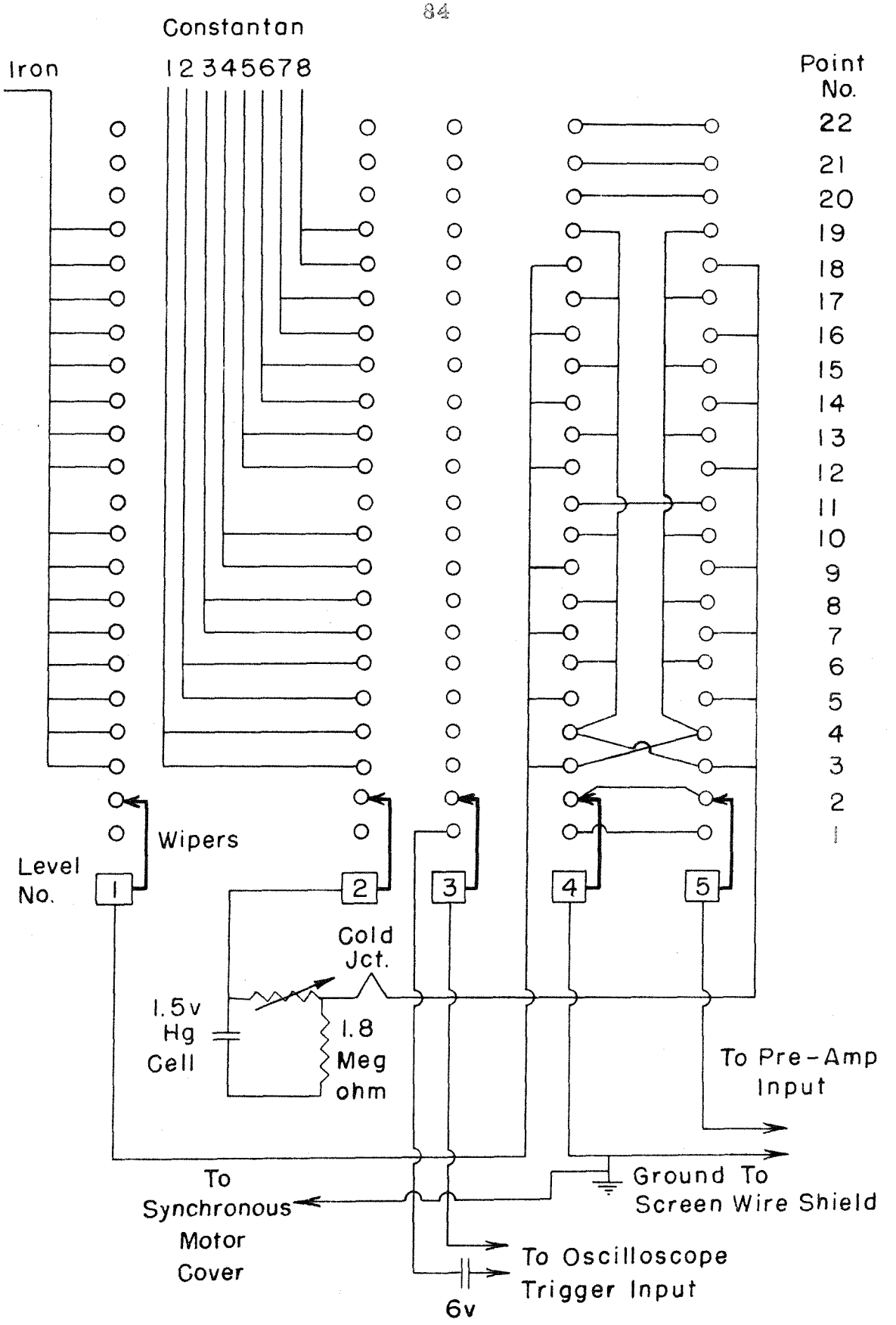

FIG. 10 – INSTRUMENTATION WIRING DIAGRAM

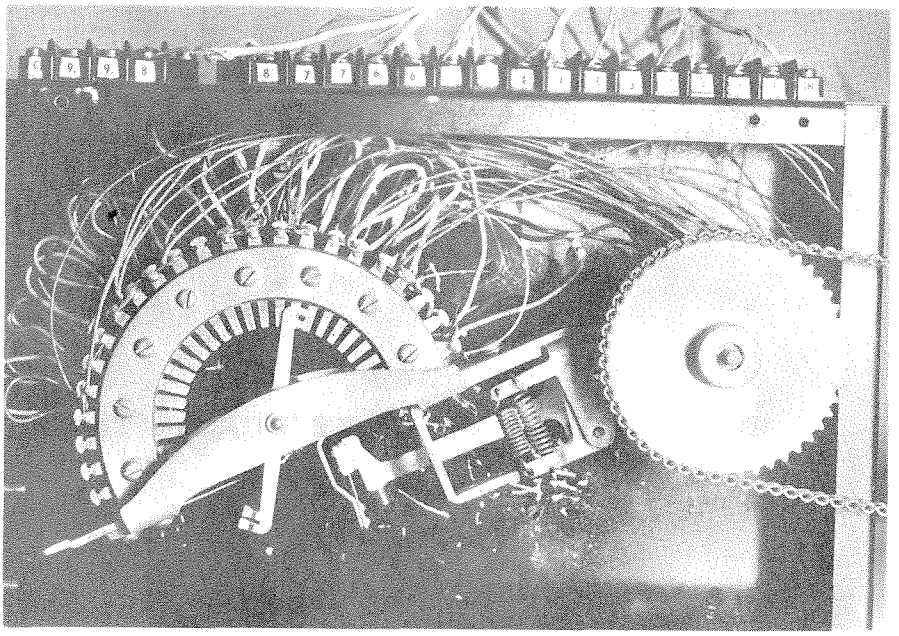

FIG. 11

STEPPING SWITCH

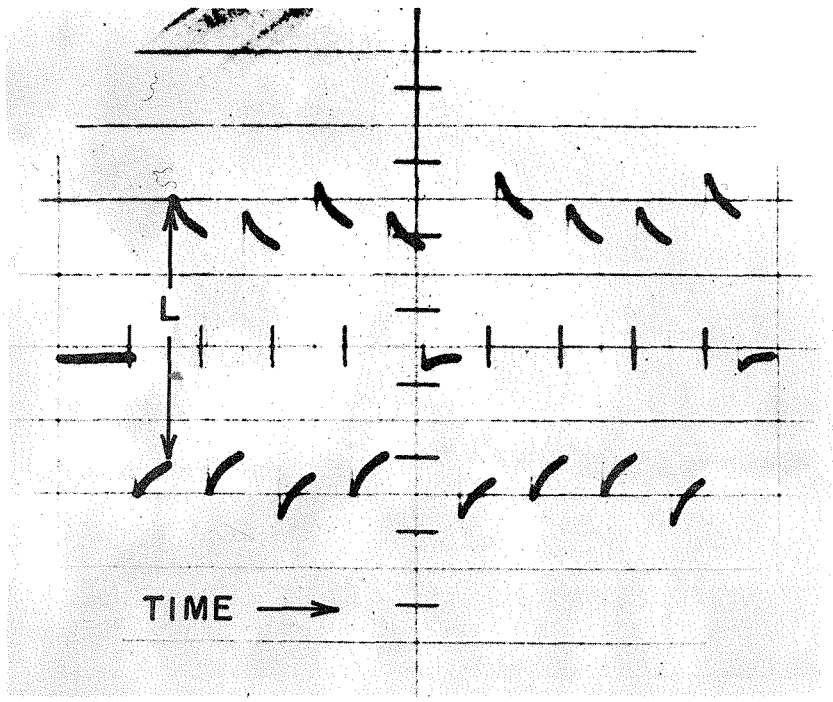

FIG. 12(a)

OSCILLOSCOPE TRACE -- SINGLE SWEEP

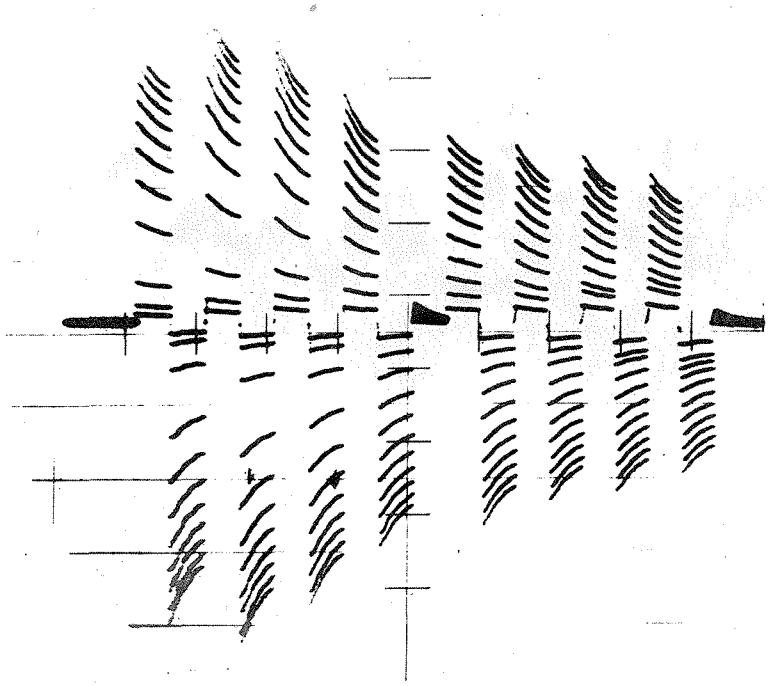

FIG. 12(b)

OSCILLOSCOPE TRACE -- MULTIPLE SWEEP

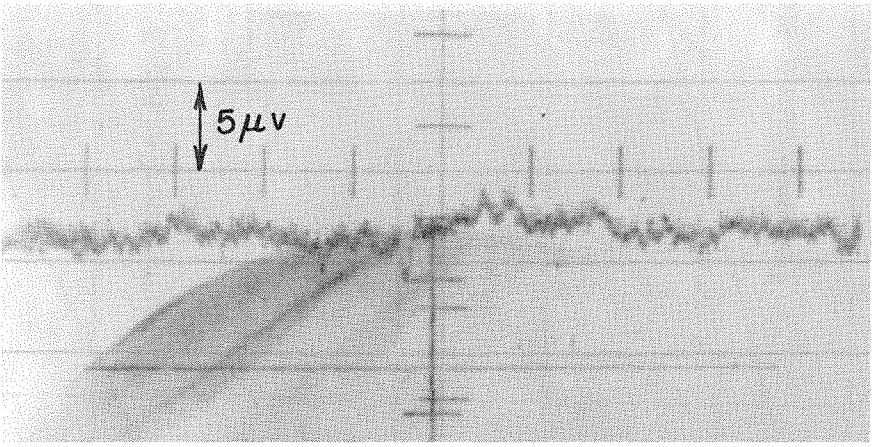

FIG. 12(c)
NOISE LEVEL OF MEASURING CIRCUIT

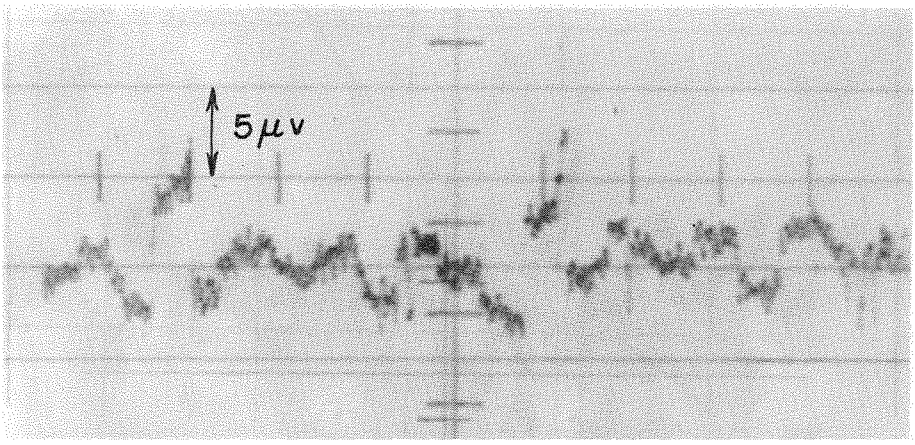

FIG. 12(d)
NOISE CAUSED BY SWITCHING

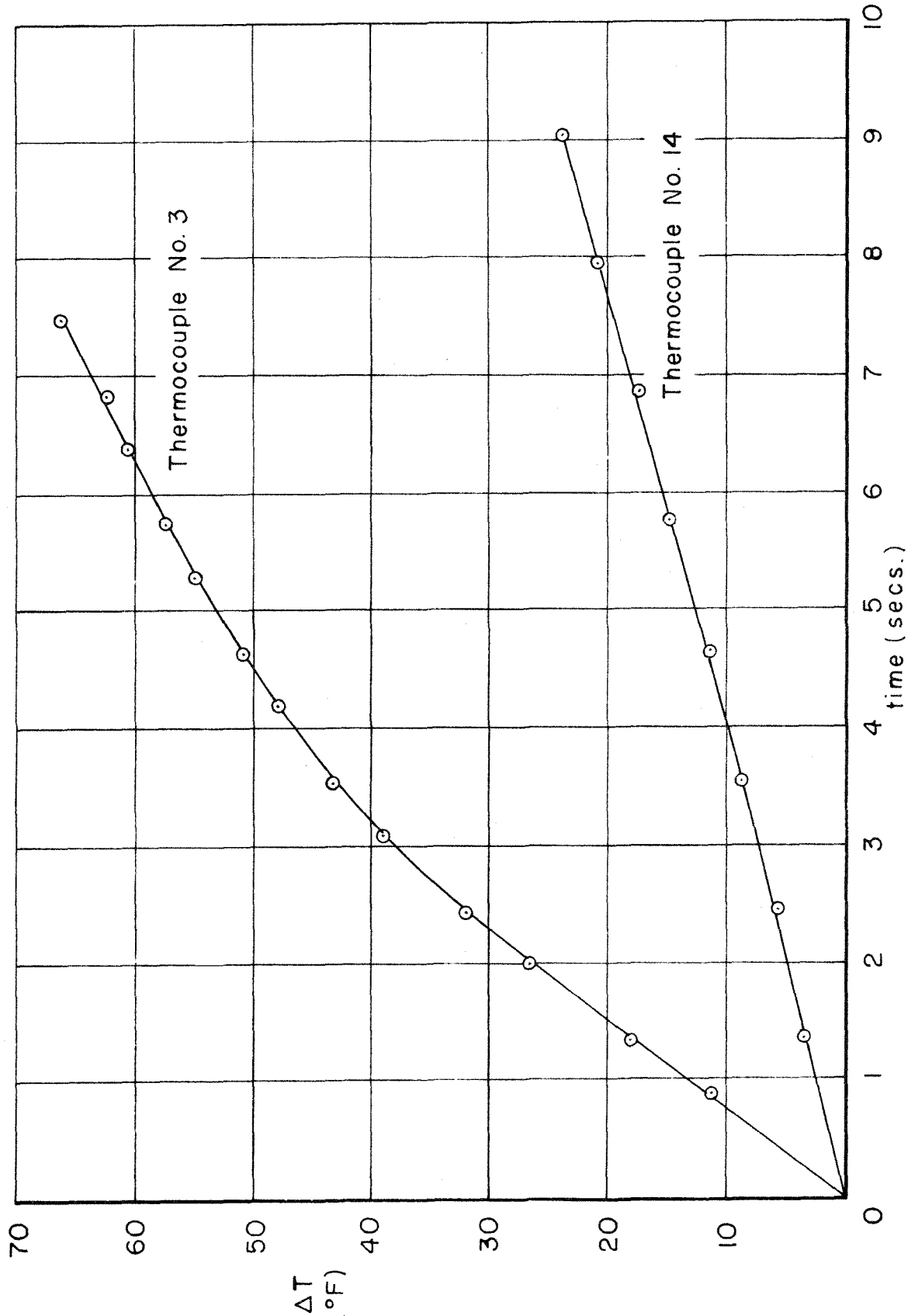

FIG. 13 – MODEL TEMPERATURES AT TWO STATIONS

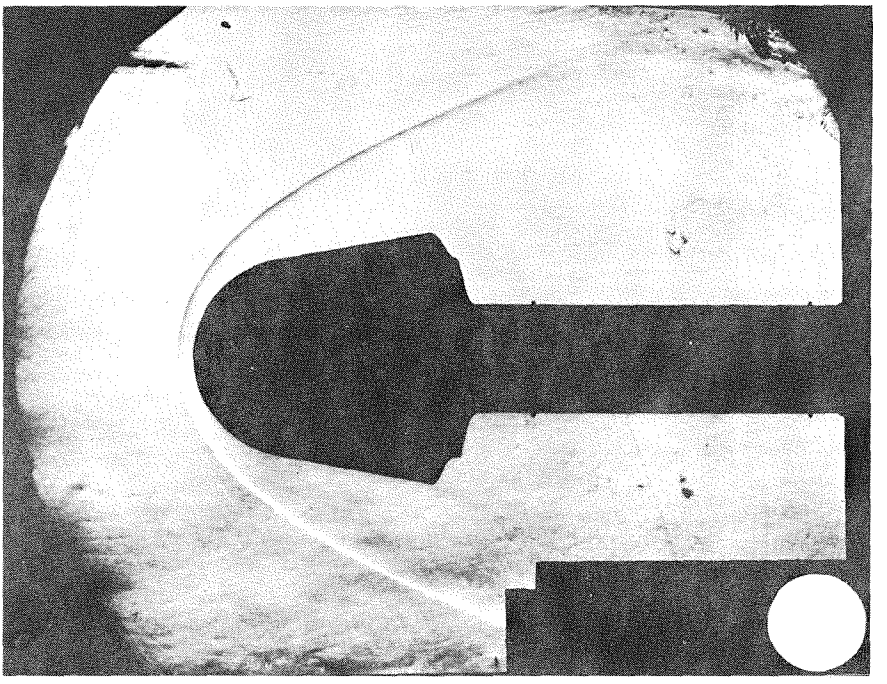

FIG. 14
SCHLIEREN PHOTOGRAPH OF MODEL HM
$\Gamma = 0$

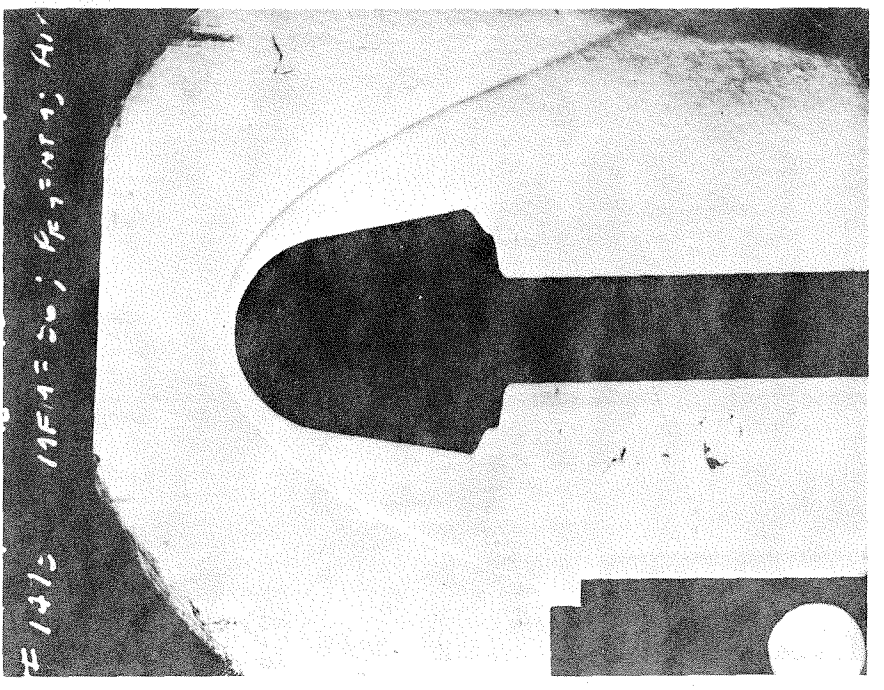

FIG. 15
SCHLIEREN PHOTOGRAPH OF MODEL HM
NITROGEN INJECTION; $\Gamma = .0019$

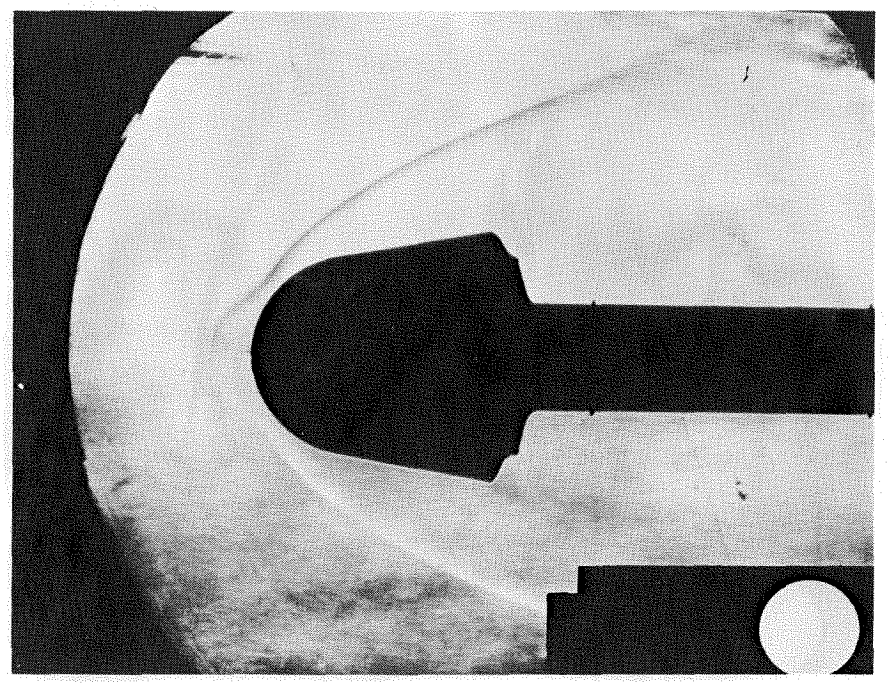

FIG. 16
SCHLIEREN PHOTOGRAPH OF MODEL HM
NITROGEN INJECTION; Γ = .019

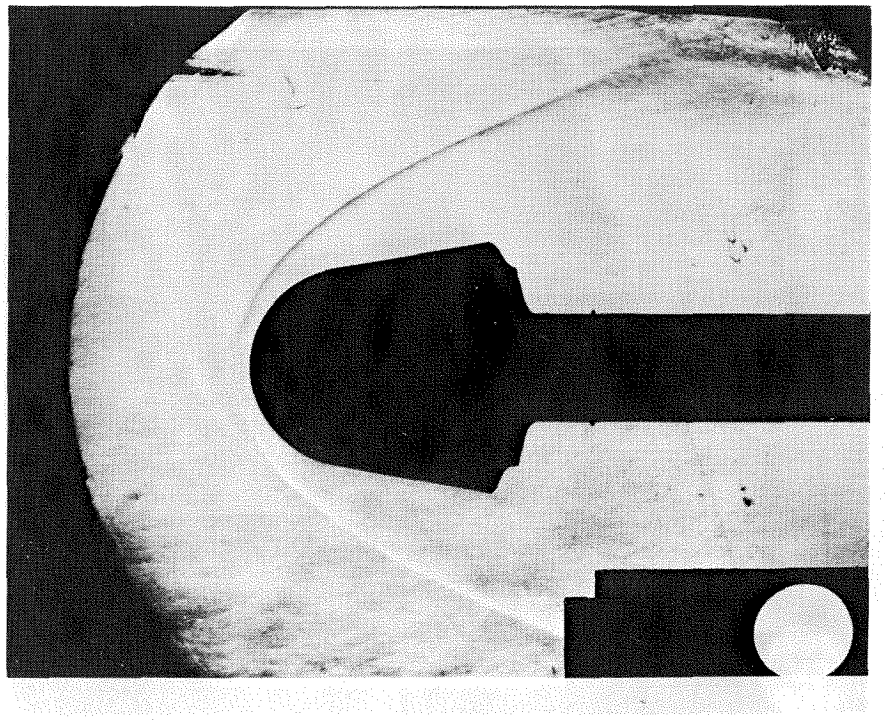

FIG. 17
SCHLIEREN PHOTOGRAPH OF MODEL HM
HELIUM INJECTION; Γ = .0010

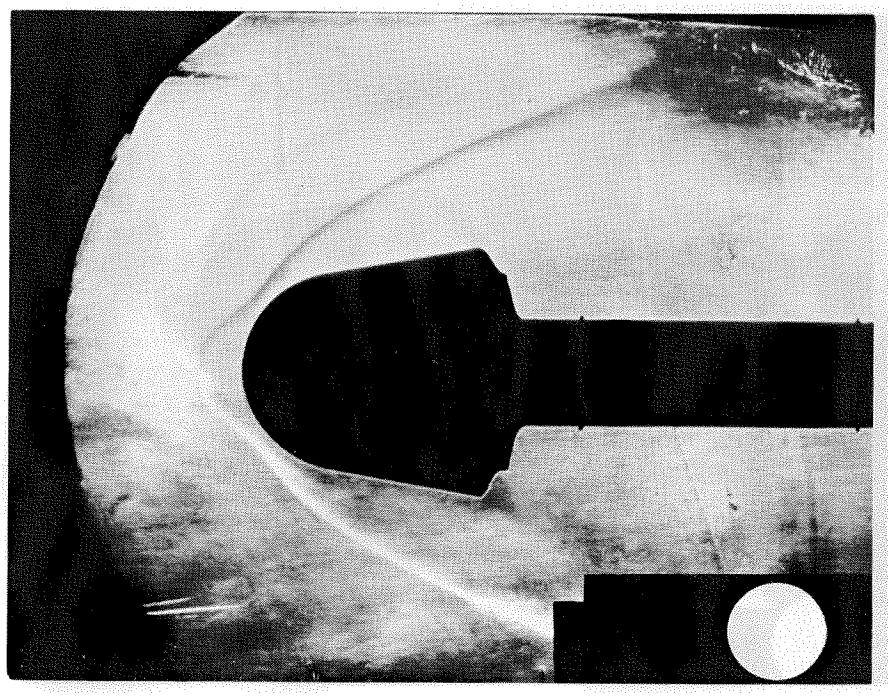

FIG. 18
SCHLIEREN PHOTOGRAPH OF MODEL HM
HELIUM INJECTION; Γ = .0064

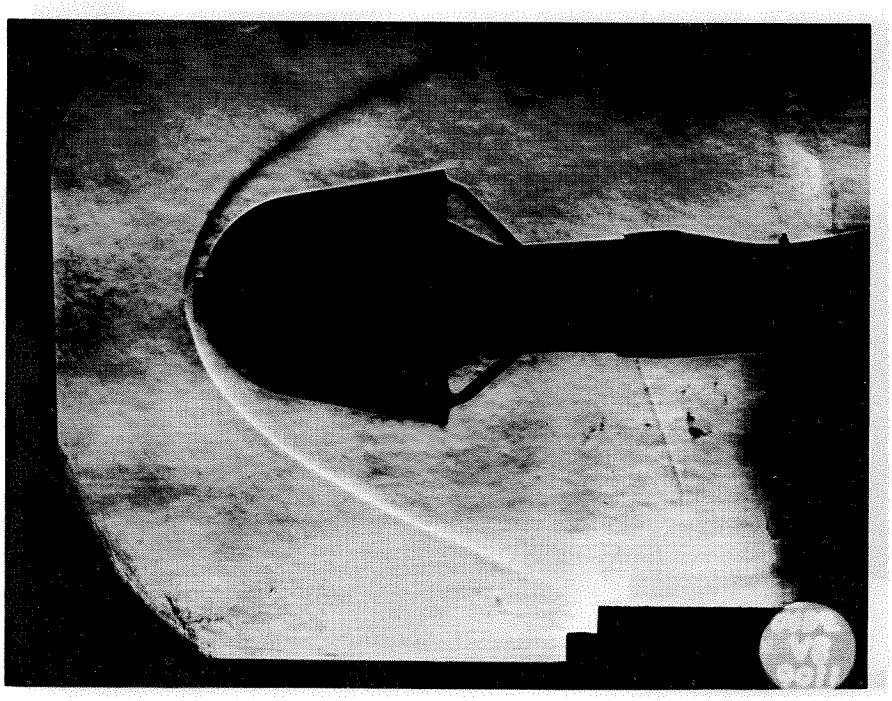

FIG. 19
SCHLIEREN PHOTOGRAPH OF MODEL HM + CA
NITROGEN INJECTION; Γ = .013

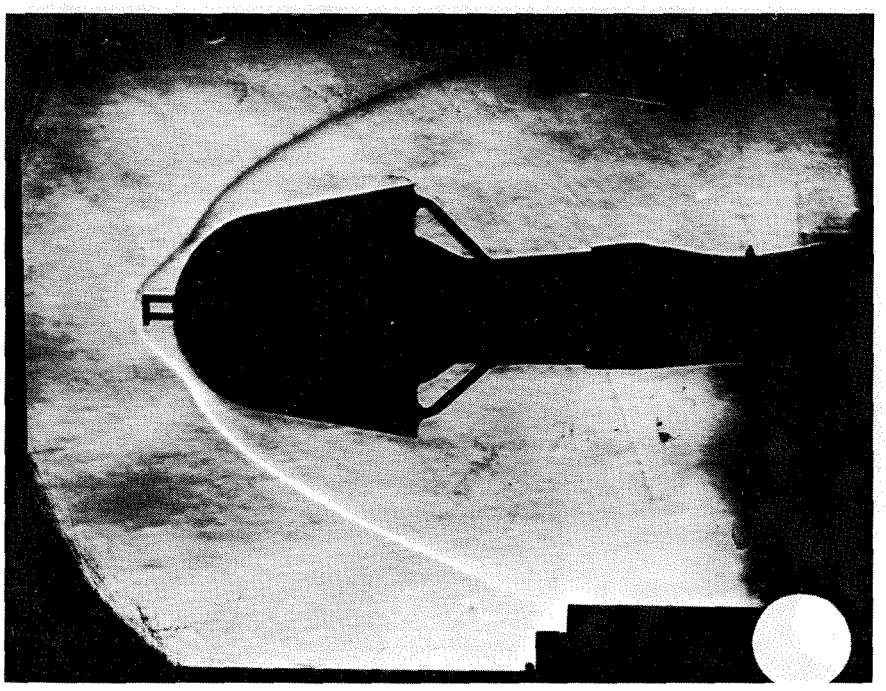

FIG. 20
SCHLIEREN PHOTOGRAPH OF MODEL HM + CC
NITROGEN INJECTION; $\Gamma = .013$

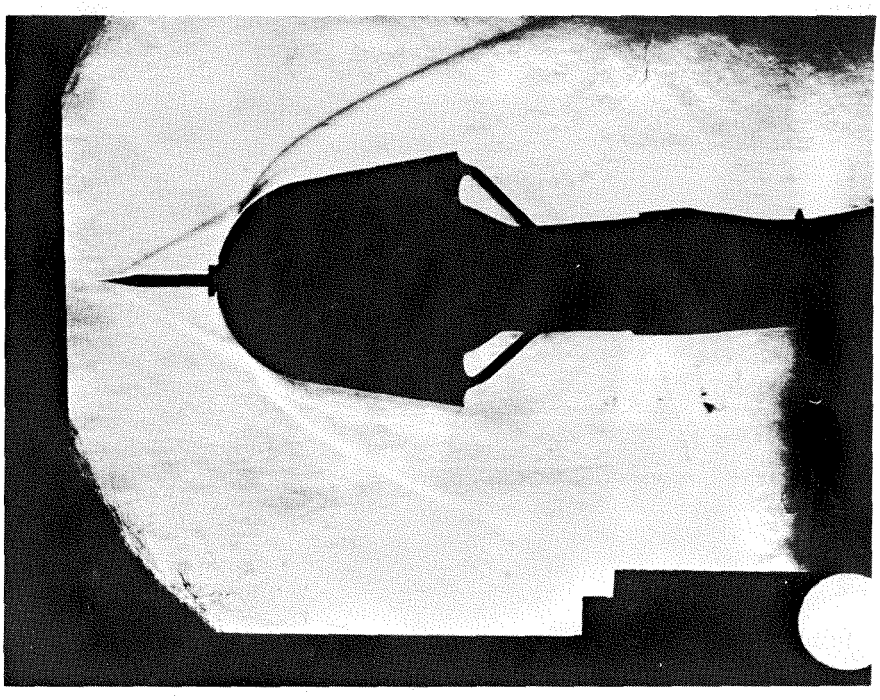

FIG. 21
SCHLIEREN PHOTOGRAPH OF MODEL HM + CA + S I
$\Gamma = 0$

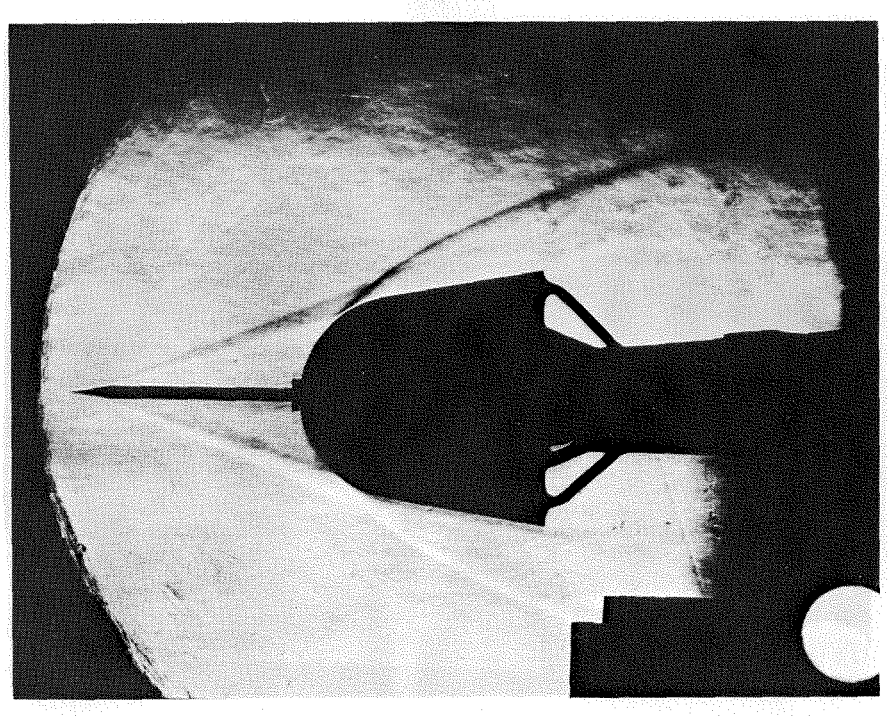

FIG. 22

SCHLIEREN PHOTOGRAPH OF MODEL HM + CA + S II

$\Gamma = 0$

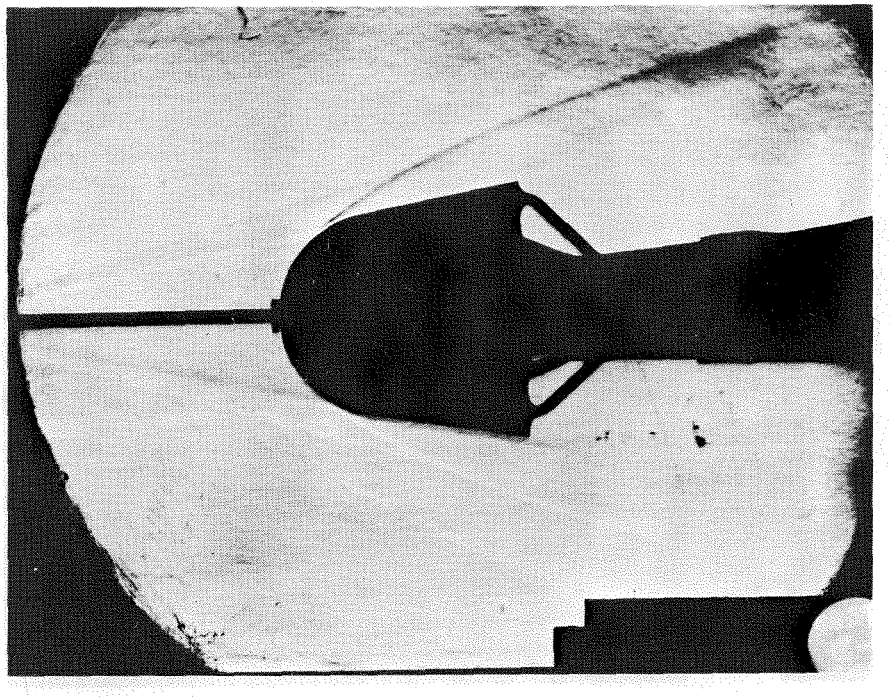

FIG. 23

SCHLIEREN PHOTOGRAPH OF MODEL HM + CA + S III

$\Gamma = 0$

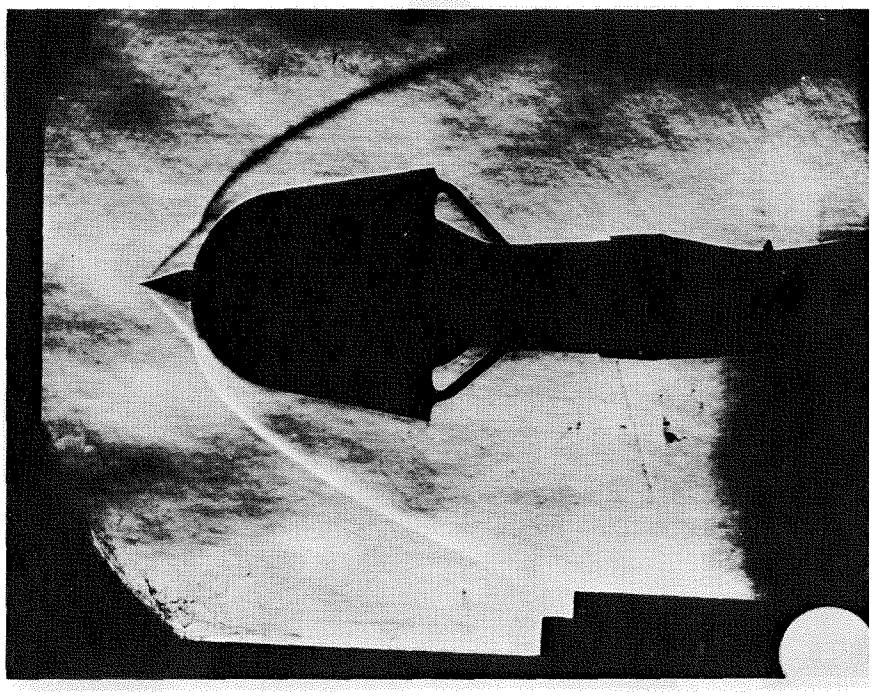

FIG. 24

SCHLIEREN PHOTOGRAPH OF MODEL HM + CA + S IV

$\Gamma = 0$

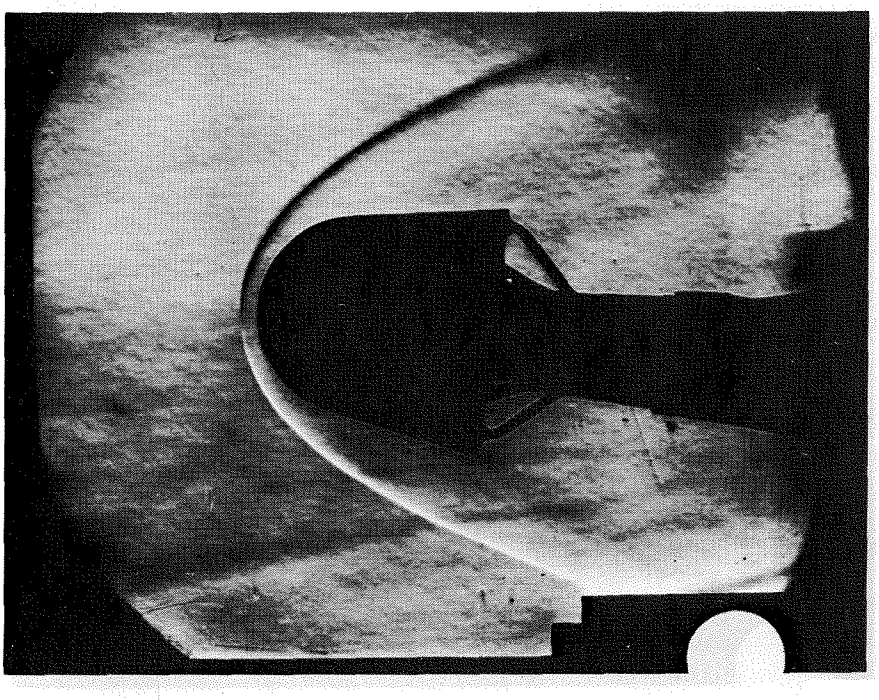

FIG. 25

SCHLIEREN PHOTOGRAPH OF MODEL HM

$\Gamma = 0$; $\alpha = 8^{\circ}$

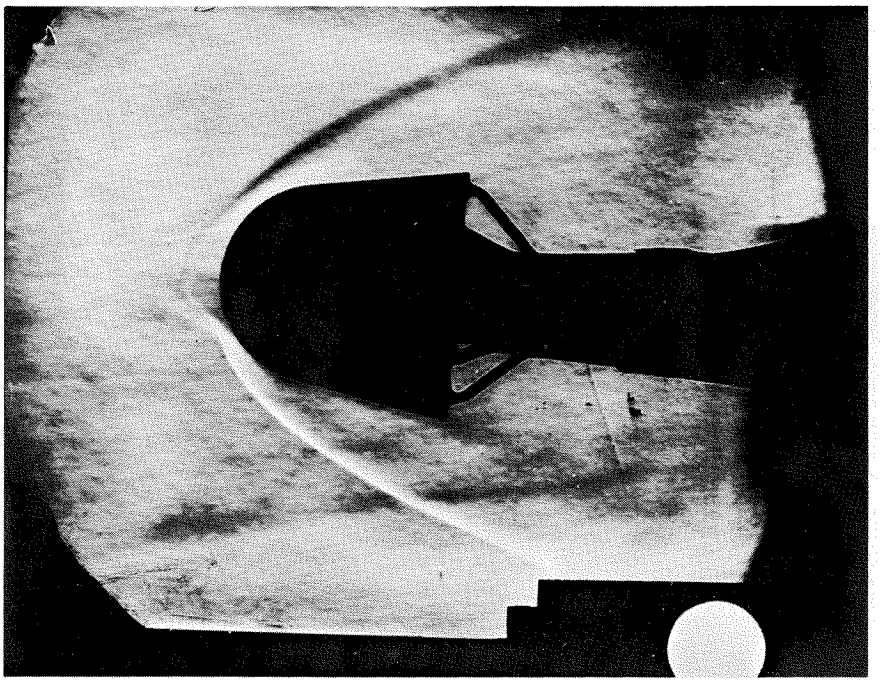

FIG. 26
SCHLIEREN PHOTOGRAPH OF MODEL HM
HELIUM INJECTION; $\Gamma = .0064$; $\alpha = 4^{\circ}$

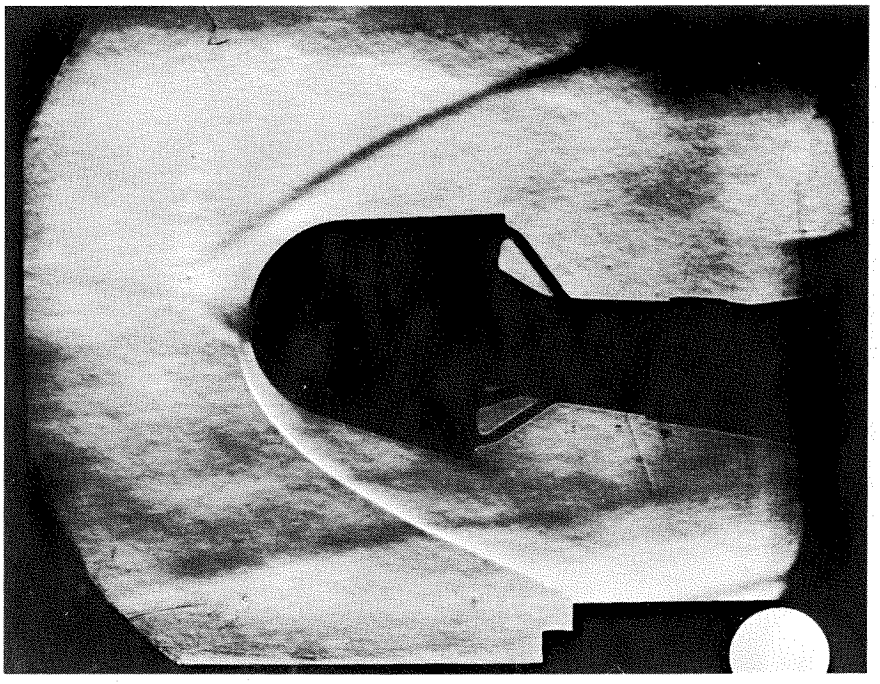

FIG. 27
SCHLIEREN PHOTOGRAPH OF MODEL HM
HELIUM INJECTION; $\Gamma = .0064$; $\alpha = 8^{\circ}$

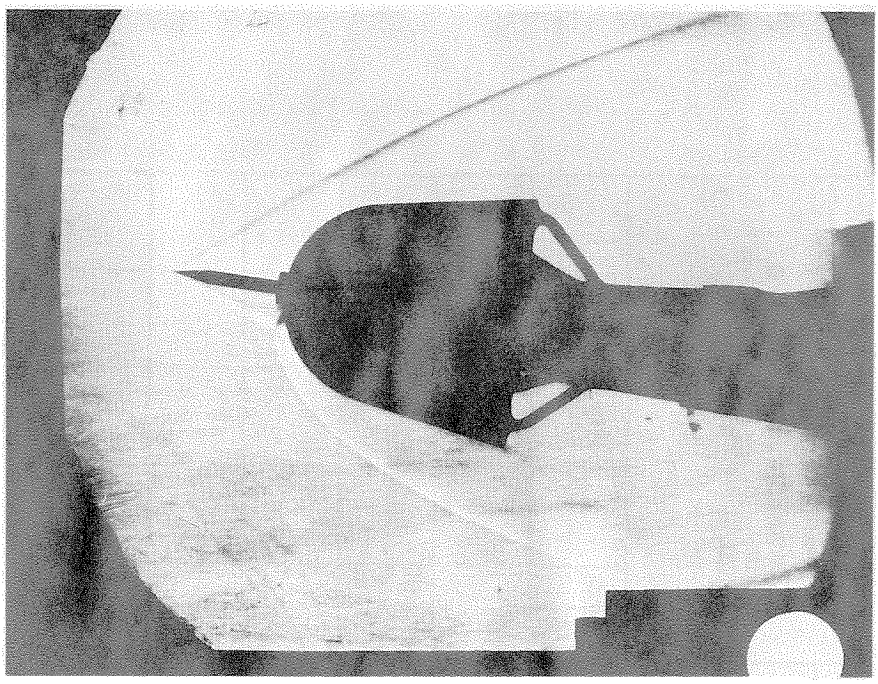

FIG. 28

SCHLIEREN PHOTOGRAPH OF MODEL HM + CA + S I

$\Gamma = 0; \alpha = 8^{\circ}$

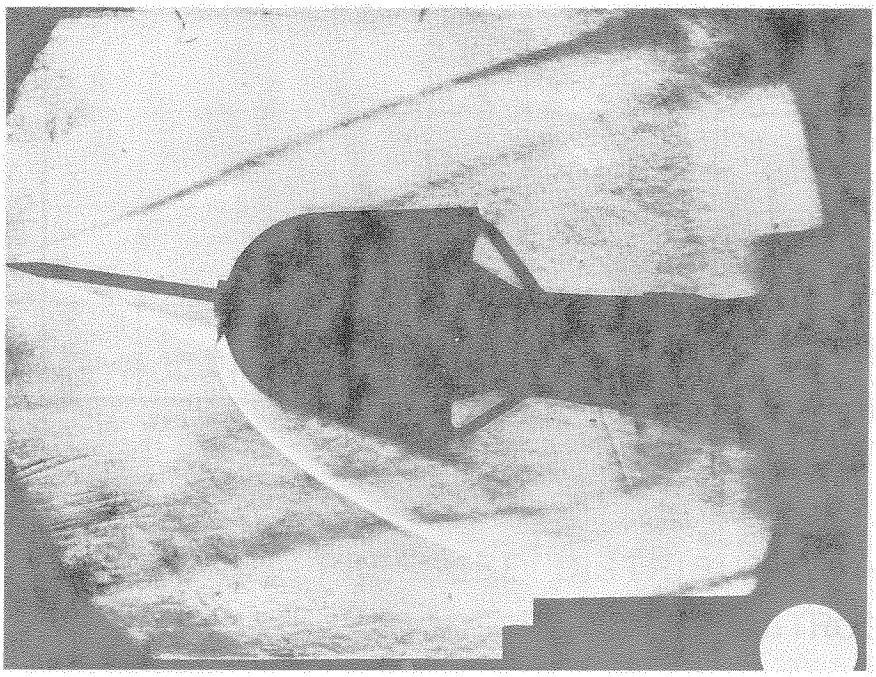

FIG. 29

SCHLIEREN PHOTOGRAPH OF MODEL HM + CA + S II

$\Gamma = 0; \alpha = 8^{\circ}$

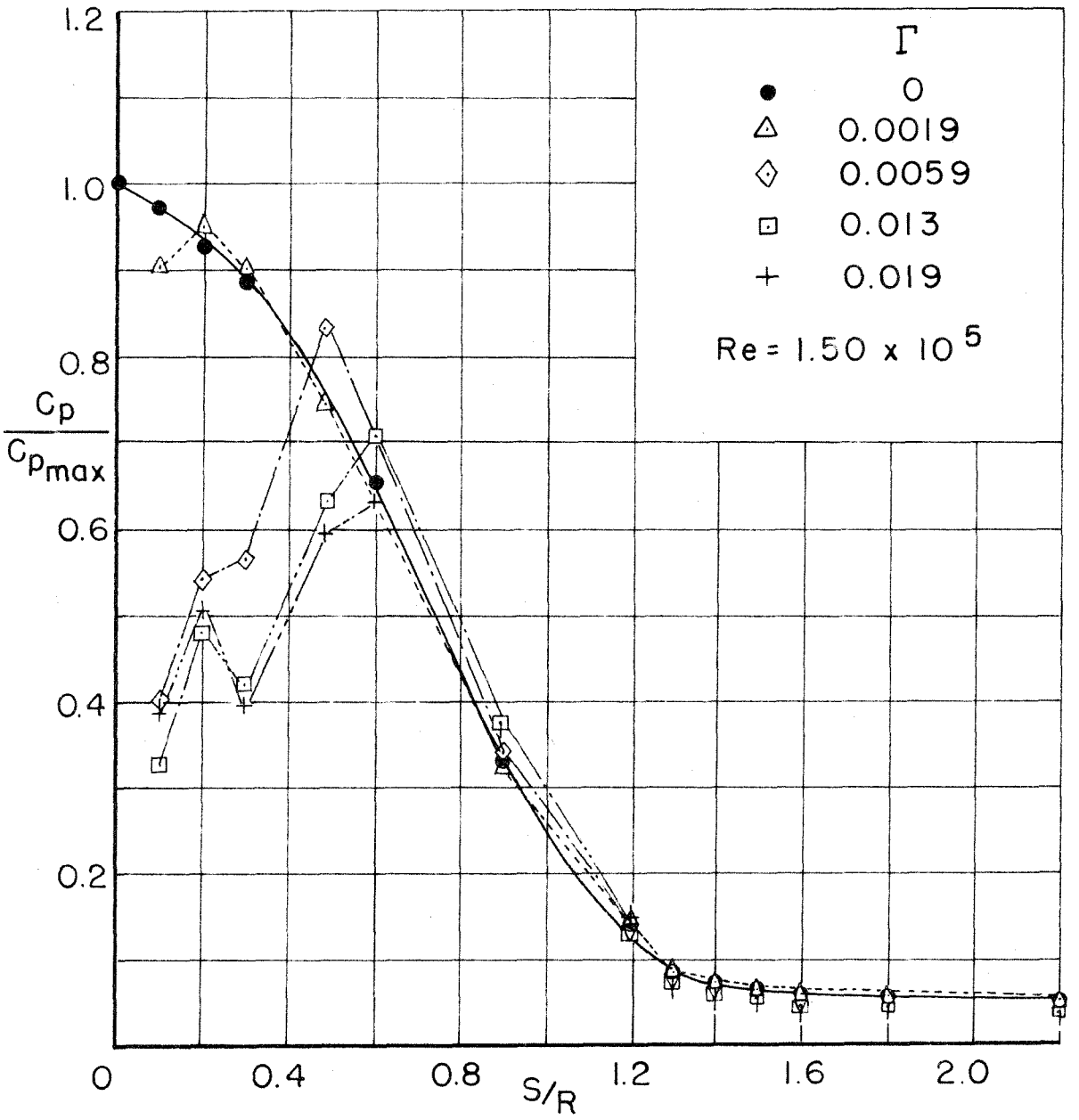

FIG.30-SURFACE PRESSURE DISTRIBUTION ON MODEL HM WITH VARIOUS RATES OF NITROGEN INJECTION

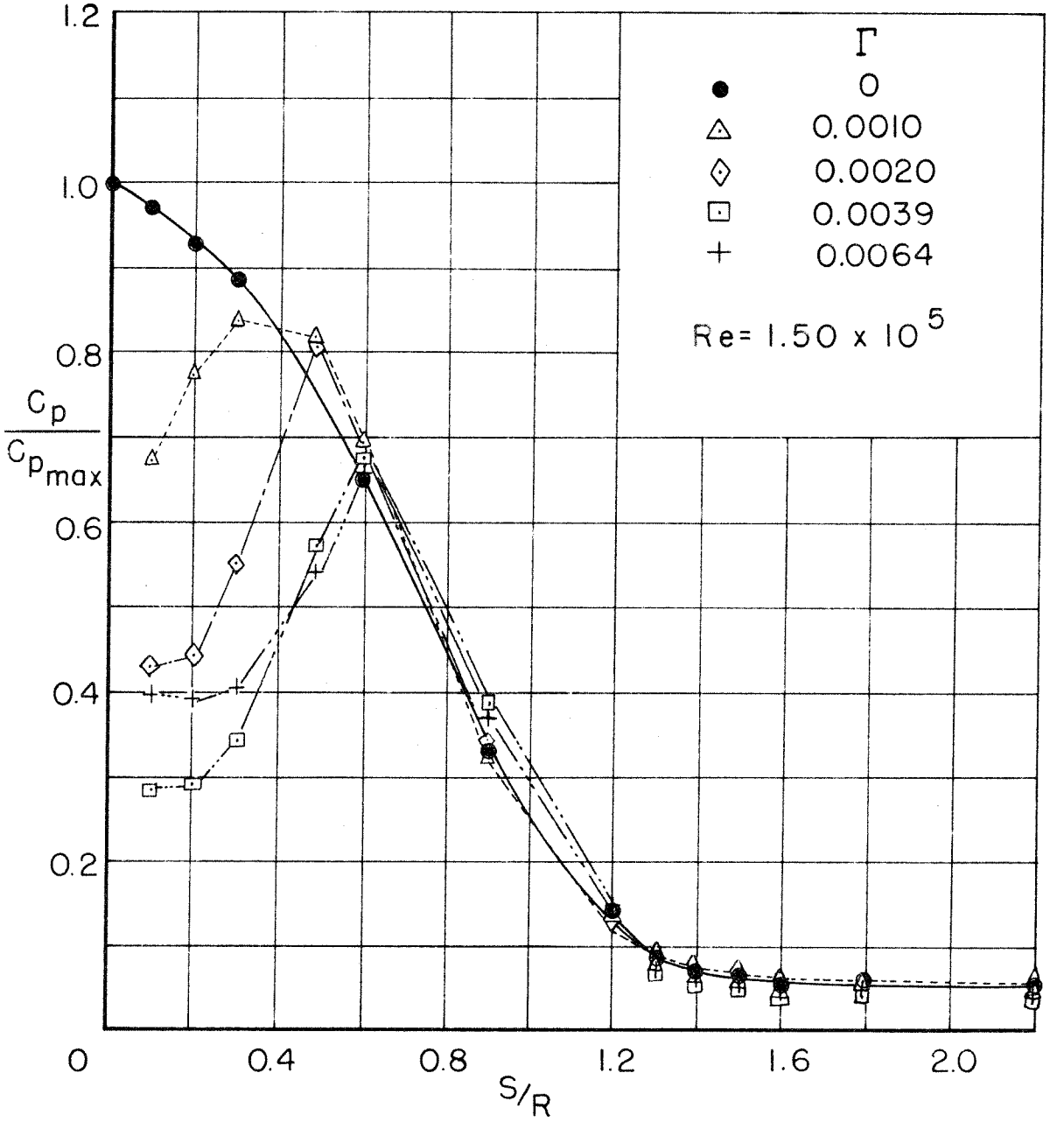

FIG.31—SURFACE PRESSURE DISTRIBUTION ON MODEL HM WITH VARIOUS RATES OF HELIUM INJECTION

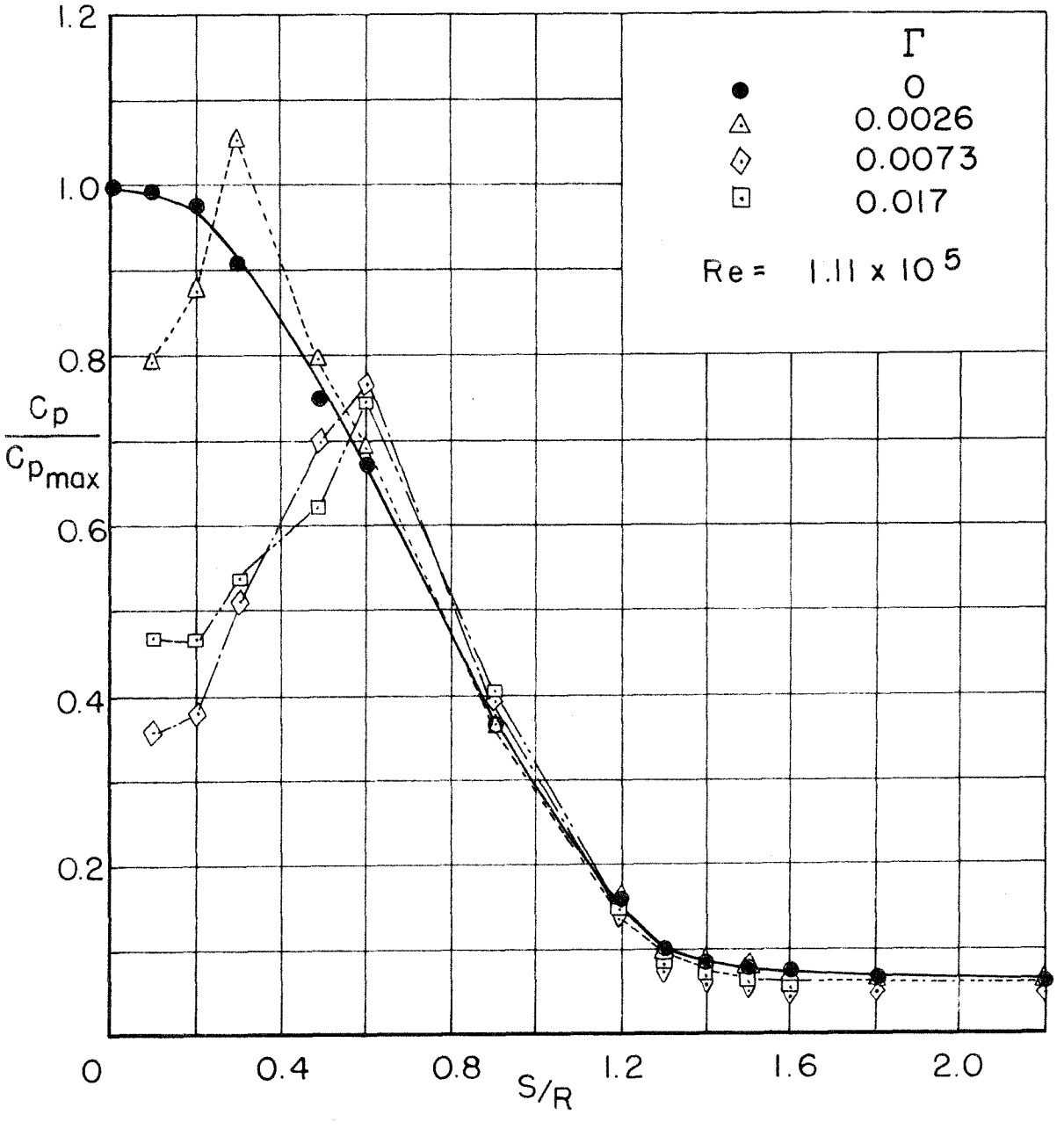

FIG. 32 - SURFACE PRESSURE DISTRIBUTION ON MODEL HM WITH VARIOUS RATES OF NITROGEN INJECTION

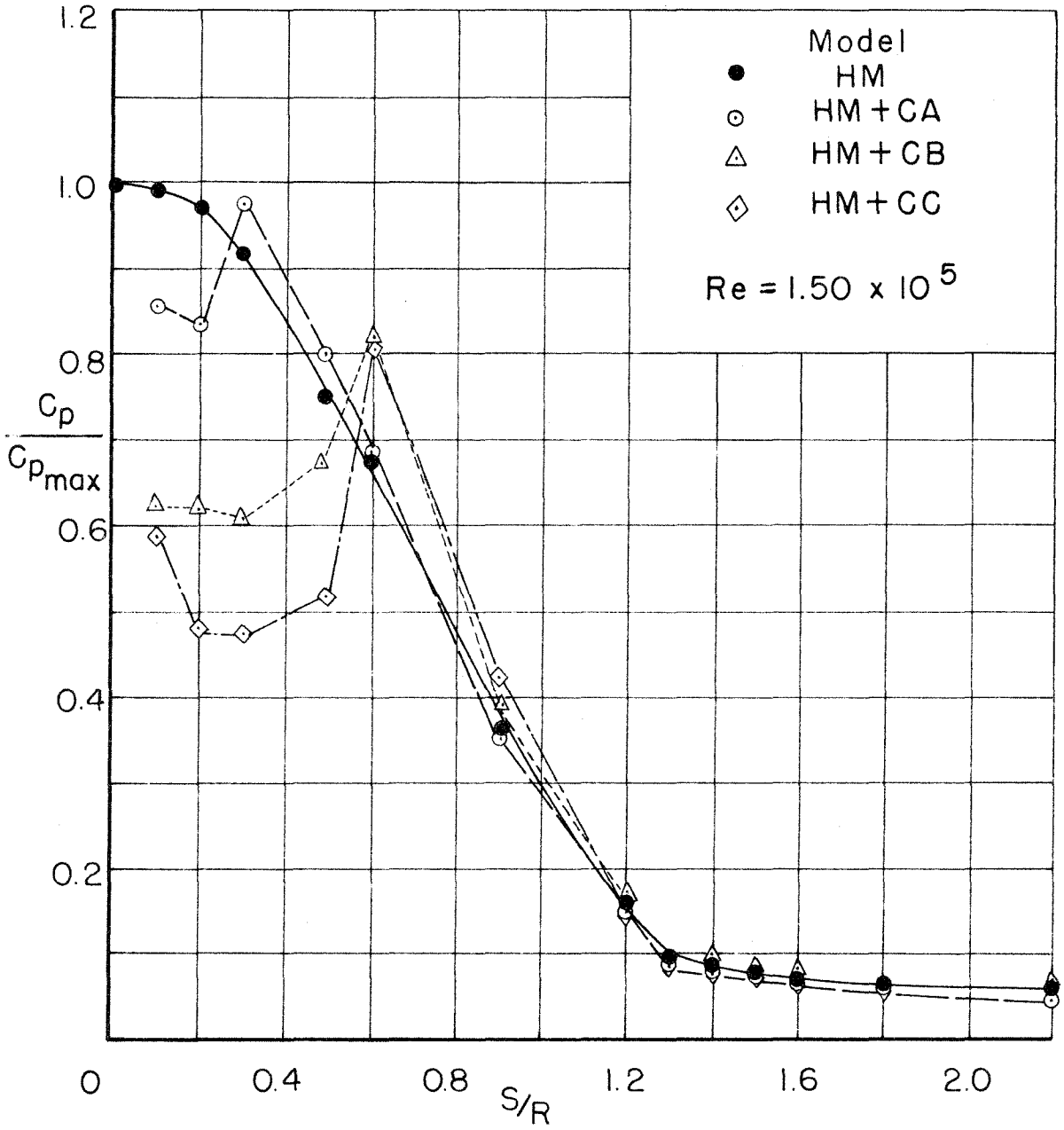

FIG. 33-SURFACE PRESSURE DISTRIBUTION ON MODEL HM WITH VARIOUS DEFLECTOR CAPS. NO INJECTION.

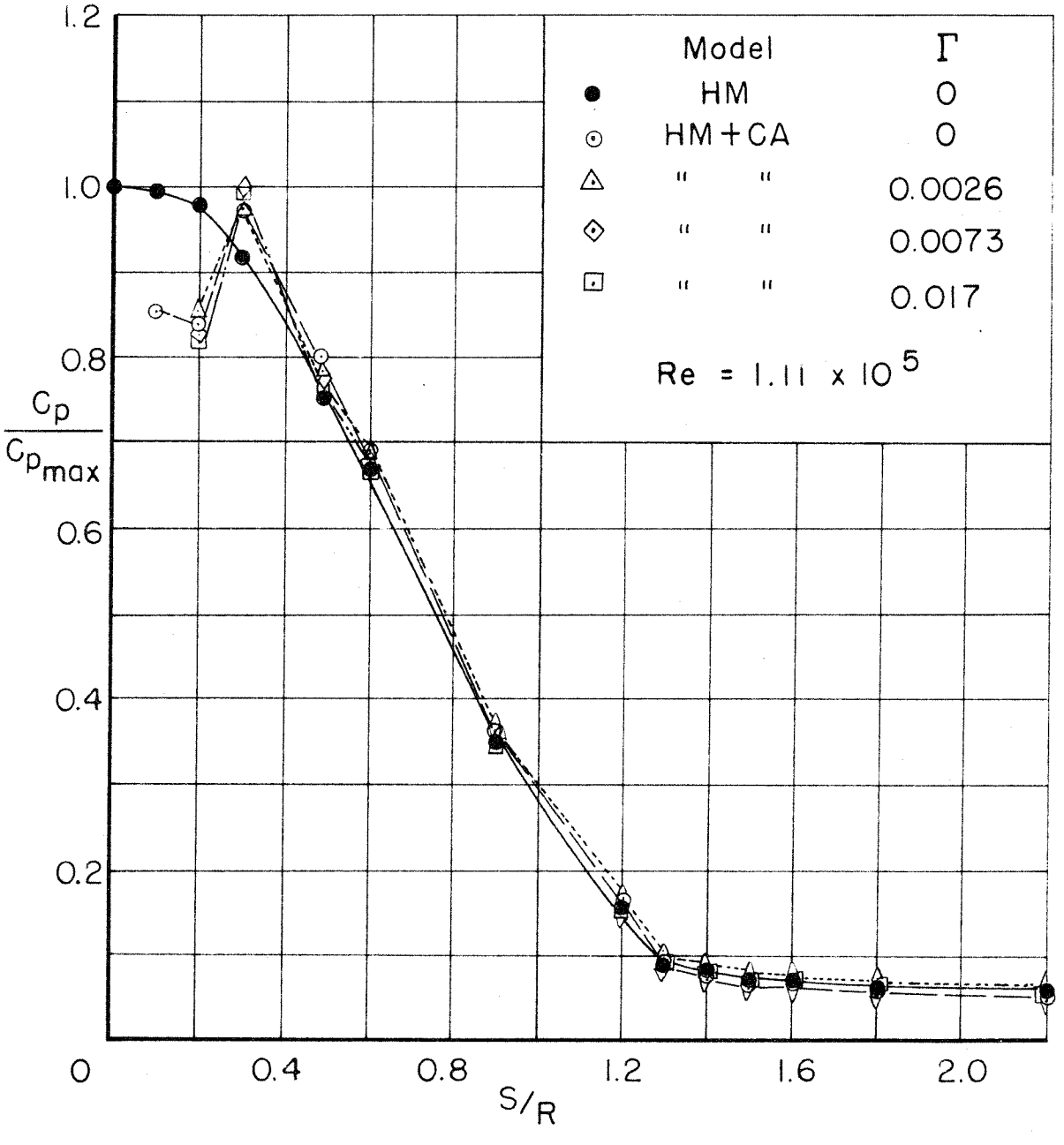

FIG. 34-SURFACE PRESSURE DISTRIBUTION ON MODEL HM + CA WITH VARIOUS RATES OF NITROGEN INJECTION

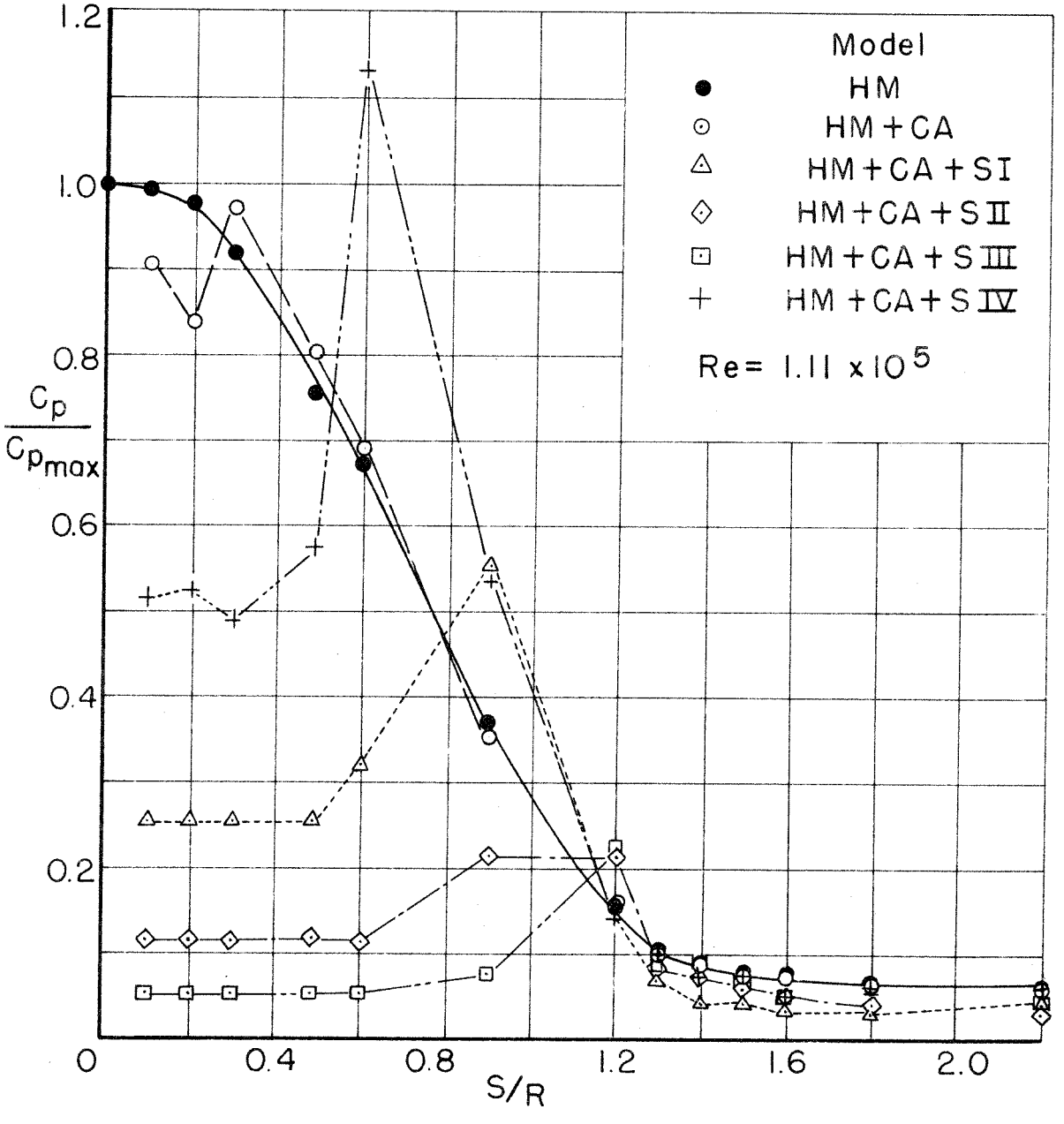

FIG. 35 – SURFACE PRESSURE DISTRIBUTION ON MODEL HM + CA WITH VARIOUS SPIKES. NO INJECTION

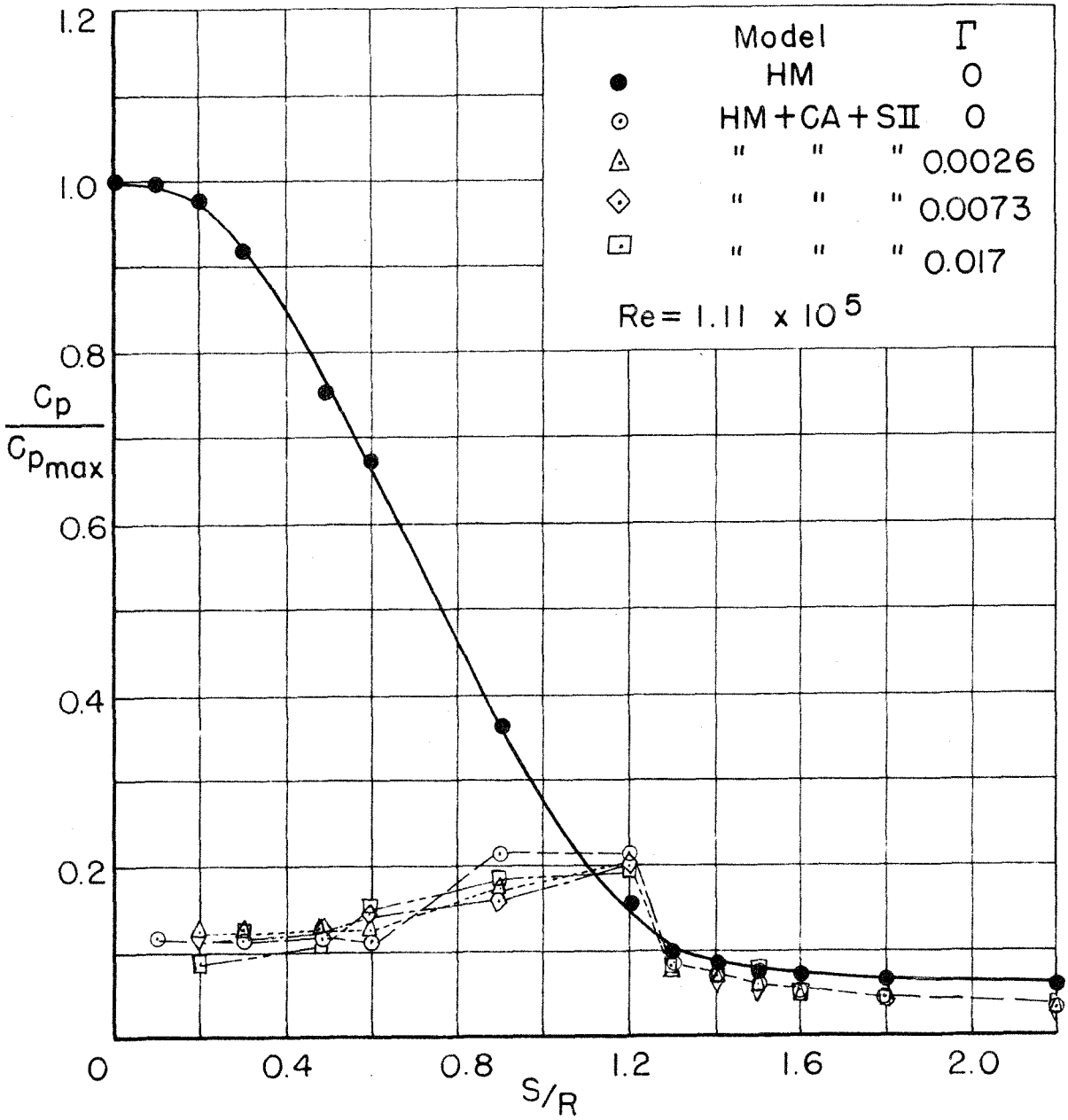

FIG. 36 - SURFACE PRESSURE DISTRIBUTION ON MODEL HM + CA + S II WITH VARIOUS RATES OF NITROGEN INJECTION

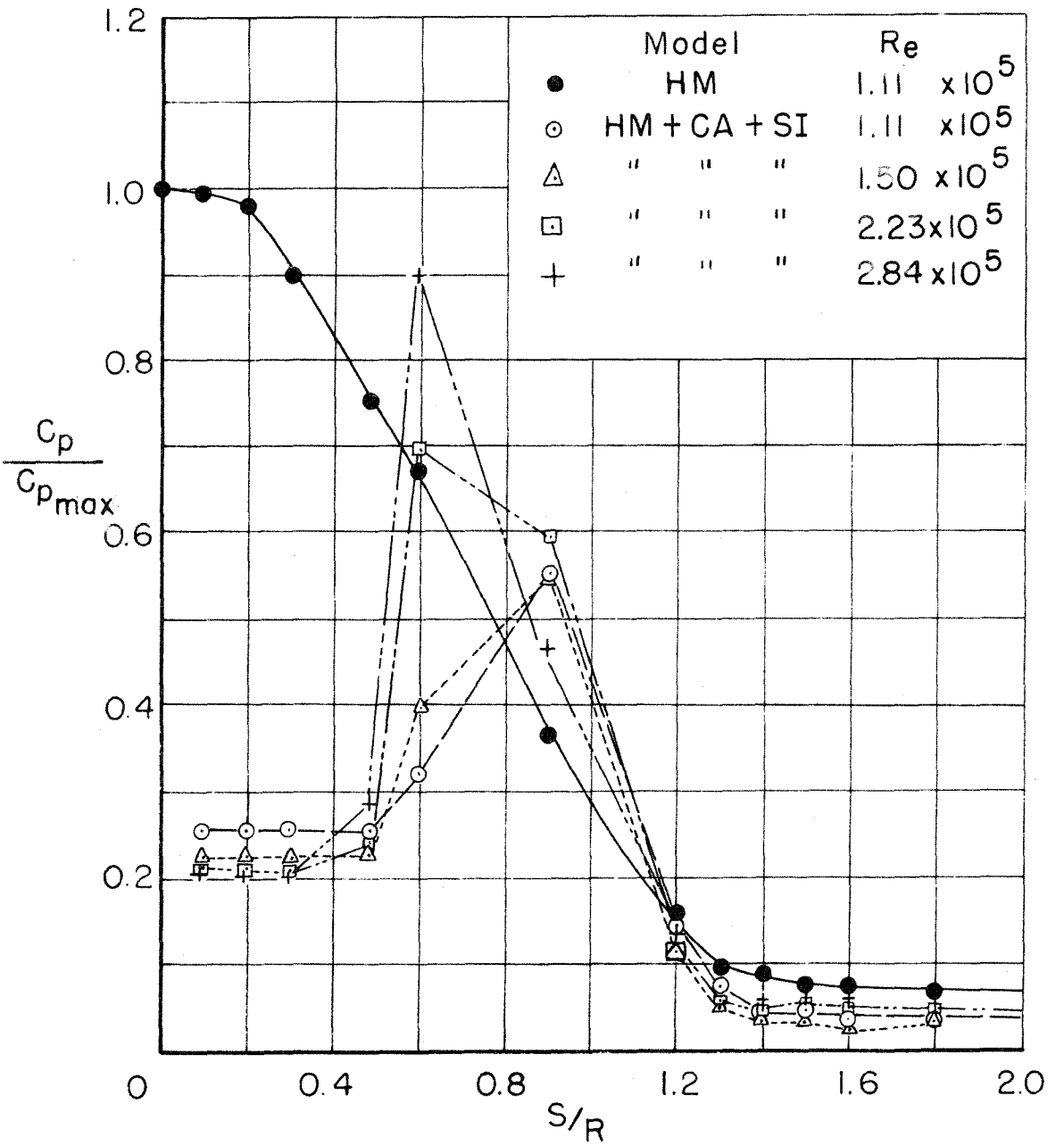

FIG. 37-SURFACE PRESSURE DISTRIBUTION AT VARIOUS REYNOLDS NUMBERS. MODEL HM + CA + SI. NO INJECTION.

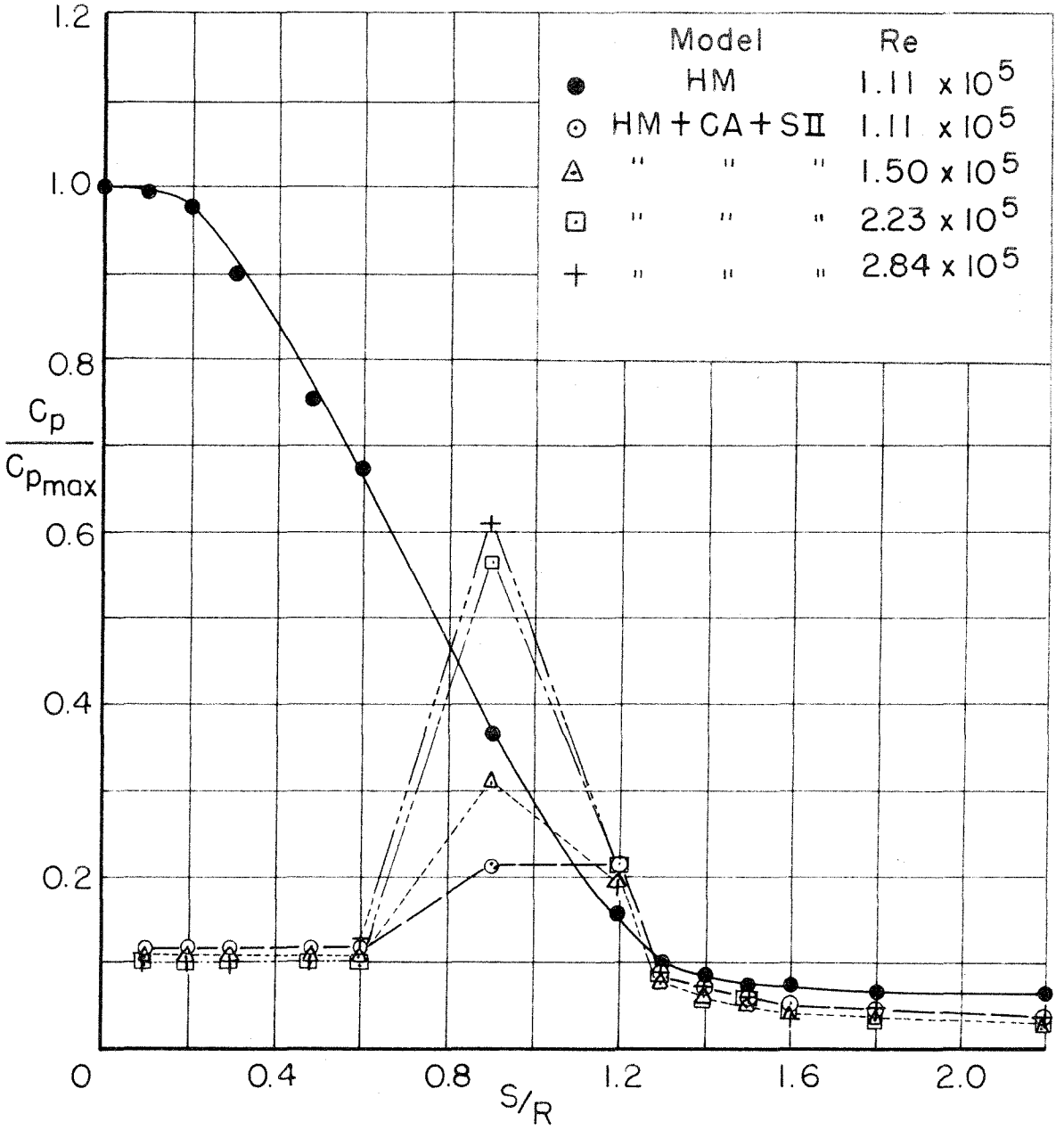

FIG. 38- SURFACE PRESSURE DISTRIBUTION AT VARIOUS REYNOLDS NUMBERS. MODEL HM + CA + S II. NO INJECTION.

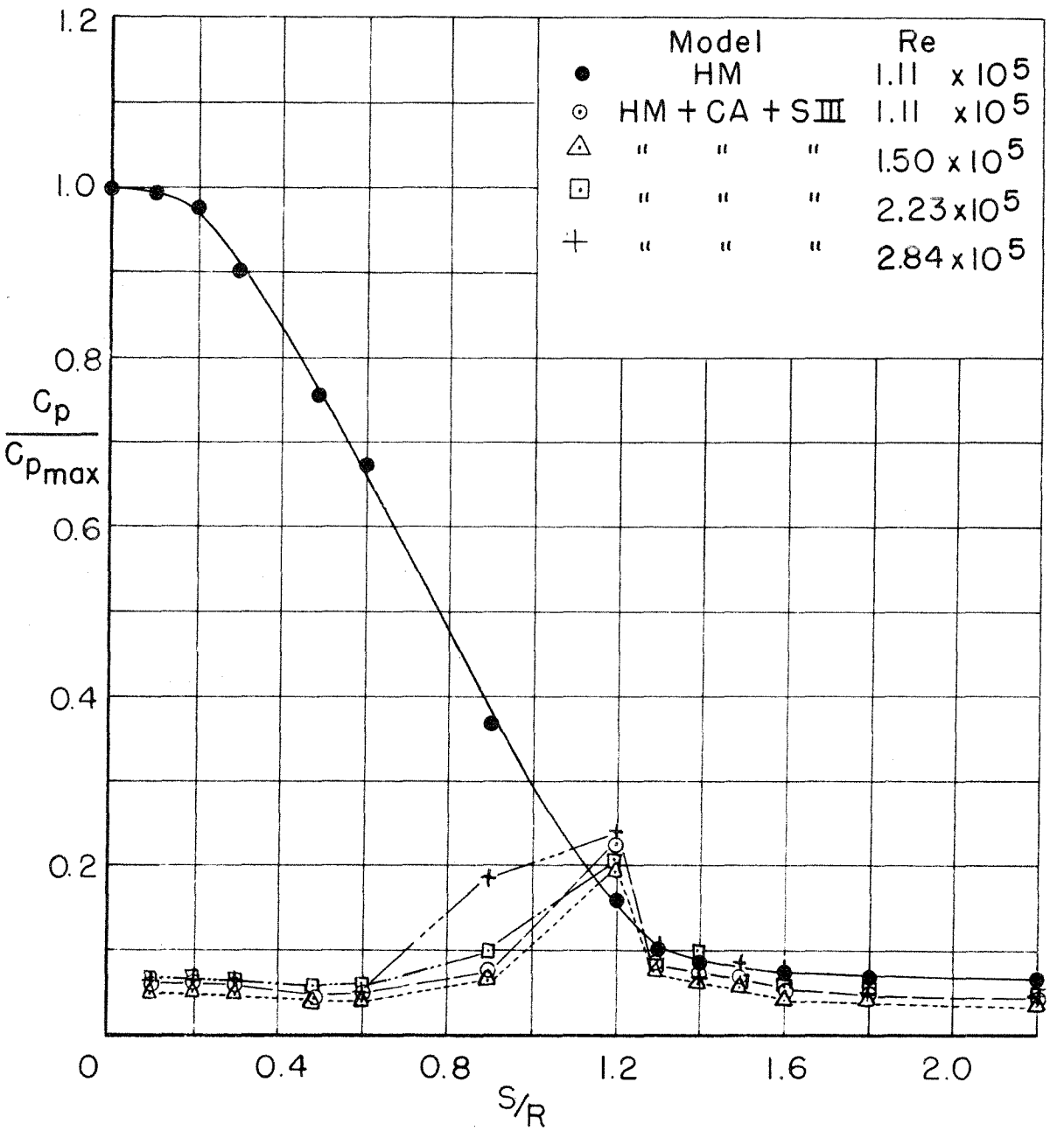

FIG. 39 – SURFACE PRESSURE DISTRIBUTION AT VARIOUS REYNOLDS NUMBERS. MODEL HM + CA + SIII. NO INJECTION.

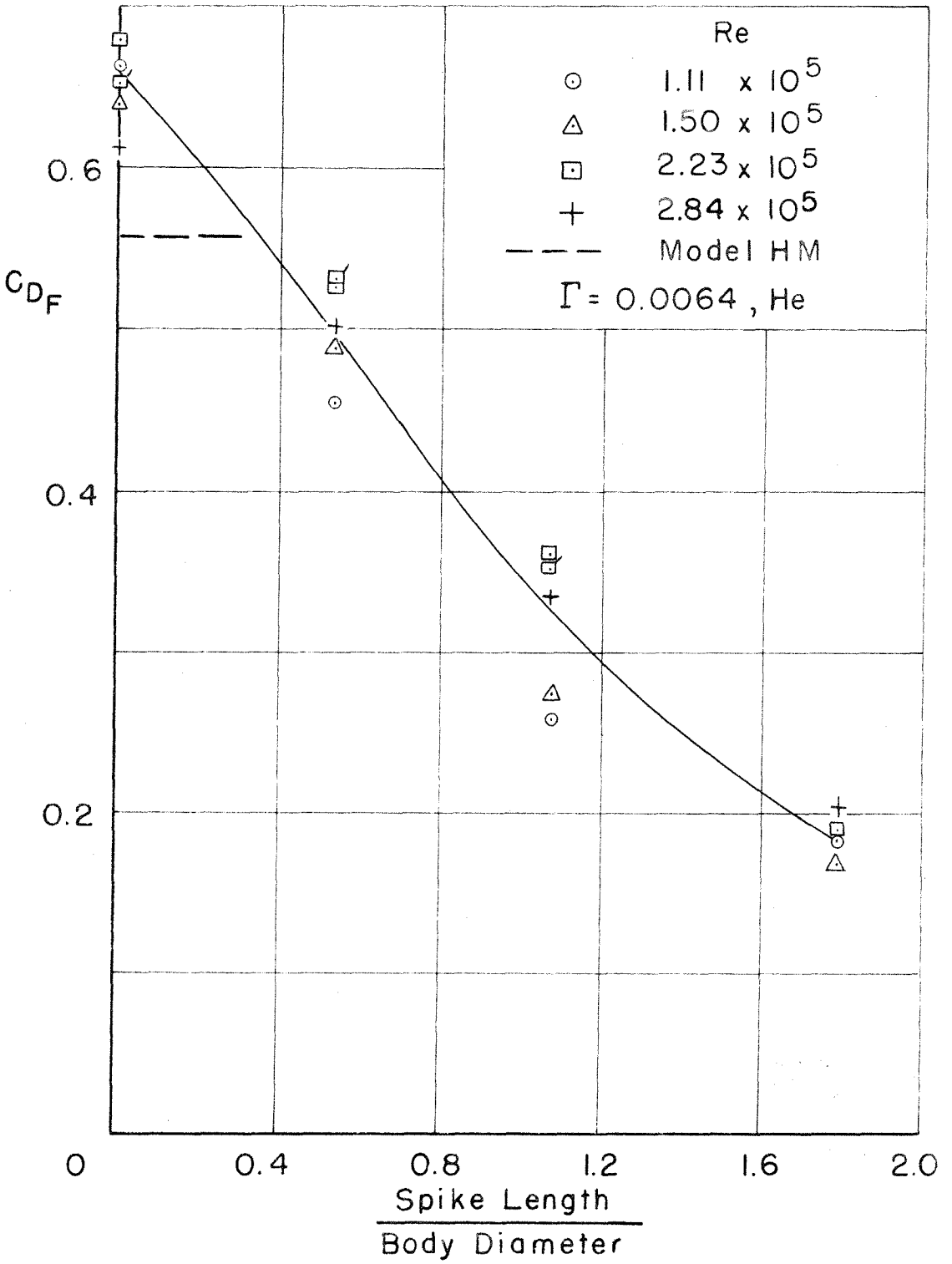

FIG. 40-PRESSURE FOREDRAG ON HEMISPHERE-CONE MODEL WITH SPIKES

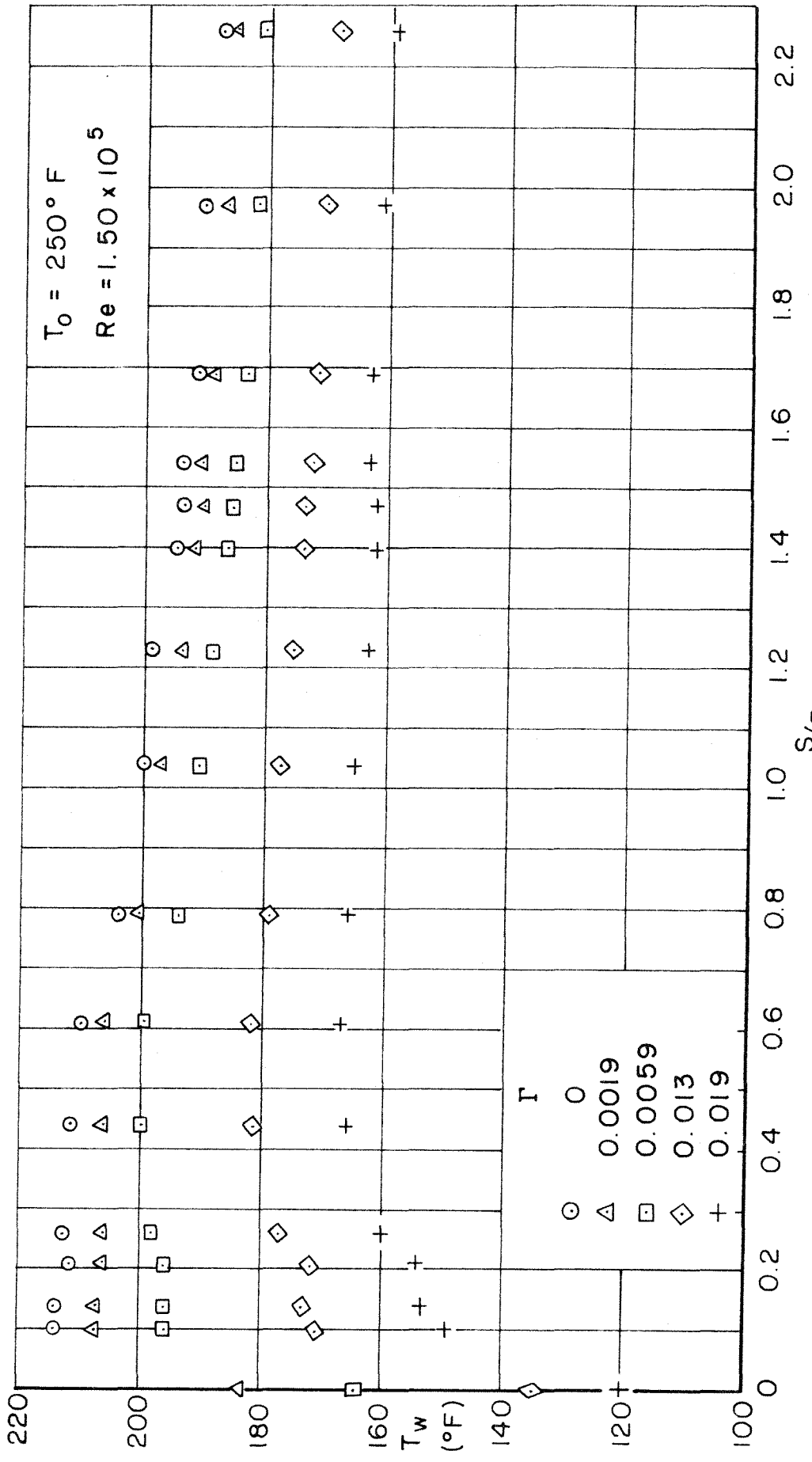

FIG. 41-EQUILIBRIUM WALL TEMPERATURE WITH VARIOUS RATES OF NITROGEN INJECTION, MODEL HM + CA

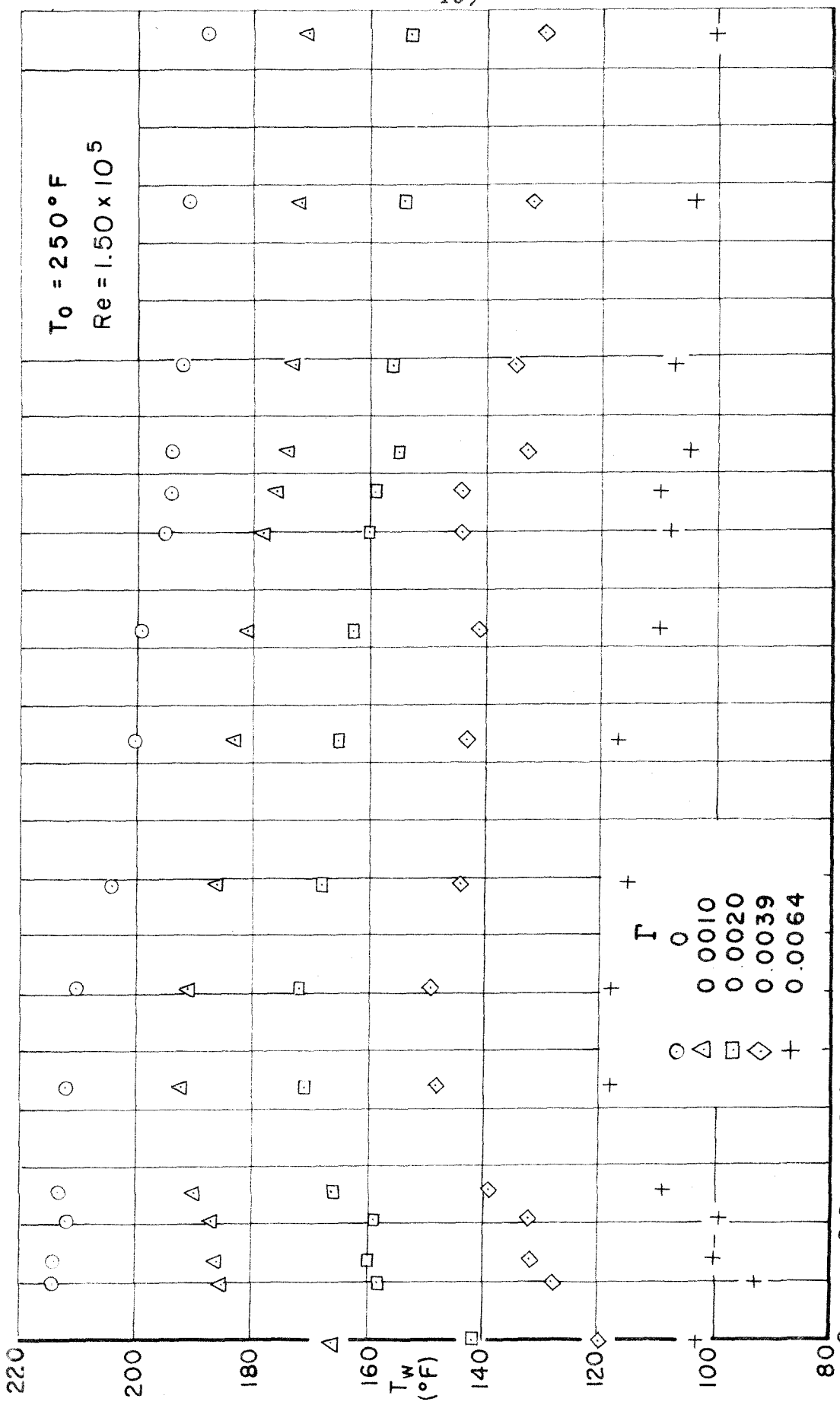

FIG.42- EQUILIBRIUM WALL TEMPERATURE WITH VARIOUS RATES OF HELIUM INJECTION, MODEL HM+CA

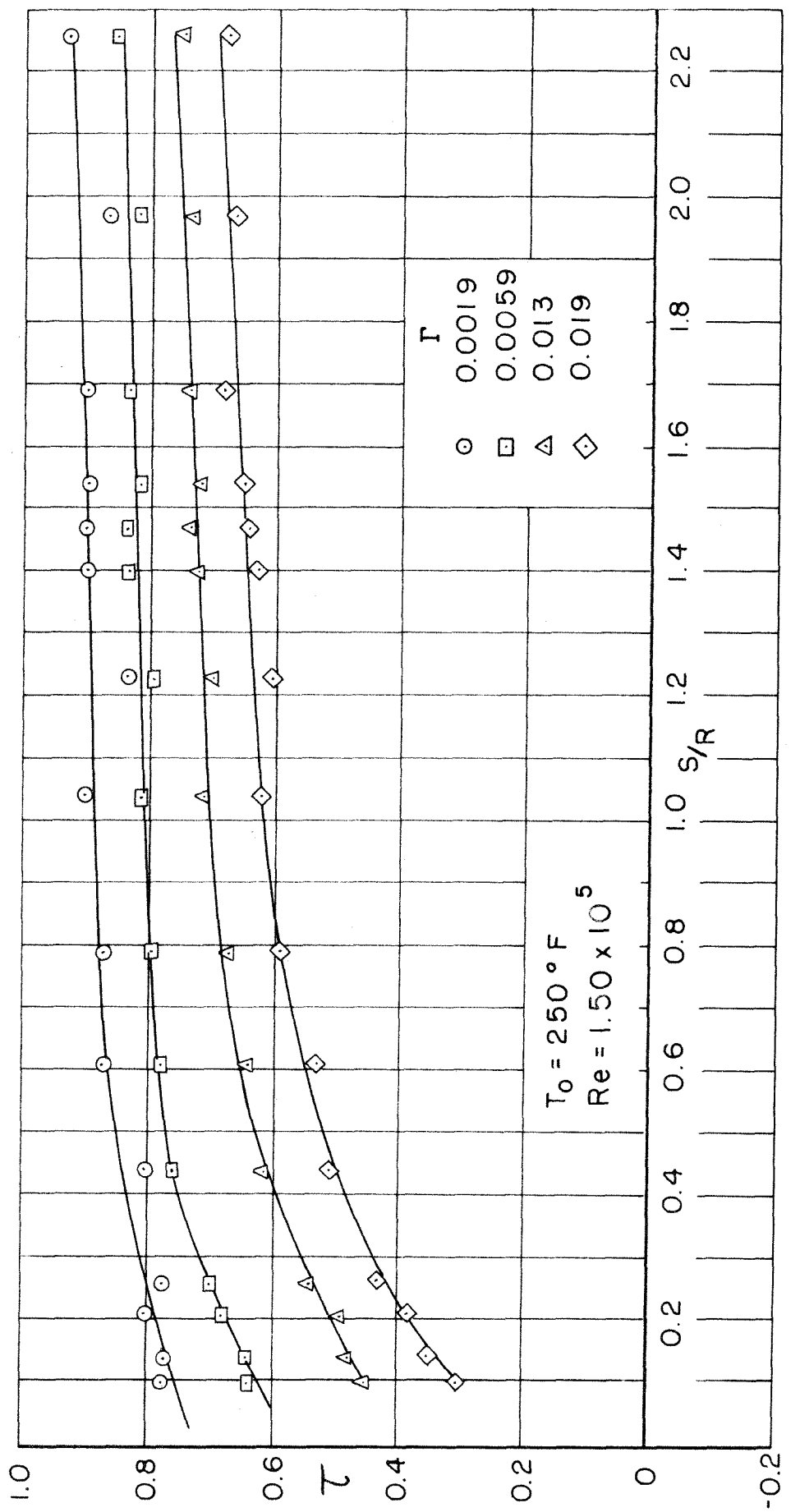

FIG. 43 - NONDIMENSIONAL TEMPERATURE RATIO WITH VARIOUS RATES OF NITROGEN INJECTION, MODEL HM + CA

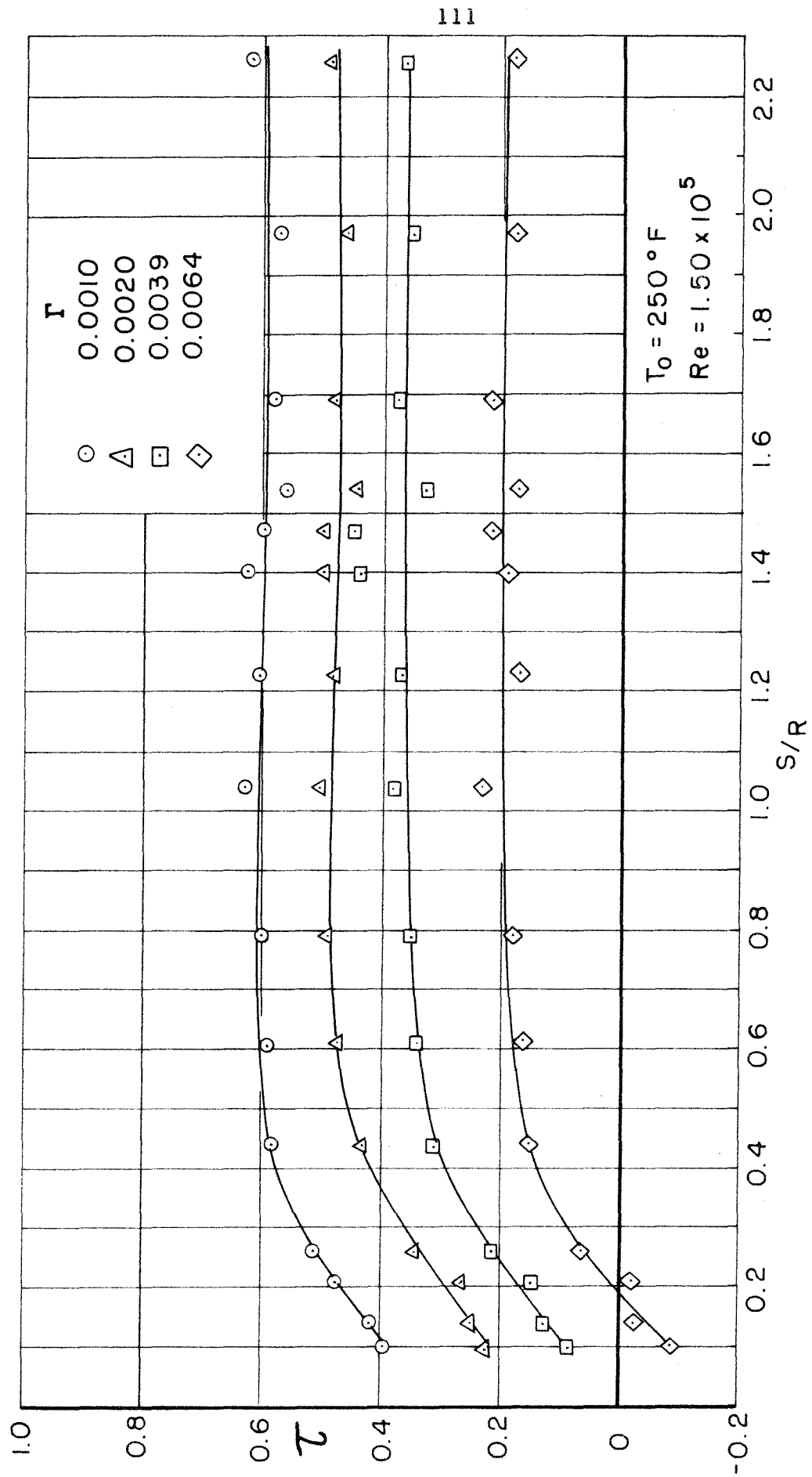

FIG. 44-NONDIMENSIONAL TEMPERATURE RATIO WITH VARIOUS RATES OF HELIUM INJECTION, MODEL HM + CA

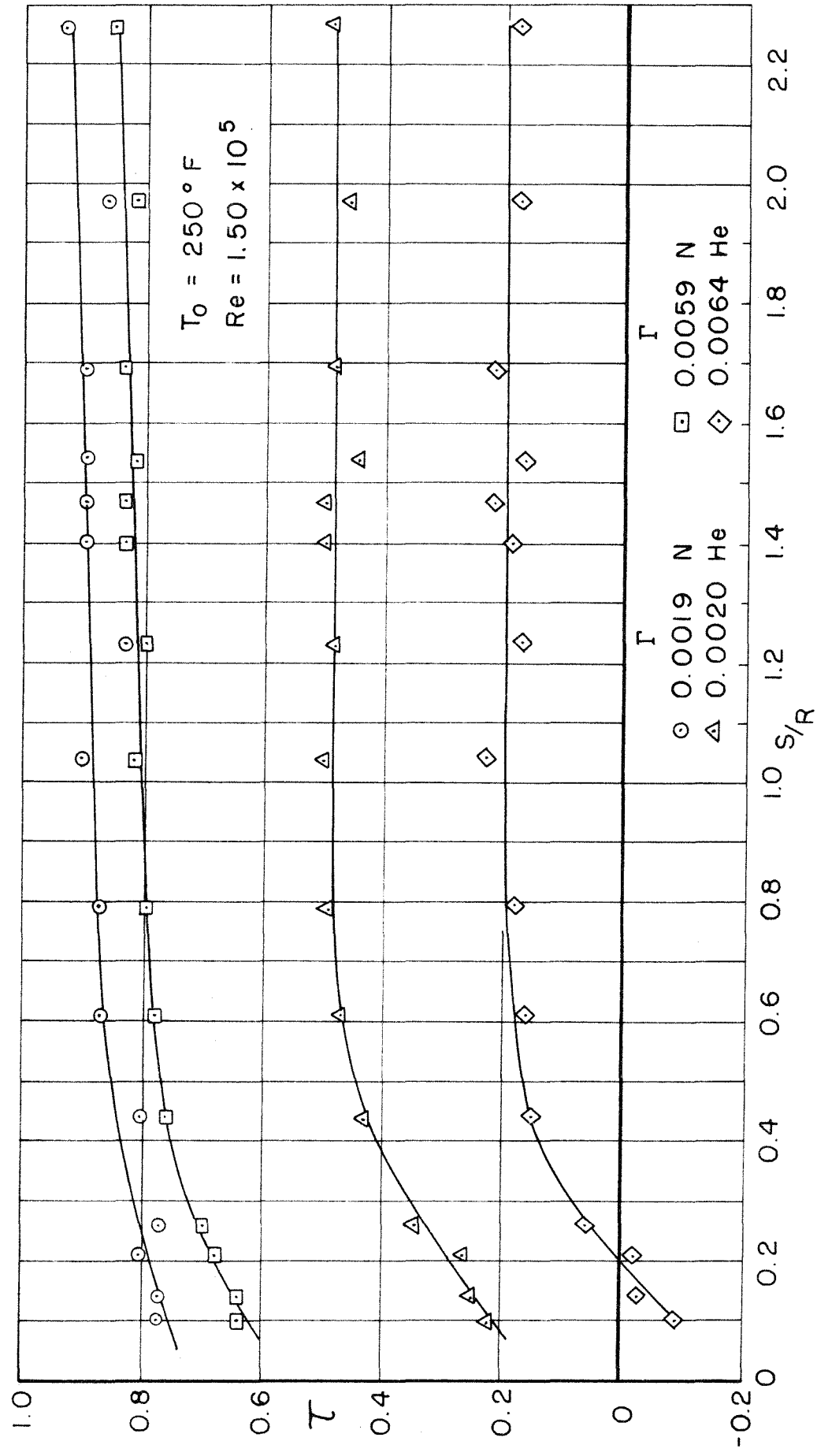

FIG. 45 – NONDIMENSIONAL TEMPERATURE RATIO WITH SAME MASS FLOWS OF NITROGEN AND HELIUM, MODEL HM + CA

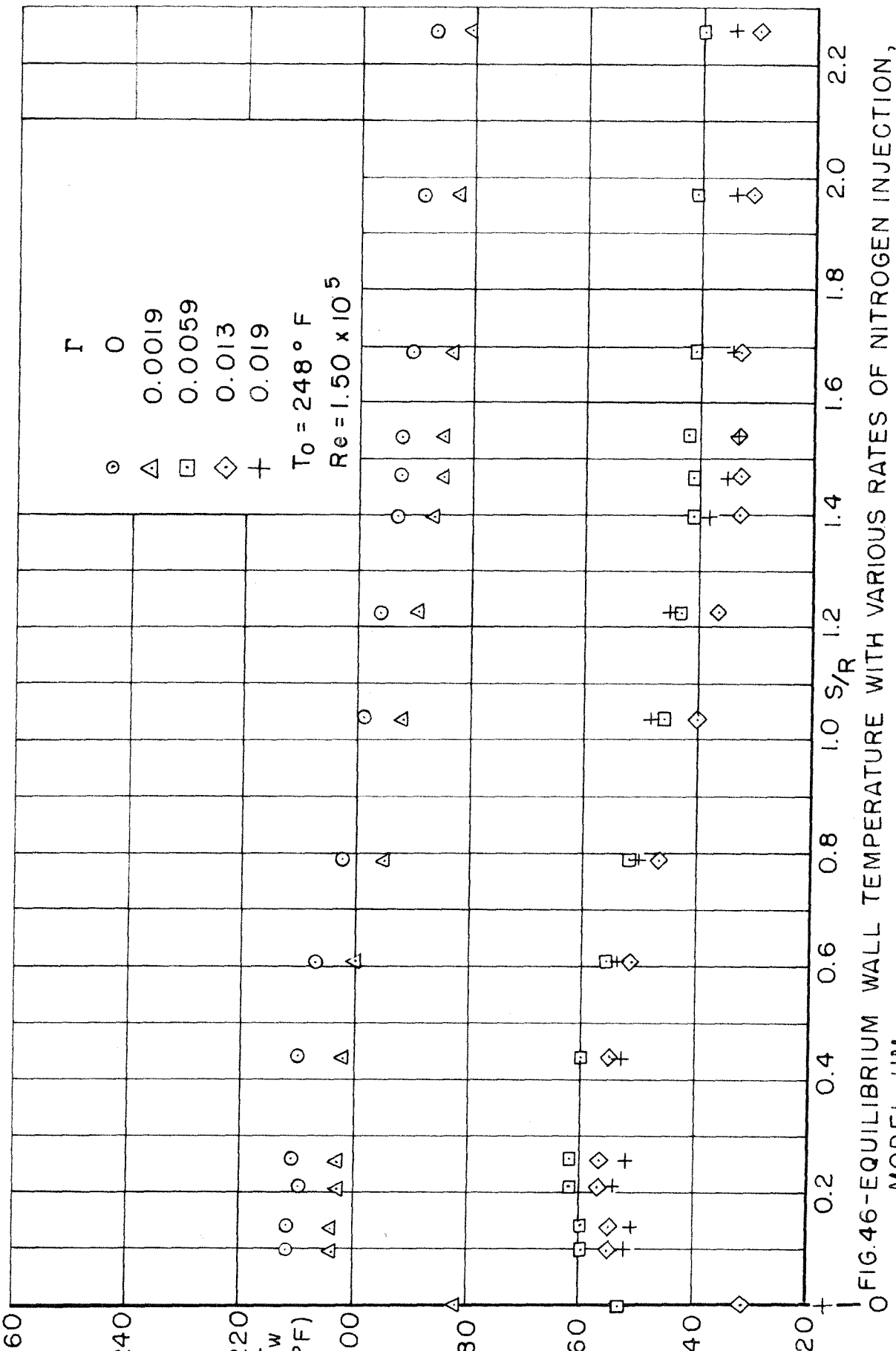

FIG. 46 - EQUILIBRIUM WALL TEMPERATURE WITH VARIOUS RATES OF NITROGEN INJECTION, MODEL HM

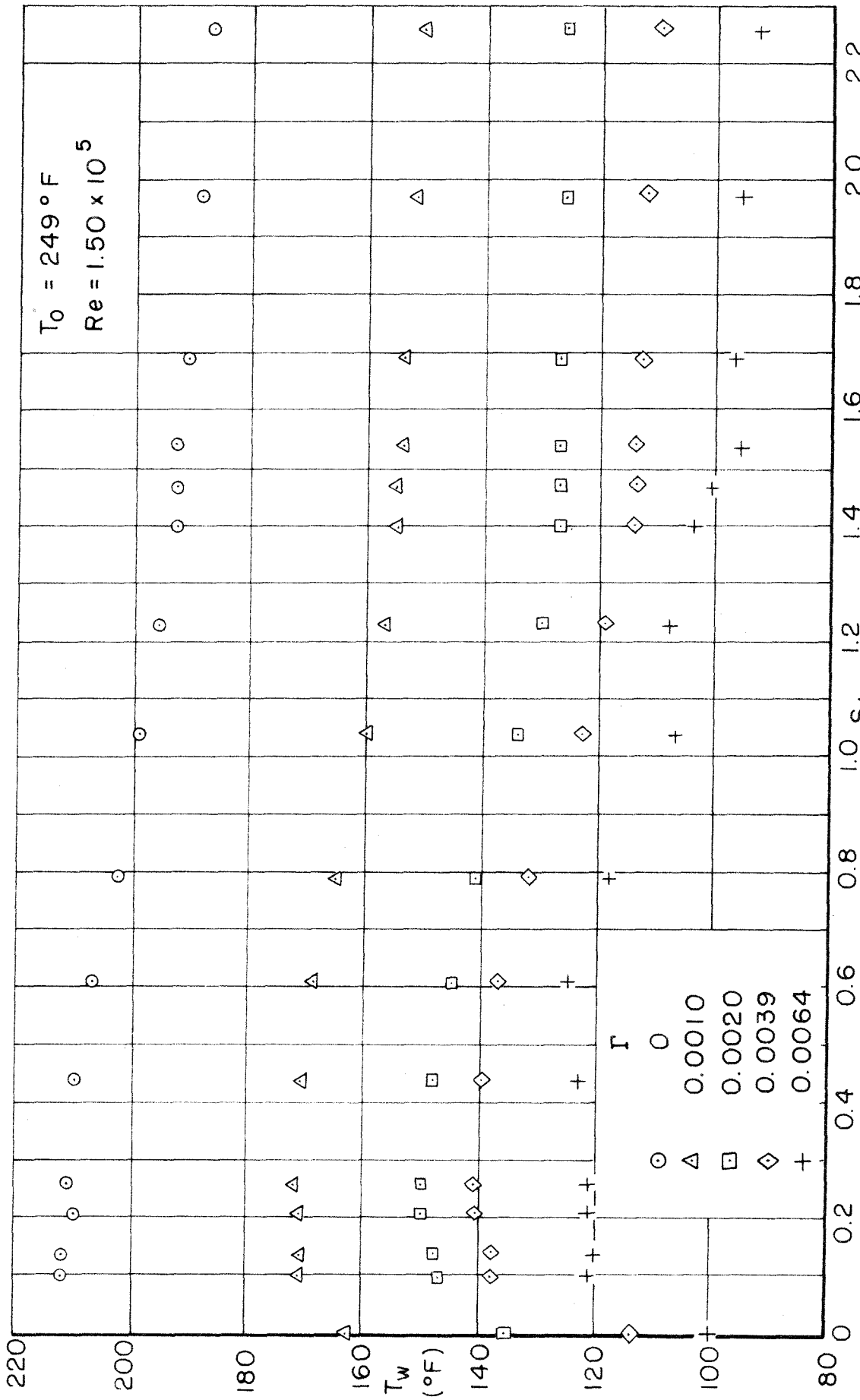

FIG. 47 – EQUILIBRIUM WALL TEMPERATURE WITH VARIOUS RATES OF HELIUM INJECTION, MODEL HM

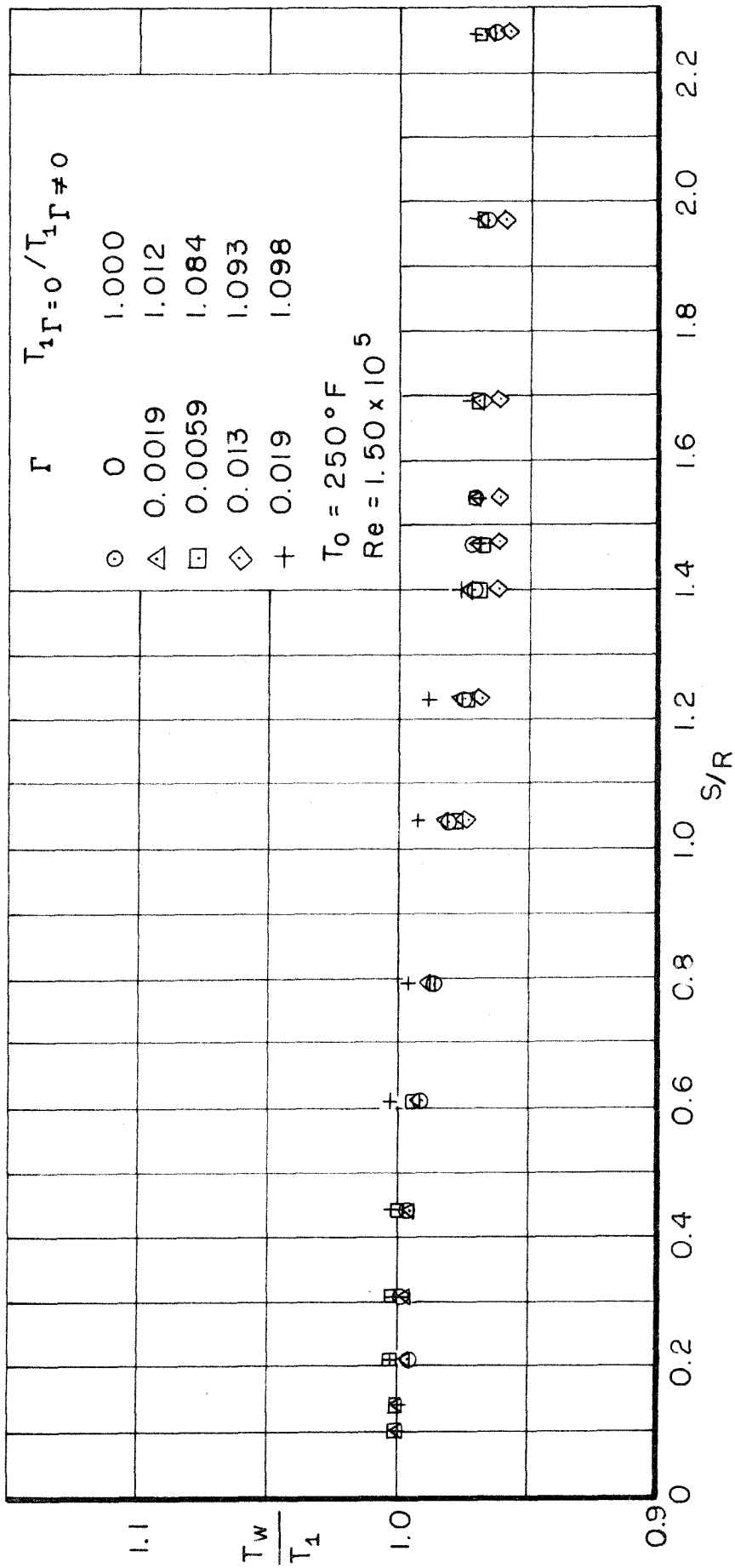

FIG. 48—NONDIMENSIONAL TEMPERATURE RATIO FOR VARIOUS RATES OF NITROGEN INJECTION, MODEL HM

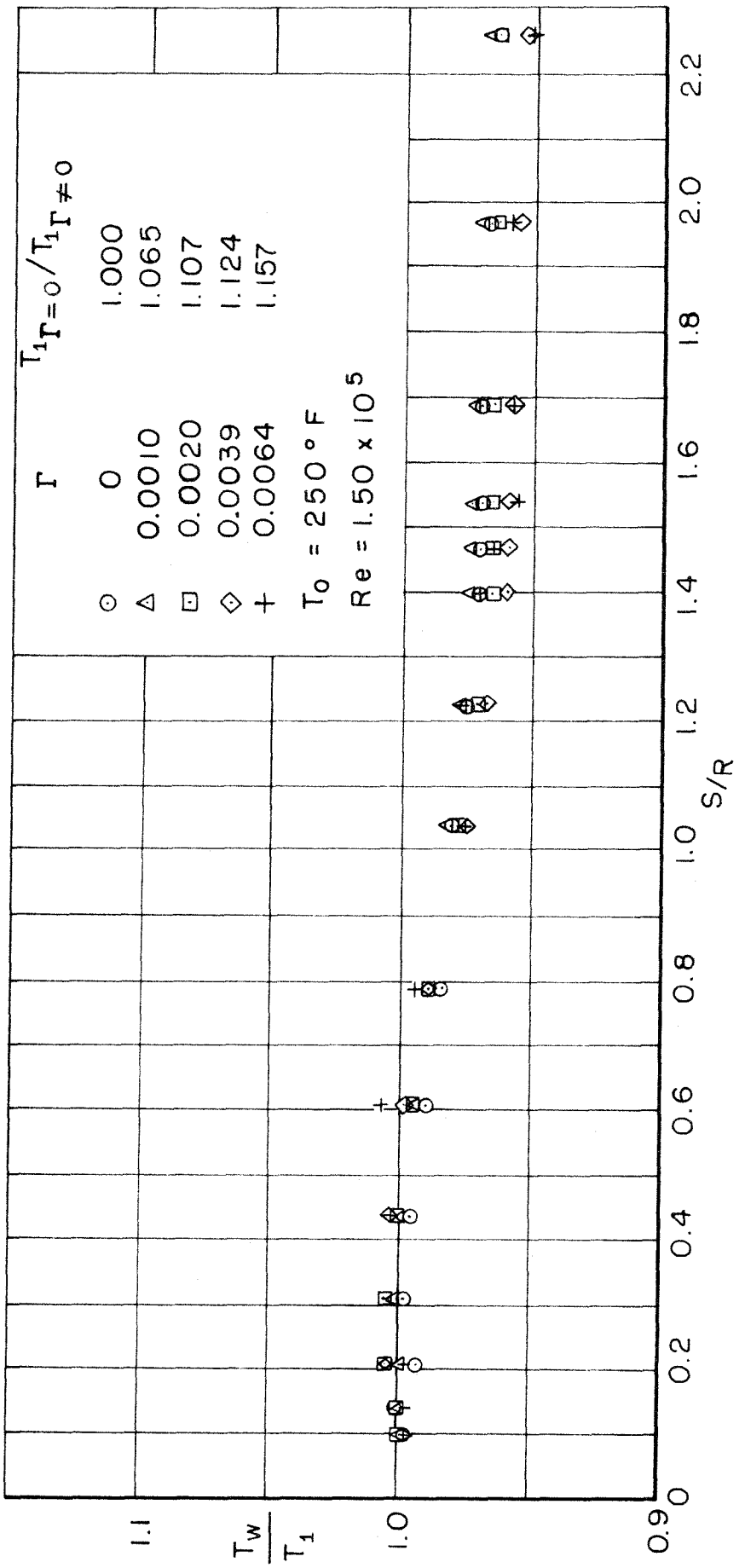

FIG. 49-NONDIMENSIONAL TEMPERATURE RATIO FOR VARIOUS RATES OF HELIUM INJECTION, MODEL HM

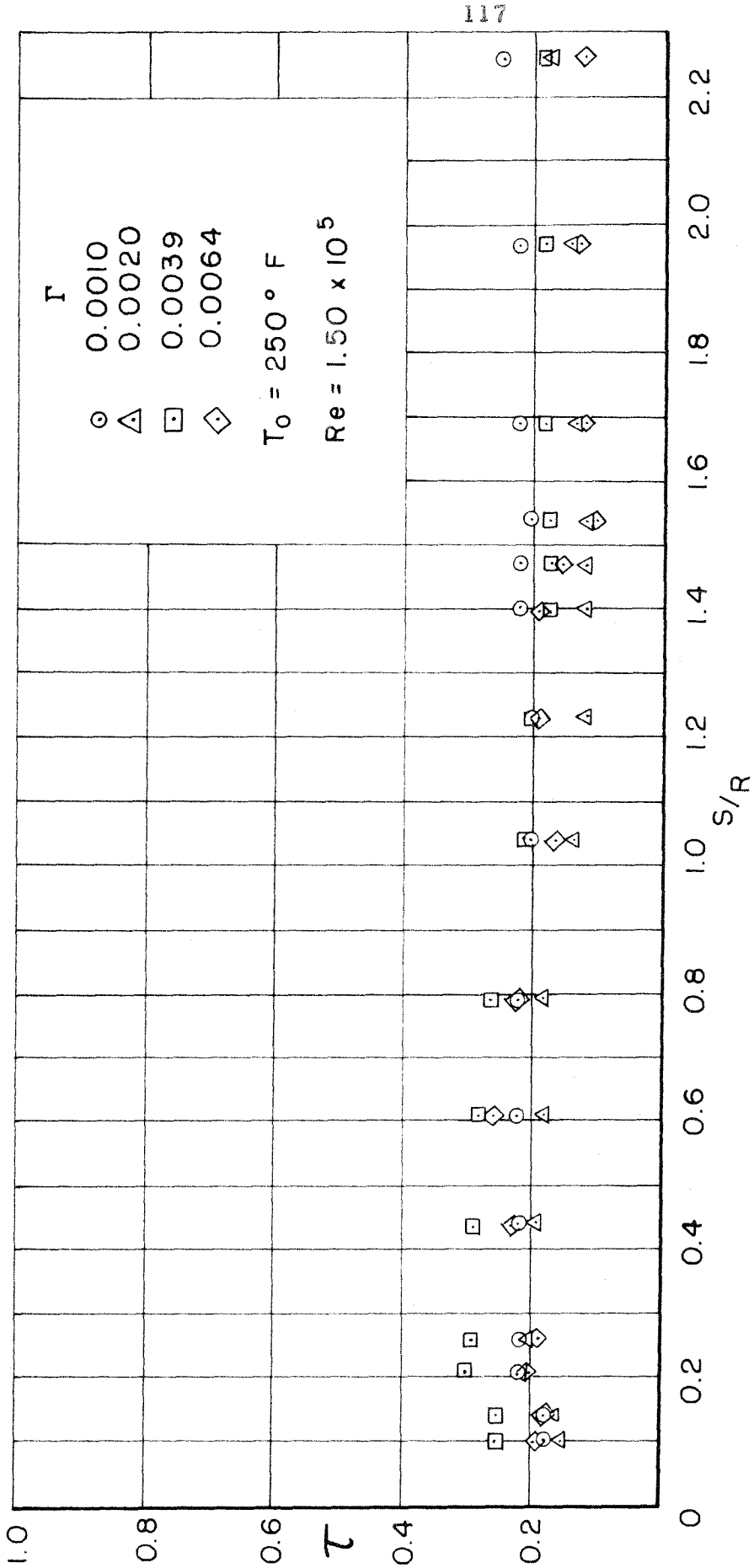

FIG. 50 - NONDIMENSIONAL TEMPERATURE RATIO WITH VARIOUS RATES OF HELIUM INJECTION, MODEL HM

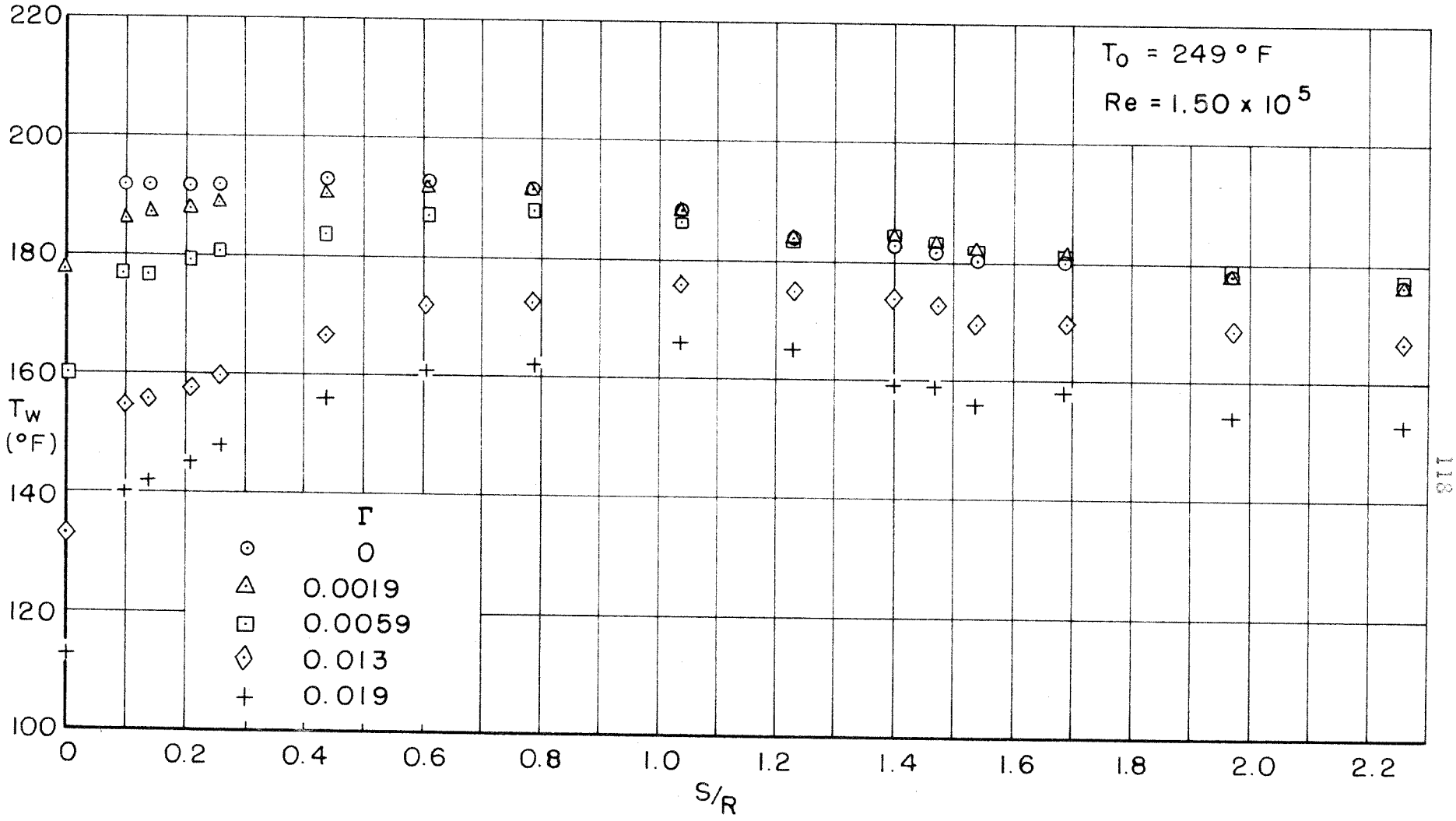

FIG. 51 – EQUILIBRIUM WALL TEMPERATURE WITH VARIOUS RATES OF NITROGEN INJECTION, MODEL HM + CA + S II

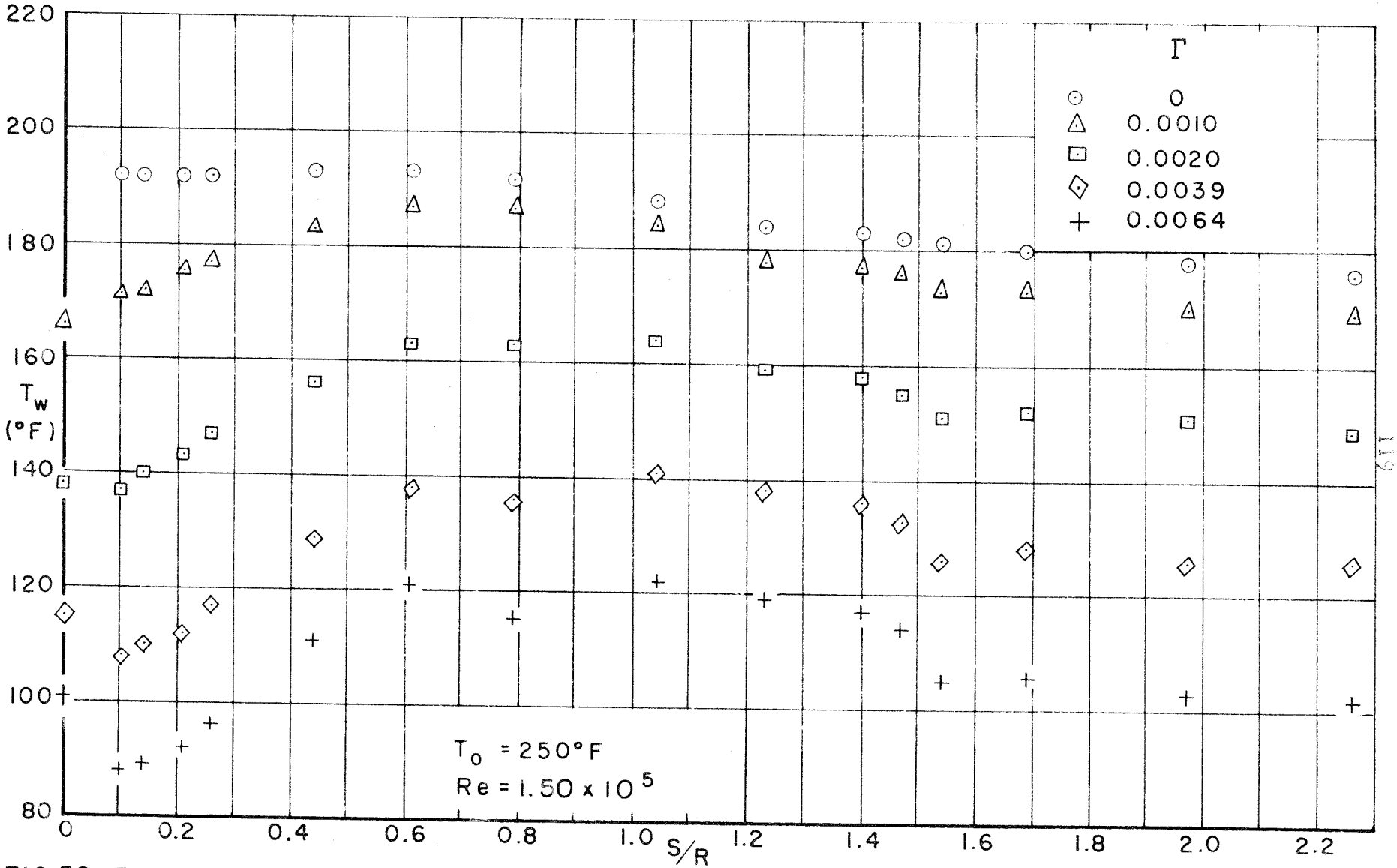

FIG.52- EQUILIBRIUM WALL TEMPERATURE WITH VARIOUS RATES OF HELIUM INJECTION, MODEL HM + CA + SII

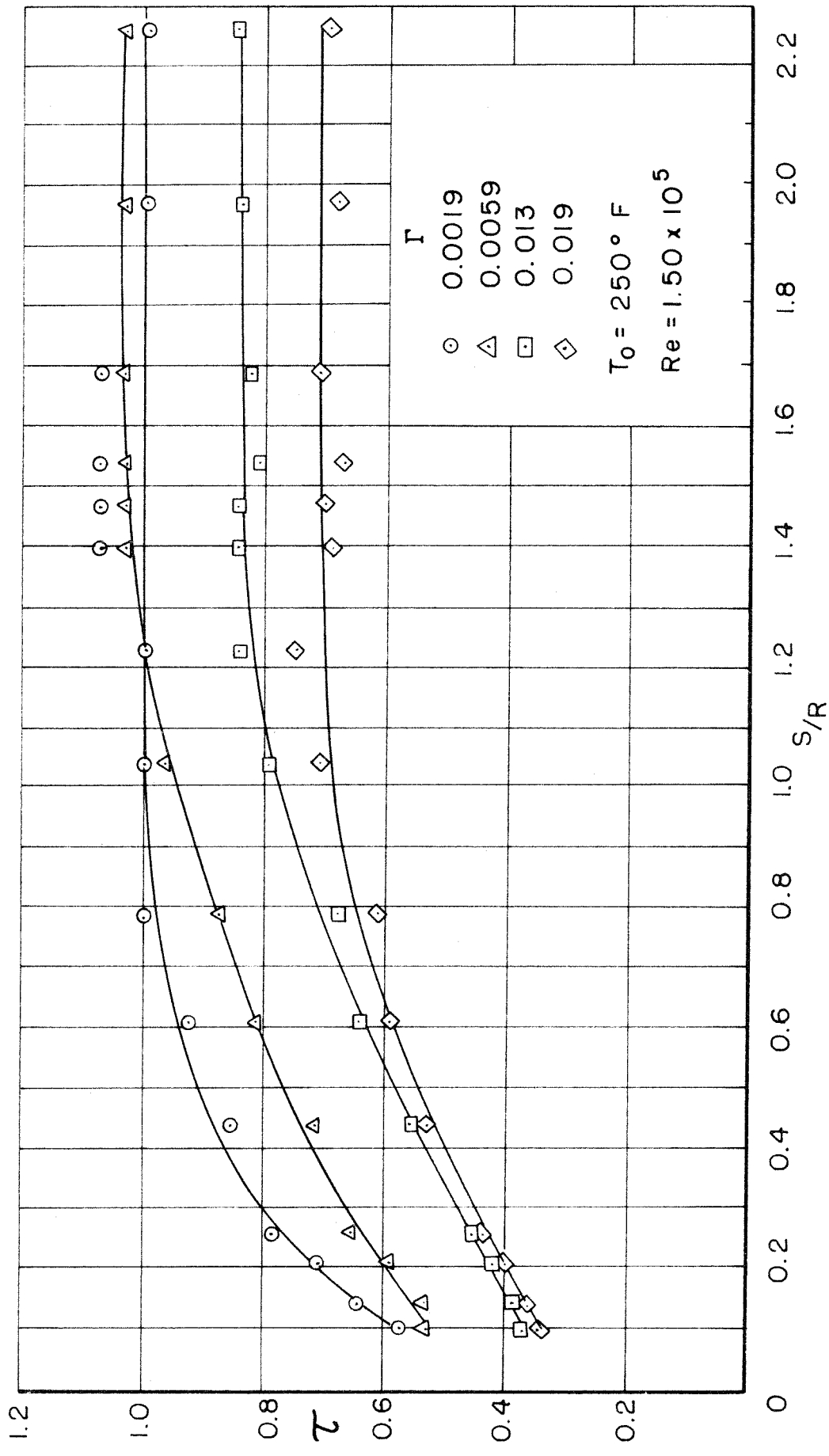

FIG. 53 – NONDIMENSIONAL TEMPERATURE RATIO WITH VARIOUS RATES OF NITROGEN INJECTION, MODEL HM + CA + S II

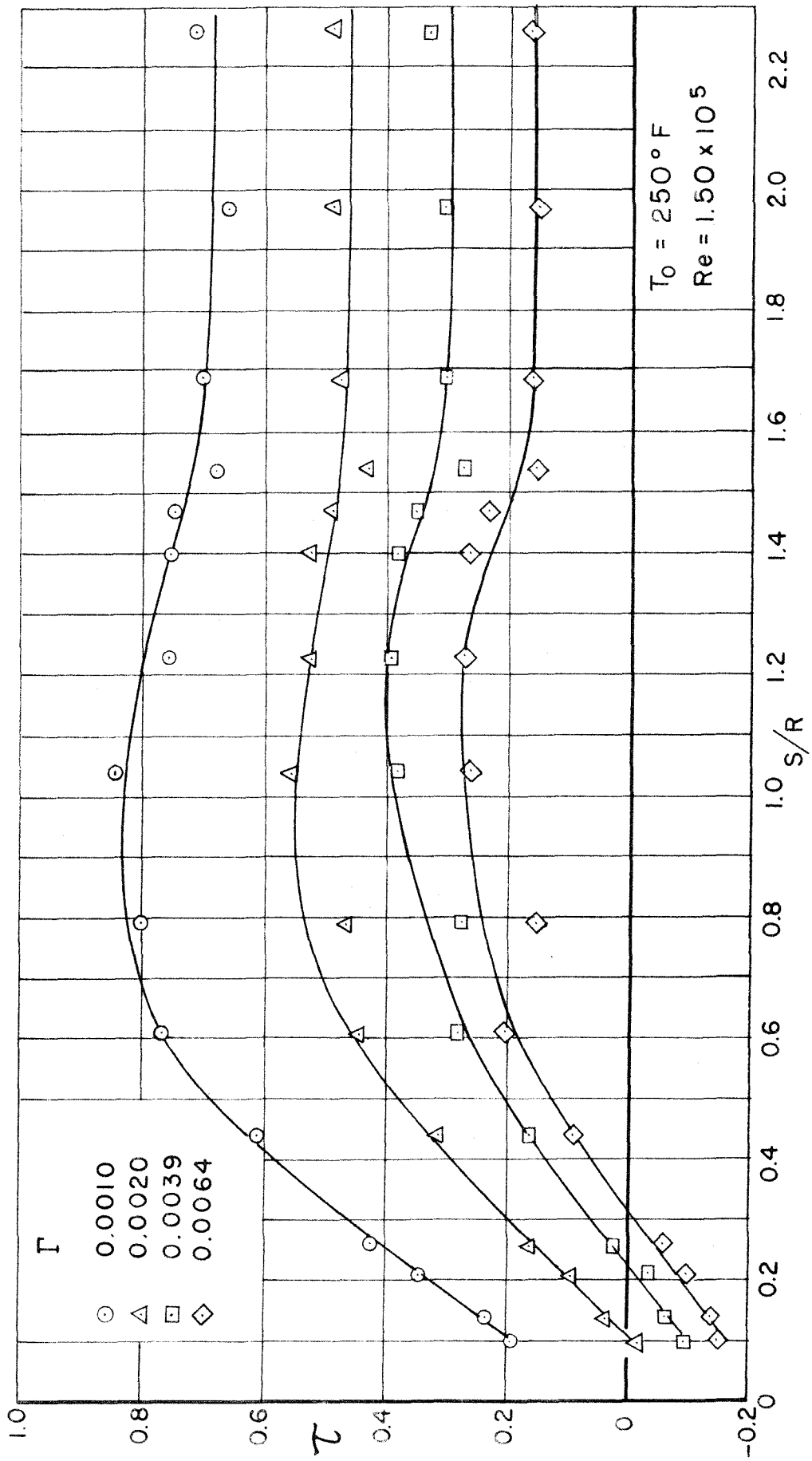

FIG. 54 - NONDIMENSIONAL TEMP. RATIO WITH VARIOUS RATES OF HELIUM INJECTION
MODEL HM + CA + SII

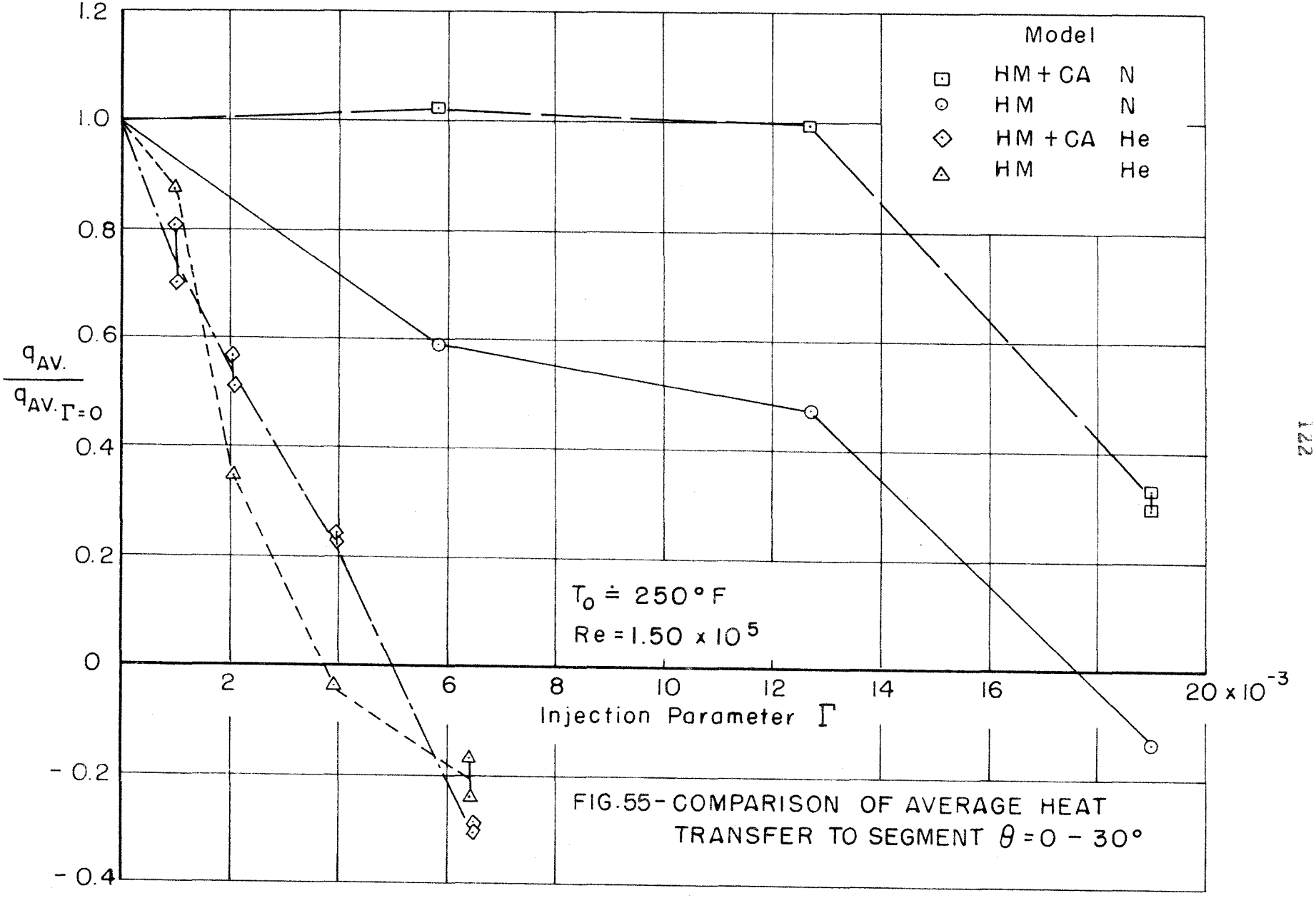

FIG.55- COMPARISON OF AVERAGE HEAT TRANSFER TO SEGMENT $\theta = 0 - 30°$

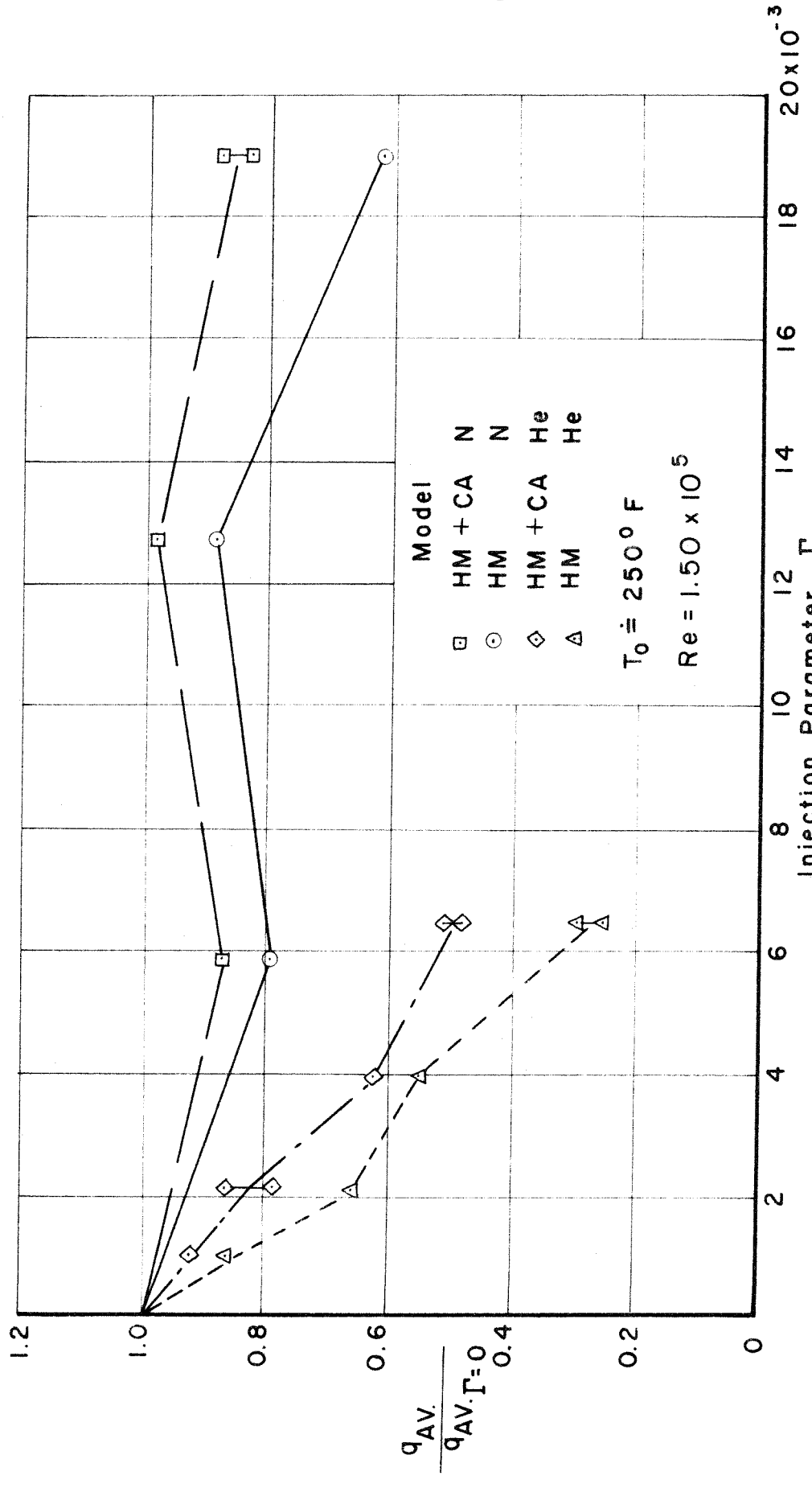

FIG.56-COMPARISON OF AVERAGE HEAT TRANSFER TO SEGMENT $\theta = 0-60^\circ$

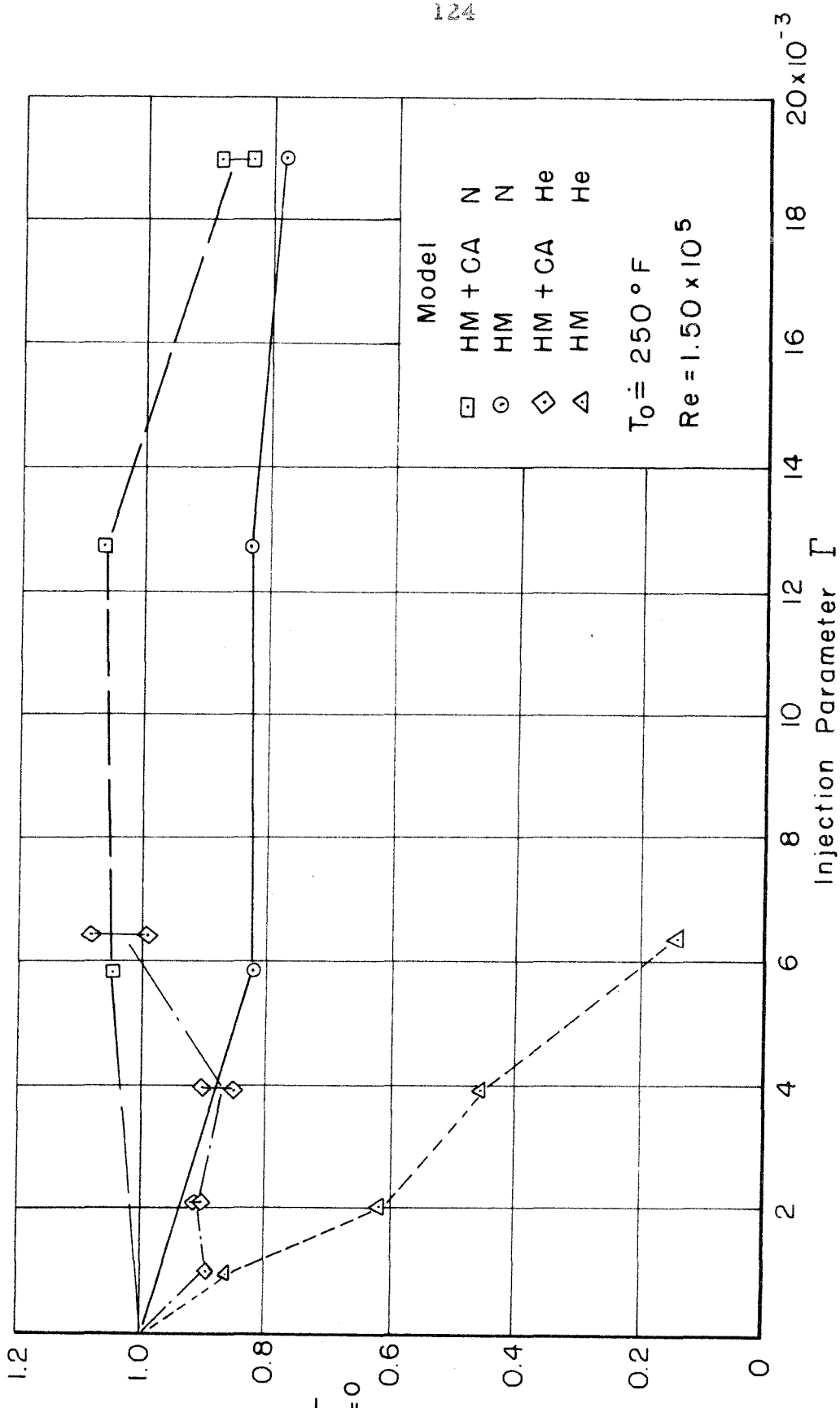

FIG.57-COMPARISON OF AVERAGE HEAT TRANSFER TO SEGMENT $\theta = 0-80°$

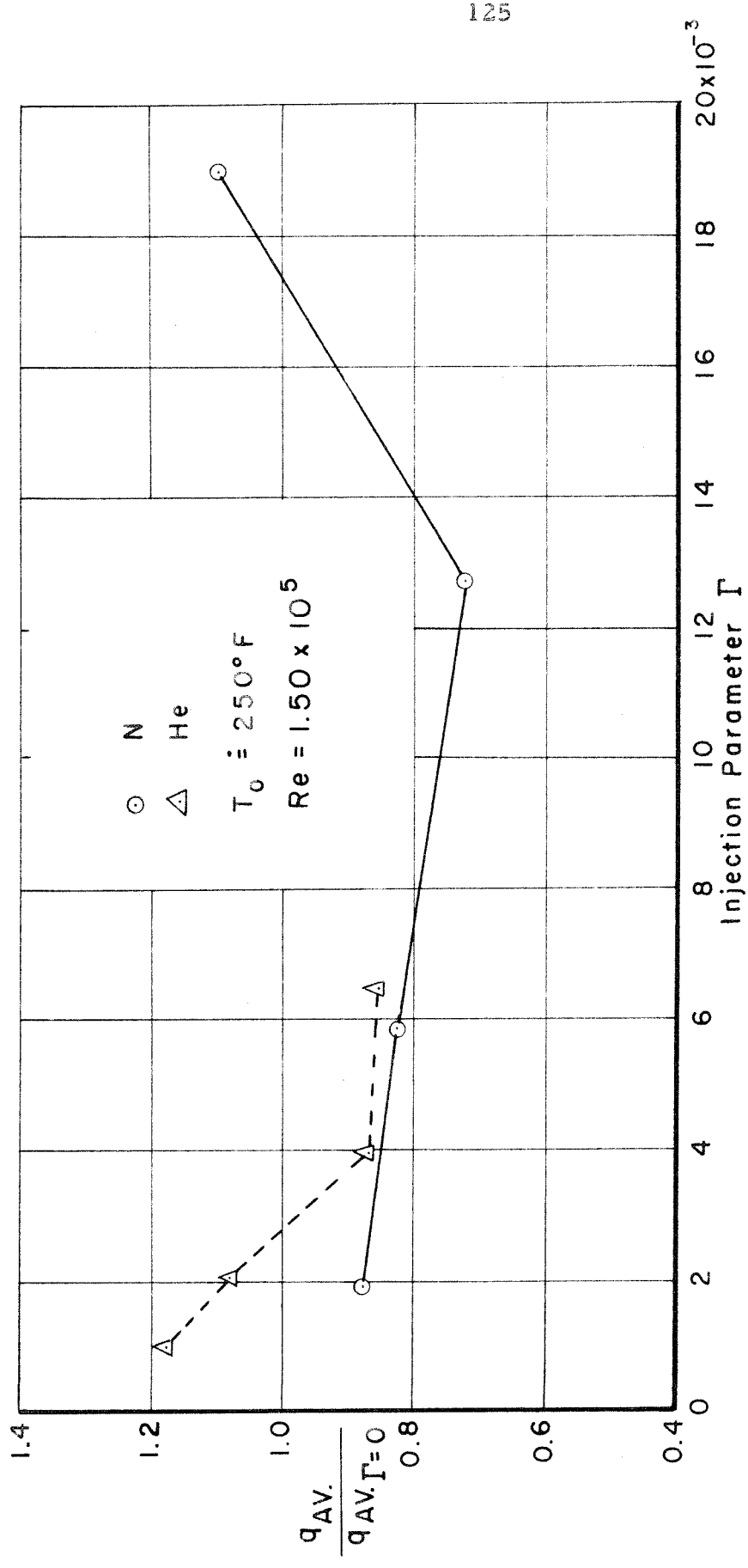

FIG.58-COMPARISON OF AVERAGE HEAT TRANSFER TO SEGMENT $\theta = 0-60°$
MODEL HM + CA + S II

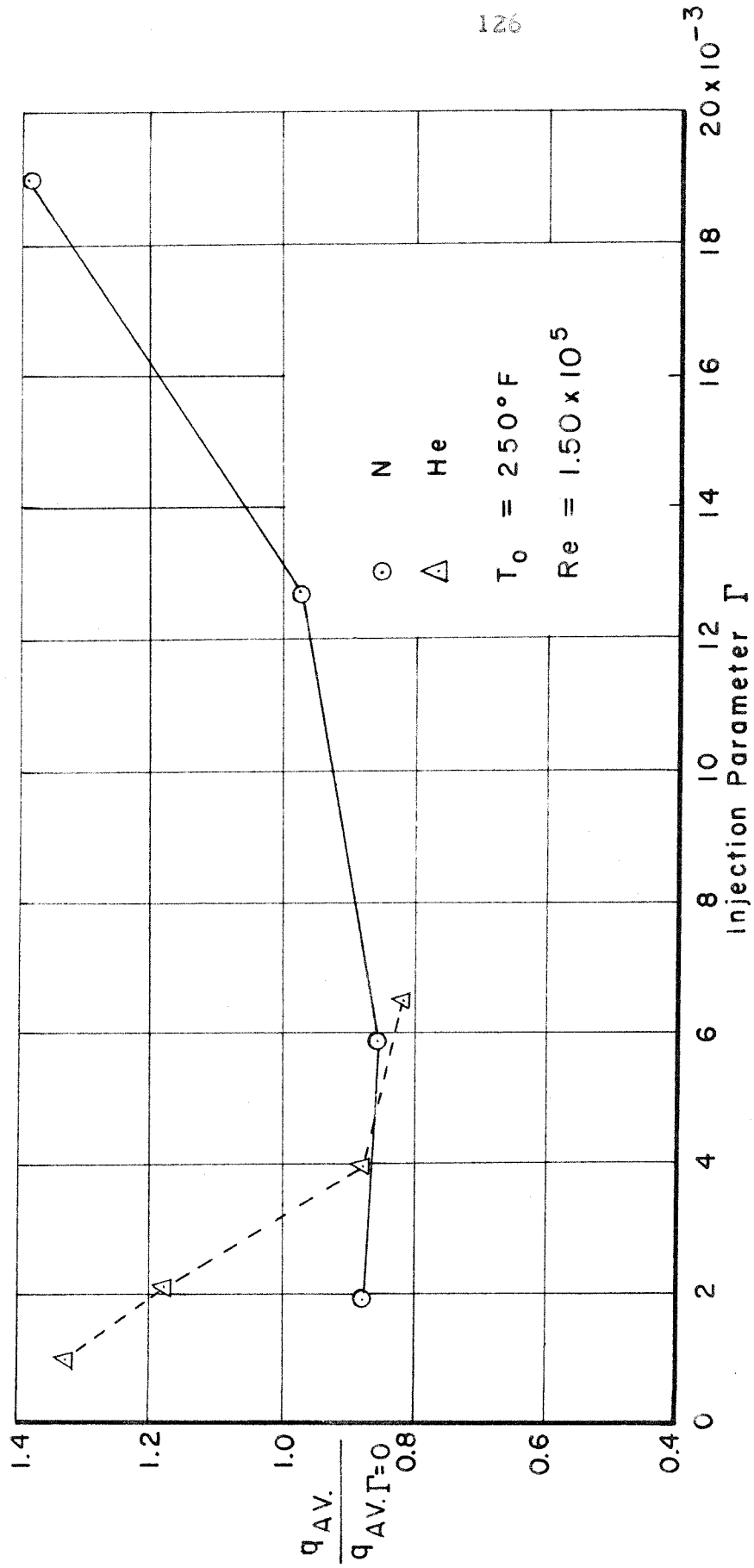

FIG.59-COMPARISON OF AVERAGE HEAT TRANSFER TO SEGMENT $\theta = 0-80°$
MODEL HM + CA + SII

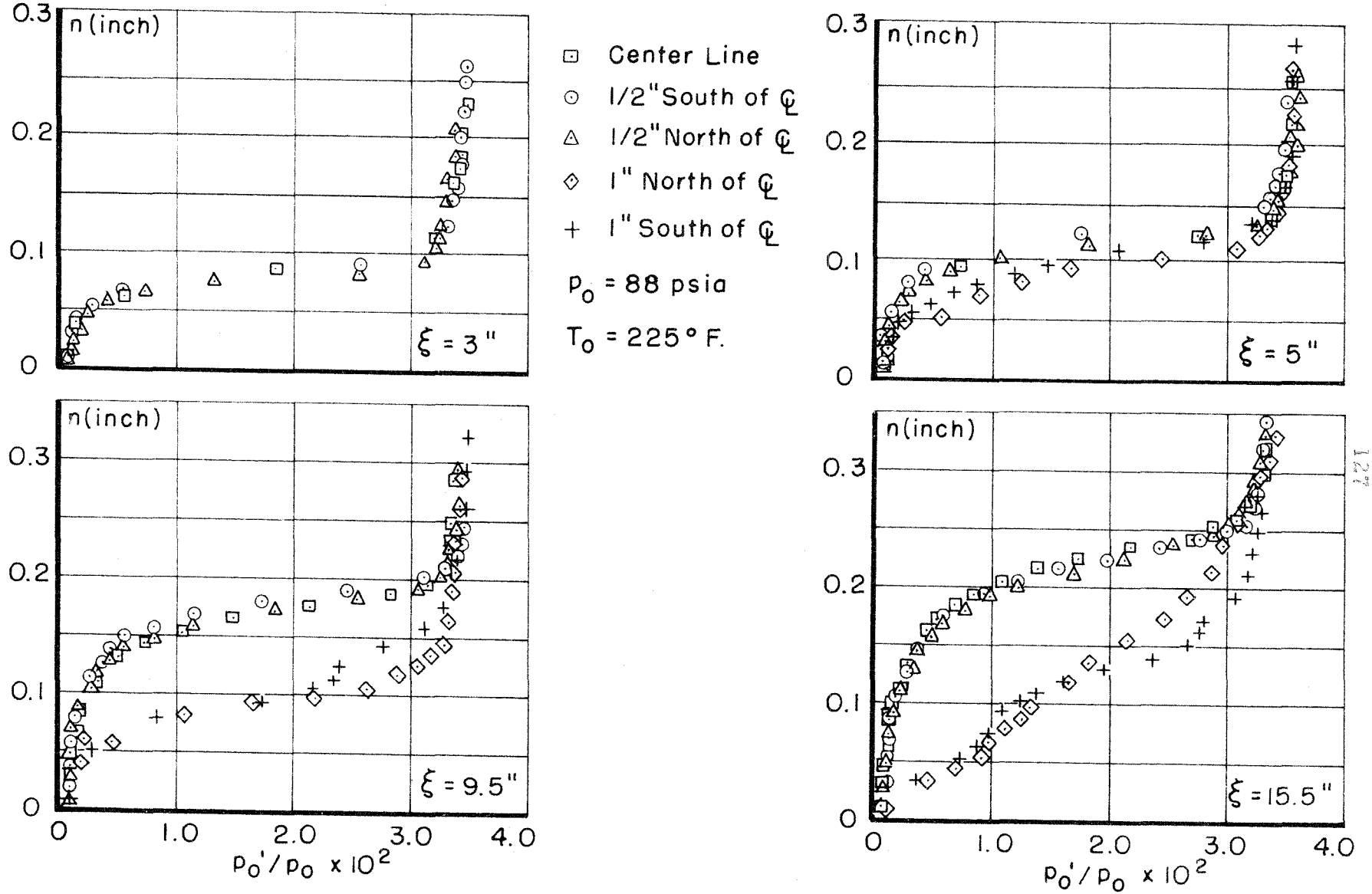

FIG. 60-TOTAL PRESSURE PROFILES THROUGH BOUNDARY LAYER ON FLAT PLATE

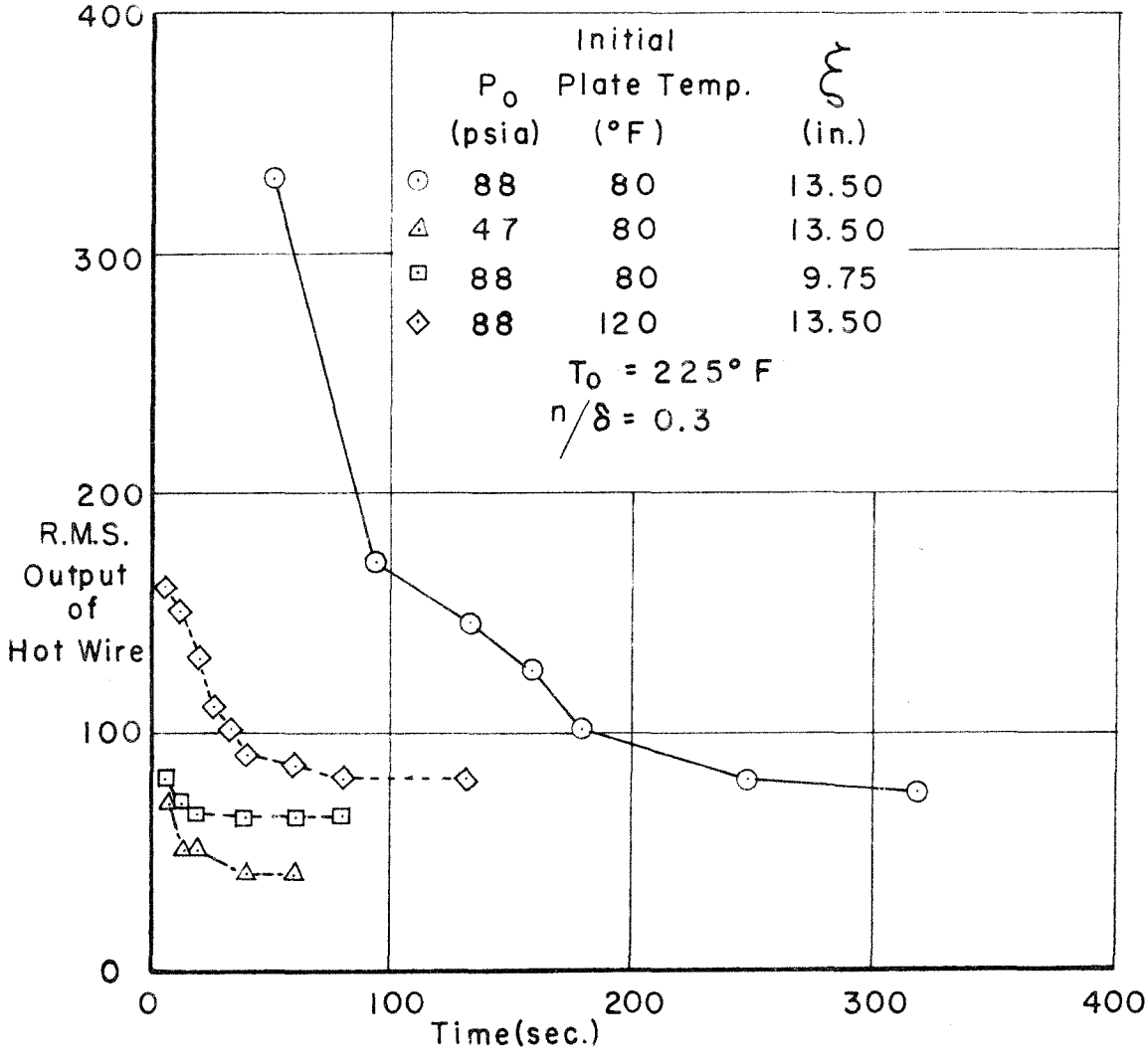

FIG. 61 — R. M. S. OUTPUT OF HOT WIRE AS A FUNCTION OF TIME